Vol. 68 • No. 11

November 2025

Microwave® Journal

SPECIAL FOCUS: 5G/6G

horizon house®

Founded in 1958

mwjournal.com

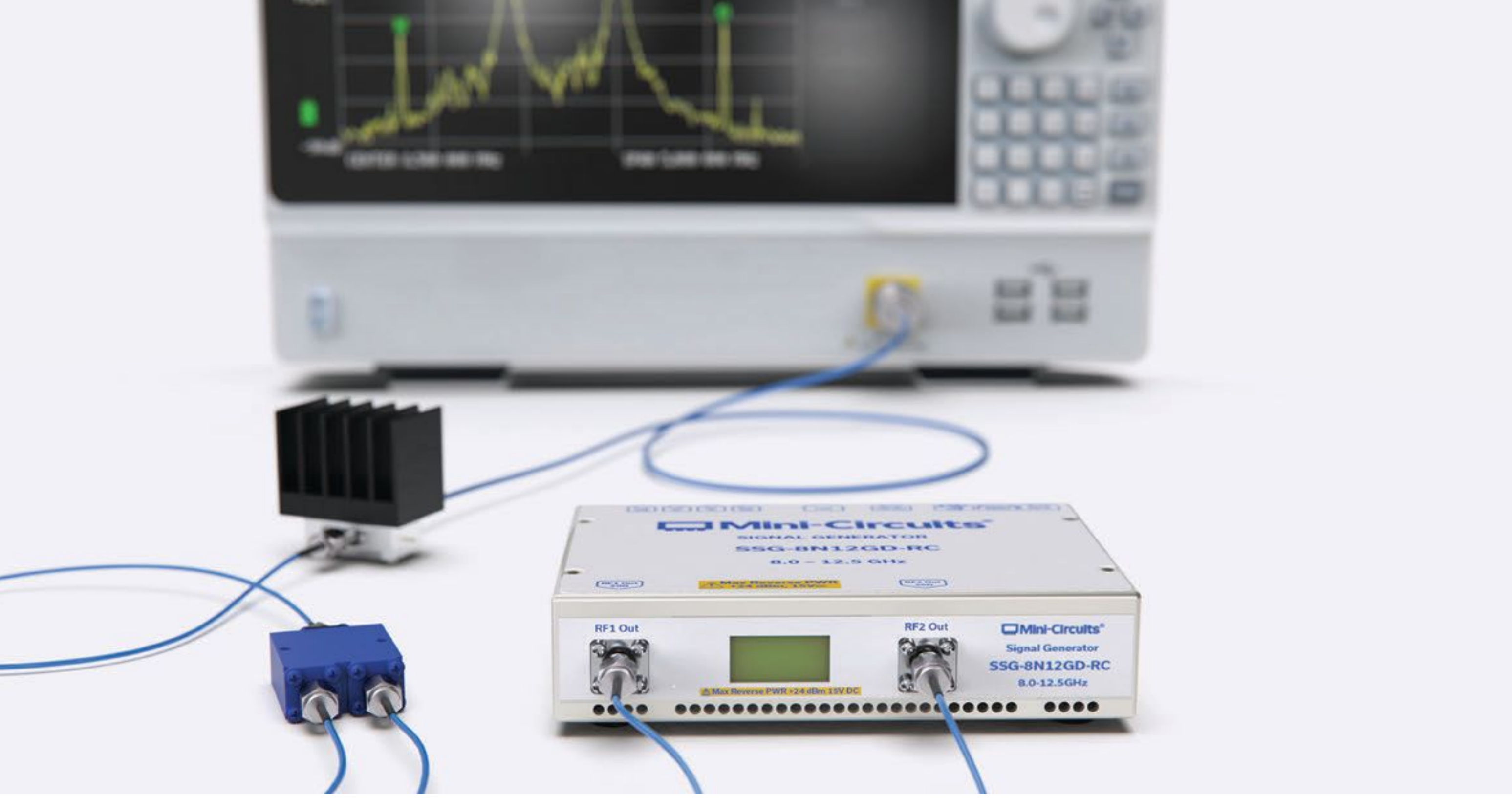

SSG SERIES

Signal Generators

Single-Channel & Dual Channel

LEARN MORE

Highlights

- Wide output power range
- Dual outputs with 360° independent phase control
- Pulsed, CW, AM, FM, and chirp modulations
- USB, Ethernet & PoE control interfaces
- Daisy chain port for multi-module control
- Compact housing, 3.6 x 5.1 x 1.2″

Model Number	Frequency	Output Power	# Channels	Release Status
SSG-8N12G-RC	8 to 12.5 GHz	-55 to 23 dBm	1	Production
SSG-8N12GD-RC	8 to 12.5 GHz	-55 to 23 dBm	2	Production
SSG-5N9G-RC	5 to 9 GHz	-55 to 23 dBm	1	Production
SSG-5N9GD-RC	5 to 9 GHz	-55 to 23 dBm	2	Production
SSG-9G-RC	0.01 to 9 GHz	-50 to 15 dBm	1	Q2, 2025
SSG-9GD-RC	0.01 to 9 GHz	-50 to 15 dBm	2	Q2, 2025
SSG-R7N6G-RC	0.7 to 6 GHz	-55 to 23 dBm	1	Q2, 2025
SSG-R7N6GD-RC	0.7 to 6 GHz	-55 to 23 dBm	2	Q3, 2025
SSG-1R5G-RC	0.02 to 1.5 GHz	-55 to 23 dBm	1	Q3, 2025
SSG-1R5GD-RC	0.02 to 1.5 GHz	-55 to 23 dBm	2	Q3, 2025

PWR SERIES

Power Sensors

Turn Your PC into a High-Performance Power Meter

LEARN MORE

- Dynamic range options spanning -60 to +20 dBm
- CW, true RMS, peak and average measurement capability
- Sample rates up to 80 million samples per second
- 50 and 75Ω models
- Software package supports automated measurement with statistical analysis and time domain plots
- No external calibration required

Model #	Control Interface	Measurement Type	Freq. Range (MHz)	Input Power Range (dBm)	Measurement Speed (ms)
PWR-40PW-RC	USB & Ethernet	Peak & Avg.	500-40000	-20 to 20	5.00E-05
PWR-18PWHS-RC	USB & Ethernet	Peak & Avg.	50-18000	-60 to 20	1.30E-05
PWR-18RMS-RC	USB & Ethernet	RMS	50-18000	-60 to 20	0.5
PWR-9PWHS-RC	USB & Ethernet	Peak & Avg.	50-9000	-60 to 20	0.000013
PWR-9RMS-RC	USB & Ethernet	RMS	50-9000	-60 to 20	0.5
PWR-8P-RC	USB & Ethernet	Peak & Avg.	10-8000	-60 to 20	0.002
PWR-8FS	USB	CW	1-8000	-30 to 20	10
PWR-8GHS	USB	CW	1-8000	-30 to 20	30
PWR-8GHS-RC	USB & Ethernet	CW	1-8000	-30 to 20	30
PWR-8PW-RC	USB & Ethernet	Peak & Avg.	10-8000	-60 to 20	0.00005


RF-LAMBDA
THE LEADER OF RF BROADBAND SOLUTIONS
BROADBAND SSPA / EMC BENCHTOP
SOLID STATE POWER AMPLIFIER
0.1-22GHZ
ULTRA BROADBAND SSPA
RFLUPA01M22GA
4W 0.1-22GHZ
RFLUPA0218GB
20W 1-19GHZ
6-18GHZ 800W
CW REMC06G18GG
18-40GHZ 200W
CW REMC18G40GQ
0. 1-6GHZ VHZ,
UHF, L, S, C BAND
RFLUPA02G06GC
100W 2-6GHZ
RFLUPA0706GD
30W 0.7-6GHZ
MADE IN
USA
6-18GHZ C, X, KU BAND
RFLUPA08G11GA
50W 8-11GHZ
RFLUPA0618GD
60W 6-18GHZ
RFLUPA06G12GB
25W 6-12GHZ
18-50GHZ K, KA, V BAND
RFLUPA18G47GC
2W 18-47GHZ
RFLUPA27G34GB
15W 27-34GHZ
RFLUPA47G53GA2
10W 47-53GHZ
RFLUPA27G34GB
30W 18-40GHZ
BENCHTOP RF MICROWAVE SYSTEM POWER AMPLIFIER
REMC02G06GE
600W 2-6GHZ
REMC18G40GC2
40W 18-40GHZ
RAMP30G65GG
8W 30-65GHZ
RAMP06G18GA
10W 6-18GHZ
RAMP00M65GA
DC-65GHZ
www.rflambda.com
sales@rflambda.com
1-888-976-8880
1-972-767-5998
San Diego, CA, US
Carrollton, TX, US
Ottawa, ONT, Canada
Frankfurt, Germany


Innovate.
Advance.
Repeat.
Breakthrough products featuring smaller footprints,
higher frequencies, greater thermal stability, and rapid delivery
Ultraminiature High Q Filters
to 10 GHz, custom diplexers
and multiplexers available
Tunable Gain Equalizer
to 50 GHz. Linear, parabolic
and ripple removal
Cryogenic Attenuators
SMT and coax models,
operate reliably at 4 mK
Filtered 38999 Connectors
3 pin configurations
12-week delivery
Get more details and see the full line-up of innovative new products at
spectrumcontrol.com/new25Q3
SPECTRUM
CONTROL ™
spectrumcontrol.com © 2025 Spectrum Control, Inc. All rights reserved


GaN

Microwave Journal

November 2025
Vol. 68 • No. 11
5G/6G & IoT
mwjournal.com

CONTENTS

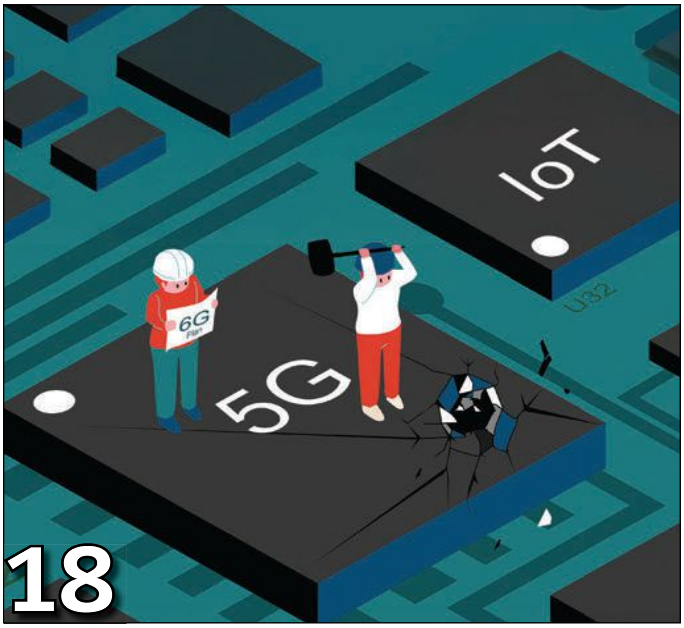

18

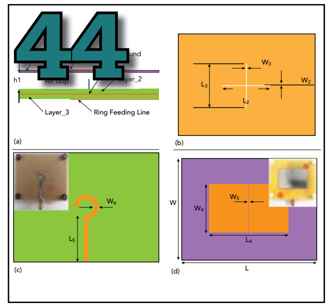

44

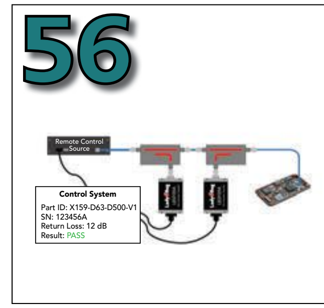

56

Cover Feature

Technical Feature

Application Note

5G 6G SPECIAL FOCUS

ACCESS NOW!
digital.microwavejournal.com

eXclusive Digital Content >>>

68 YEARS OF PUBLISHING EXCELLENCE

Microwave Journal

CONTENTS

mwjournal.com

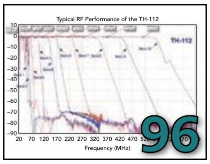

Product Feature

Tech Brief

Departments

Microwave Journal (USPS 396-250) (ISSN 0192-6225) is published monthly by Horizon House Publications Inc., 685 Canton St., Norwood, MA 02062. Periodicals postage paid at Norwood, MA 02062 and additional mailing offices.

POSTMASTER: Send address corrections to Microwave Journal, PO Box 1028, Lowell, MA 01853 or e-mail mwj@e-circ.net.com. Subscription information: (978) 671-0446. This journal is issued without charge upon written request to qualified persons working in the RF & microwave industry. Other subscriptions are: domestic, $130.00 per year, two-year subscriptions, $200.00; foreign, $225.00 per year, two-year subscriptions, $400.00; back issues (if available) and single copies, $20.00 domestic and $30.00 foreign. Claims for missing issues must be filed within 90 days of date of issue for complimentary replacement.

EXECUTIVE EDITORIAL OFFICE

685 Canton Street, Norwood, MA 02062
Tel: (781) 769-9750
FAX: (781) 769-5037
e-mail: mwj@mwjournal.com

EUROPEAN EDITORIAL OFFICE

16 Sussex Street, London SW1V 4RW, England
Tel: Editorial: +44 207 596 8730 Sales: +44 207 596 8740
FAX: +44 207 596 8749

SUBSCRIPTION SERVICES

Send subscription inquiries and address changes to:
Tel: (978) 671-0446
e-mail: mwj@e-circ.net

www.mwjournal.com

Printed in the USA


GaN

Microwave Journal ONLINE .COM

LEARNING CENTER On-Demand

Designing with Juliano and Katerina eLearning Series: Frequency Selective Surfaces
Sponsored by: Ansys

Online Panel: 5G/6G Advances
Sponsored by: Qorvo, MathWorks and CADFEM

WHITE PAPERS

ANALOG DEVICES — AHEAD OF WHAT'S POSSIBLE™
Benefits of Ultralow Noise Switching Regulator in Noise-Sensitive RF Applications

Coilcraft
The Fundamentals of Electromagnetic Compliance

Look for additional content from:
saetta labs
WÜRTH ELEKTRONIK

Executive Interview

Sundeep Rangan, NYU Professor of Electrical & Computer Engineering and newly appointed Director of **NYU WIRELESS**, discusses the research being done by the center in wireless technology along with projects for 6G technology.

Join Us Online

Follow us @Pathindle @MWJEditor

Join us at the RF and Microwave Community

Become a fan at facebook.com/microwavejournal

Microwave Journal podcasts include the RF/microwave update series, Frequency Matters, plus interviews with industry experts and executives.

Catch *Frequency Matters,* the industry update from *Microwave Journal,* microwavejournal.com/FrequencyMatters

Visit us @ mwjournal.com

A NEW RECORD!

Mini-Circuits MMICs Strike 10W!

LEARN MORE

PMA6 Series

PMA5 Series

PMA3 Series

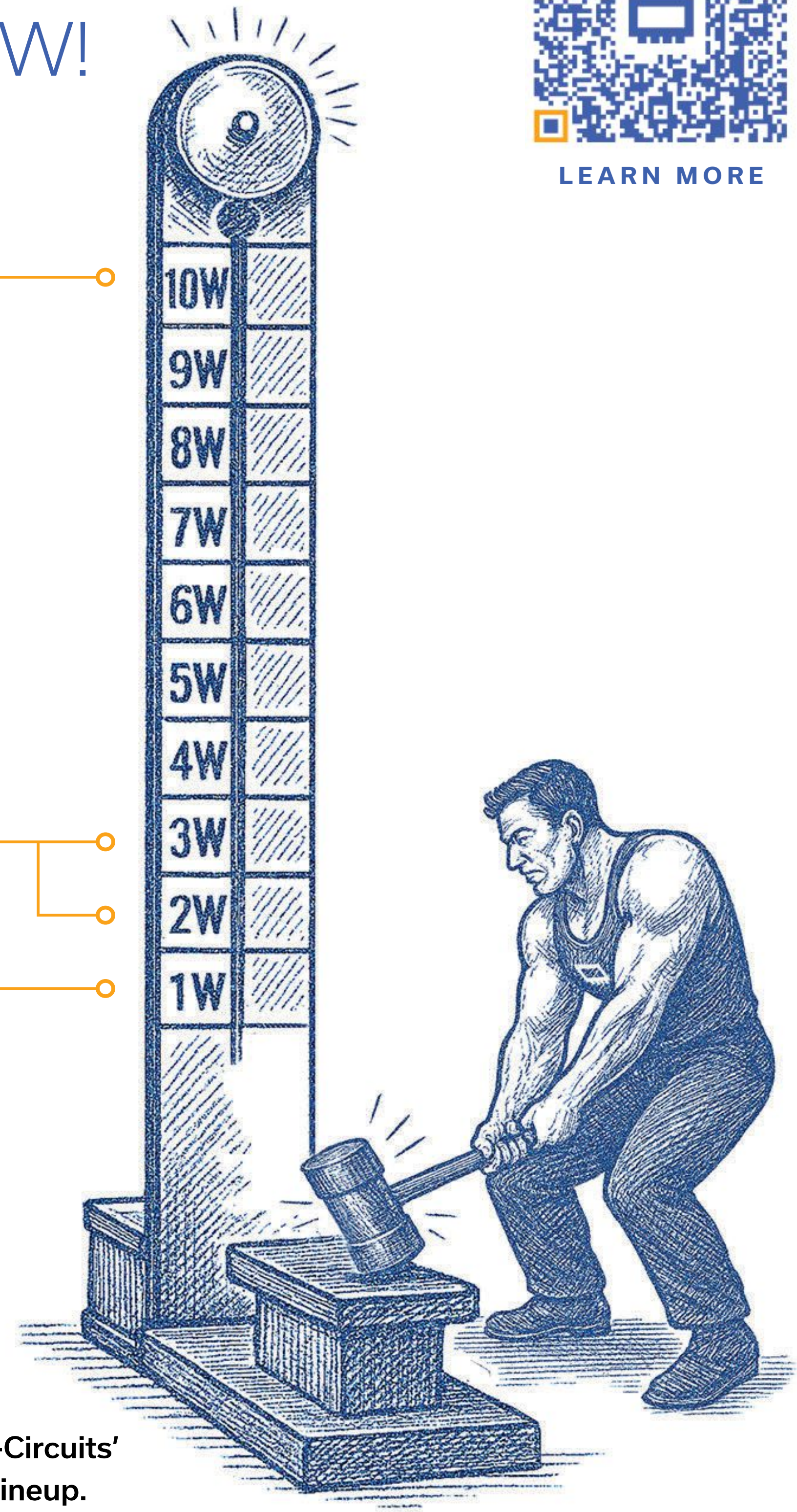

There's more muscle than ever in Mini-Circuits' growing GaAs MMIC power amplifier lineup.
Check out our new PMA6-series with P_{SAT} up to 10W, and look out for more innovations on the way!

YOUR TRUSTED PARTNER
FROM DC TO mmWAVE

Mini-Circuits®

STAY CONNECTED TO COMING EVENTS

MARK YOUR CALENDAR

NOVEMBER

18-20
Space Tech Expo EU
Bremen, Germany
www.spacetechexpo-europe.com

DECEMBER

2-5
APMC 2025
Jeju, South Korea
www.apmc2025.org

6-10
IEDM 2025
San Francisco, Calif.
www.ieee-iedm.org

9-11
AOC 2025
National Harbor, Md.
https://aoc2025.org

14-18
MAPCON 2025
Kochi, Kerala, India
https://ieeemapcon.org

JANUARY

6-9
CES 2026
Las Vegas, Nev.
www.ces.tech

18-21
IEEE Radio & Wireless Week
Los Angeles, Calif.
https://www.radiowirelessweek.org

FEBRUARY

7-9
IEEE IMFW
Hong Kong, China
www.imfw-ieee.org

24-26
DesignCon
Santa Clara, Calif.
www.designcon.com

MARCH

9-11
German Microwave Conference
Karlsruhe, Germany
www.gemic2026.kit.edu

Register online at mwjournal.com

ONLINE PANEL SERIES

11/12
5G/6G Advances

Call for Papers Deadlines

1/6
Annual Microwave Power Symposium (IMPI)

2/9
International Conference on Microwave Acoustics & Mechanics (IC-MAM)

FOR DETAILS VISIT MWJOURNAL.COM/EVENTS

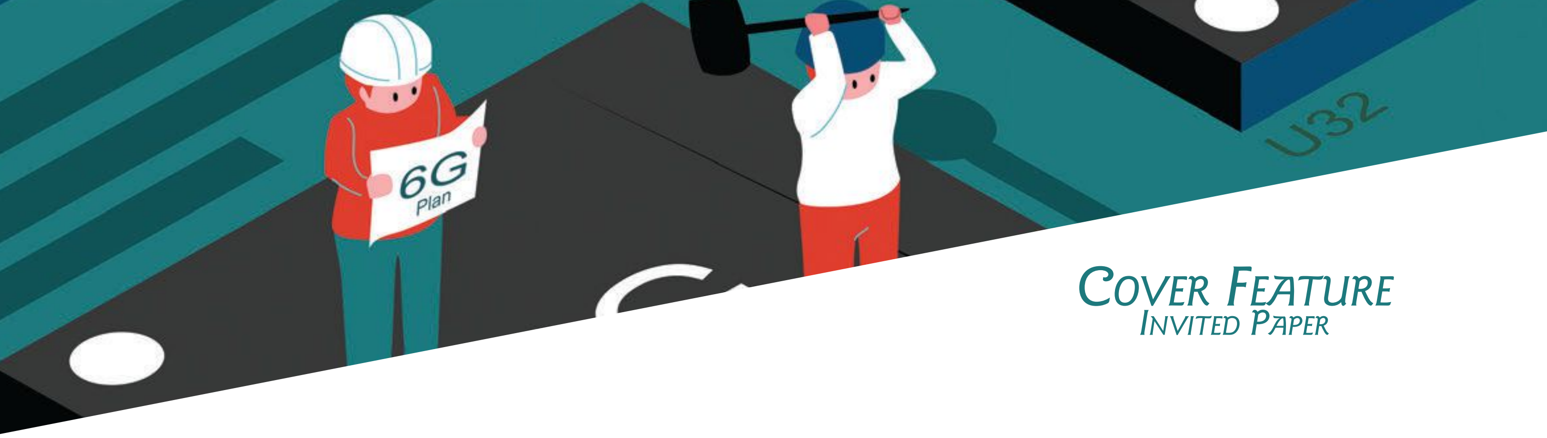

IoT RF Front-End Challenges and Solutions

Luis Andia
Soitec, Bernin, France

CELLULAR COMMS EVOLUTION FOR IOT

The evolution of cellular communications has been pivotal in meeting the specific needs of IoT. With 3GPP Releases 10 to 12 (4G LTE-Advanced), enhancements were introduced to support low-data-rate, robust and power-efficient connectivity.[1] This marked a critical turning point, further accelerated by the emergence of 5G reduced capability (RedCap), which caters to devices requiring more throughput than LPWAN solutions, such as NB-IoT, but less than full-scale eMBB. RedCap achieves lower complexity and cost by limiting antenna count, bandwidth (20 MHz maximum) and modulation schemes (64QAM or optional 256QAM).[2]

A key enabler of rapid innovation in smartphones, and increasingly in IoT devices, is the modularization of the RF front-end (RFFE). This modular approach allows designers to selectively integrate optimized components for various frequency bands and functionalities. IoT devices, such as connected watches, benefit from this by repurposing proven smartphone RFFE modules, resulting in faster time-to-market and reduced design complexity. Modularity offers an added advantage: the reuse of proven, reliable RF technologies such as RF-

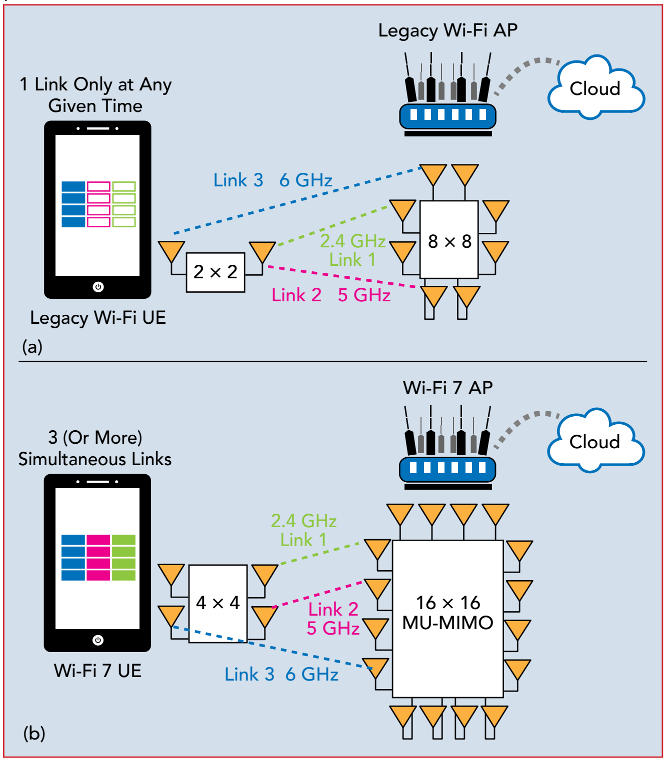

Fig. 1 **Wi-Fi (a) without MLO and (b) with MLO.**

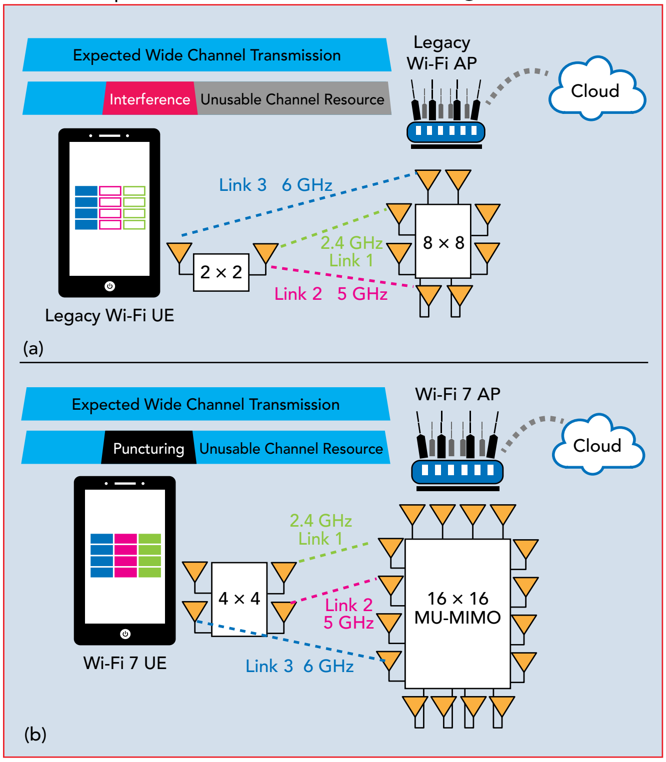

Fig. 2 **Wi-Fi channel (a) without and (b) with puncturing.**

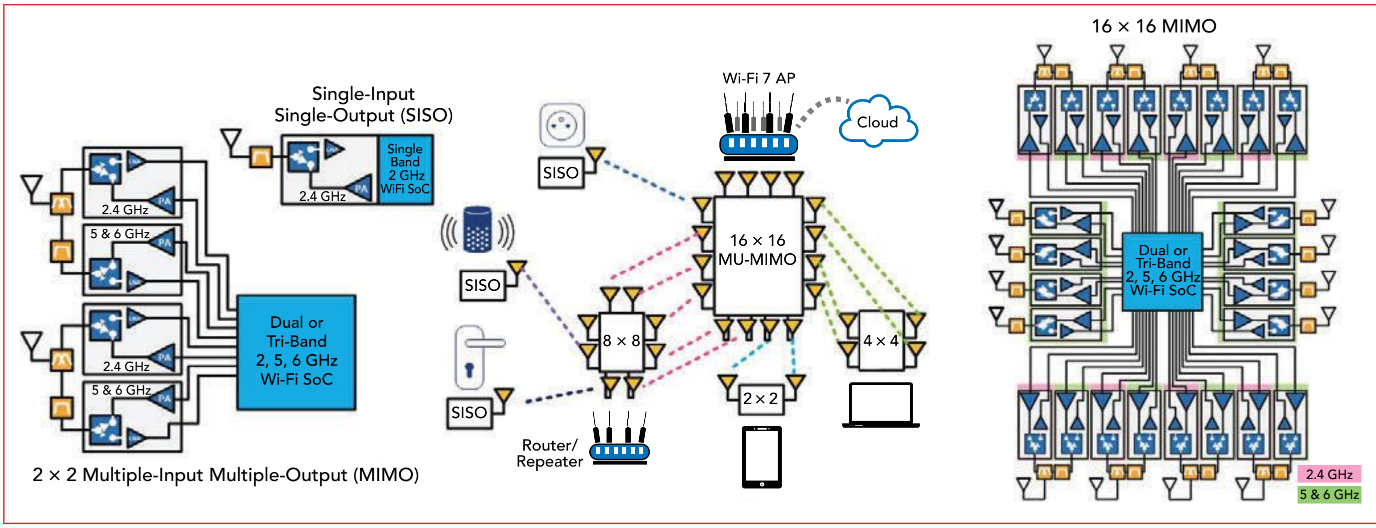

Fig. 3 **Example of Wi-Fi multi-user MIMO RFFE modular design.**

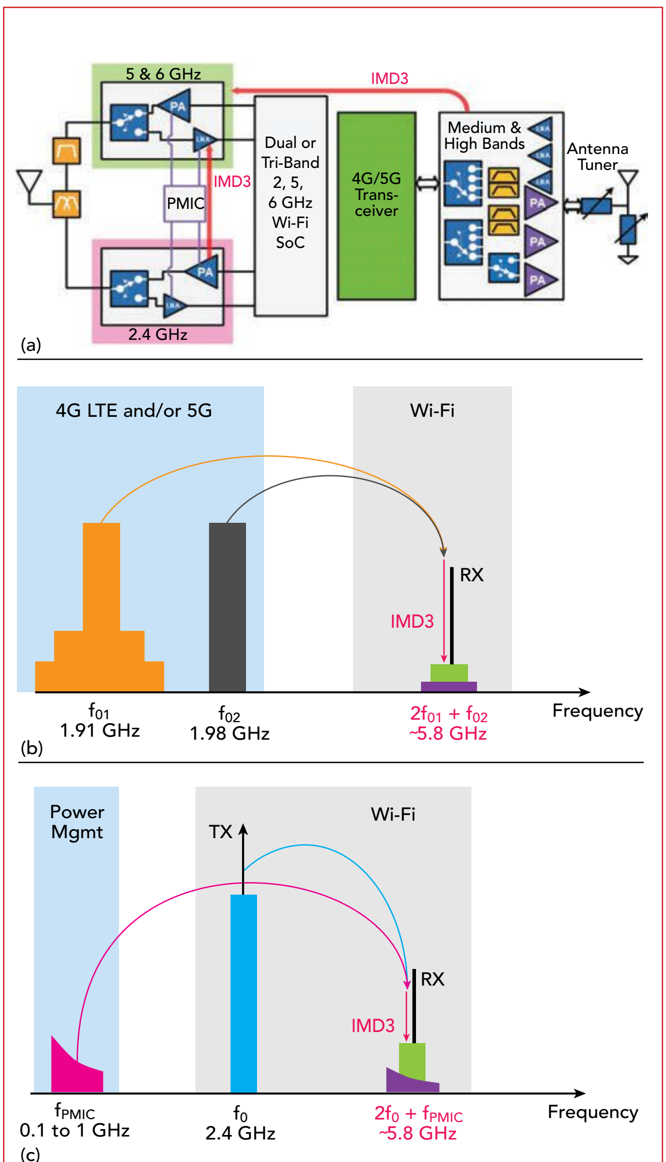

Fig. 4 **(a) RFFE IMD3 interferers generated by (b) cellular and Wi-Fi and (c) PMIC and Wi-Fi signals.**

silicon-on-insulator (SOI), piezo-on-insulator (POI) and fully depleted (FD)-SOI.

WI-FI COMMS EVOLUTION FOR IOT

Wi-Fi 7 brings significant improvements to IoT environments, especially in dense deployments. It increases modulation order from 1024QAM to 4096QAM, doubling peak data rates. It also expands multi-user capabilities through multi-user MIMO, now supporting up to 16 x 16 streams. These features increase network capacity, range and reliability.

To support higher network demands, Wi-Fi 7 incorporates multi-link operation (MLO), allowing devices to maintain simultaneous connections across multiple frequency bands, including 2.4 GHz, 5 GHz and 6 GHz, as demonstrated in ***Figure 1***. This reduces latency and minimizes disruptions during frequency handovers. Additionally, the multi-user resource unit feature enhances interference resistance by selectively blocking only affected channel sections, maintaining optimal performance, as seen in ***Figure 2***.

An additional innovation is the use of non-linear power amplifiers (PAs) in the Wi-Fi RFFE, which reduces power consumption by up to 25 percent compared to traditional linear amplifiers.[3] These PAs are linearized by AI-assisted digital predistortion (DPD) for calibration.[4] Integration of RF-SOI-based switches, low noise amplifiers (LNAs) and PAs in compact dies supports a broad range of compact IoT designs, as shown in ***Figure 3***.

Finally, dual 5G and Wi-Fi connectivity ensures robust, seamless transitions for IoT gateways and routers. This integration supports multi-gigabit throughput and ultra-low latency, critical for both consumer applications and industrial use cases.

IOT RFFE CHALLENGES AND SOLUTIONS

As IoT devices proliferate, RFFE modules face increasing demands for performance, integration and interference management. This overview highlights key semiconductor challenges and solutions across Wi-Fi and cellular applications. The insights gained are applicable across other wireless technologies as well.


Has Amplifier Performance or
Delivery Stalled Your Program?

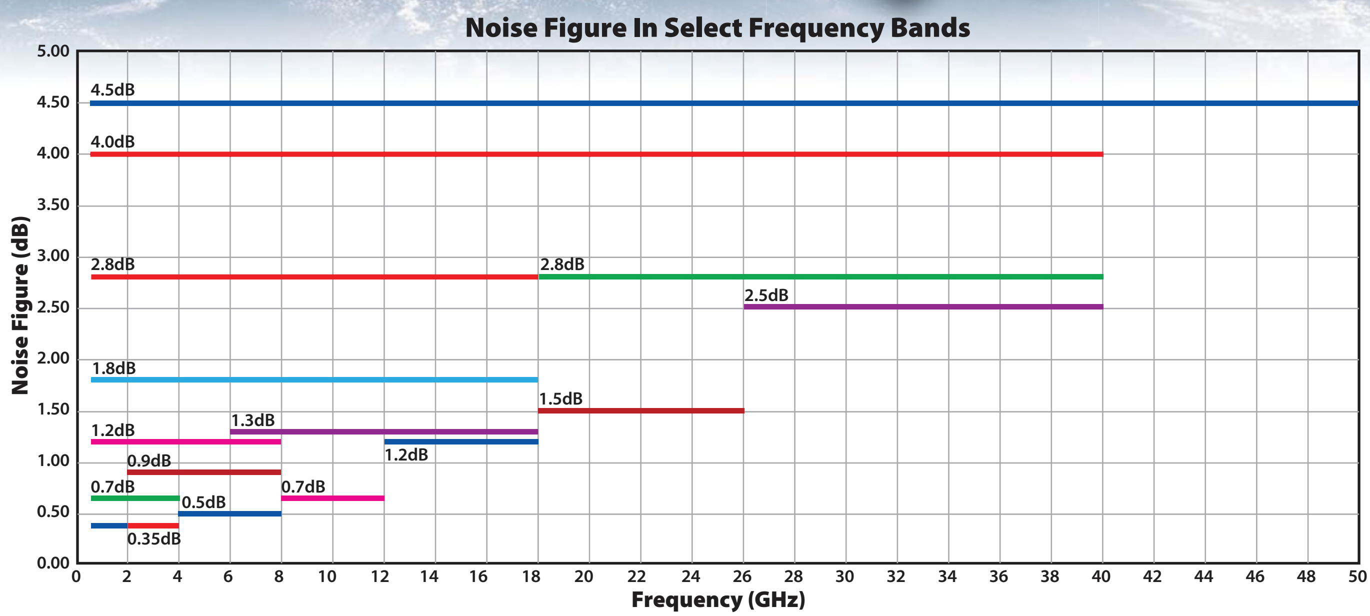
Noise Figure In Select Frequency Bands
Noise Figure (dB)
5.00
4.50
4.00
3.50
3.00
2.50
2.00
1.50
1.00
0.50
0.00
4.5dB
4.0dB
2.8dB
2.8dB
2.5dB
1.8dB
1.5dB
1.3dB
1.2dB
1.2dB
0.9dB
0.7dB
0.7dB
0.5dB
0.35dB
0 2 4 6 8 10 12 14 16 18 20 22 24 26 28 30 32 34 36 38 40 42 44 46 48 50
Frequency (GHz)

ENSURING RFFE SIGNAL INTEGRITY

CMOS on RF-SOI substrates enables high performance switches with excellent isolation and low insertion loss.[5] For example, a true wireless stereo earbud uses an RF-SOI switch to suppress parasitic signals, improving audio quality while reducing power consumption and extending range.

Interference is a common challenge in dense RF environments. Third-order intermodulation (IMD3) can arise from harmonic mixing of nearby cellular and Wi-Fi frequencies or between power management ICs and transmission signals. These interferences can compromise reception. ***Figure 4*** shows an example of these interferences at 5.8 GHz.

Soitec's trap-rich RF-SOI substrates (RFeSI™) minimize harmonic distortions such as HD2, HD3 and IMD3 wherever they may appear in the RFFE.[6,7] Compared to high-resistivity SOI (HR-SOI), these engineered substrates further suppress signal distortion, as shown in ***Figure 5***, where:

- RFeSI™: Soitec's RF enhanced signal integrity trap-rich RF-SOI substrate
- RFeSI90: RFeSI™ with CPW HD2 below -90 dBm at 15 dBm power
- RFeSI80: RFeSI™ with CPW HD2 below -80 dBm at 15 dBm power
- RFeSI lite: RFeSI™ for IoT "lite" complexity
- HR-SOI: High resisitivity non-trap-rich SOI substrate.

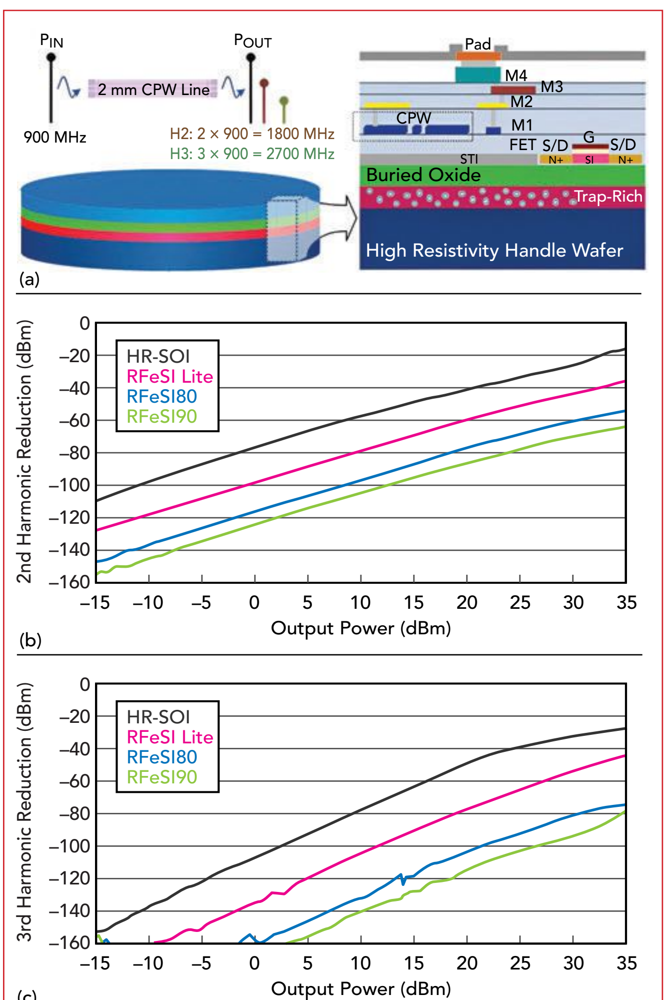

▲ Fig. 5 **(a) CPW on an RFeSI™ and its measured (b) HD2 and (c) HD3 on different substrates.**

MITIGATING COUPLED-NOISE INTERFERERS

Internal crosstalk (e.g., clocks or digital control) and external noise (e.g., motors, lightning, industrial equipment) often impact IoT devices. ***Figure 6*** demonstrates the various interference paths and the effectiveness of Soitec's substrates in reducing crosstalk. RFeSI™ substrates consistently outperform HR-SOI in suppressing noise across a wide frequency spectrum, improving system robustness.

Figure 7 demonstrates the reduction of digital noise across different Soitec RF-SOI substrates. The plots show that using RFeSI™ leads to a cleaner RF signal.

ENHANCED RF ACOUSTIC FILTERS

RF filters such as surface acoustic wave (SAW) and bulk acoustic wave (BAW) types are key to performance

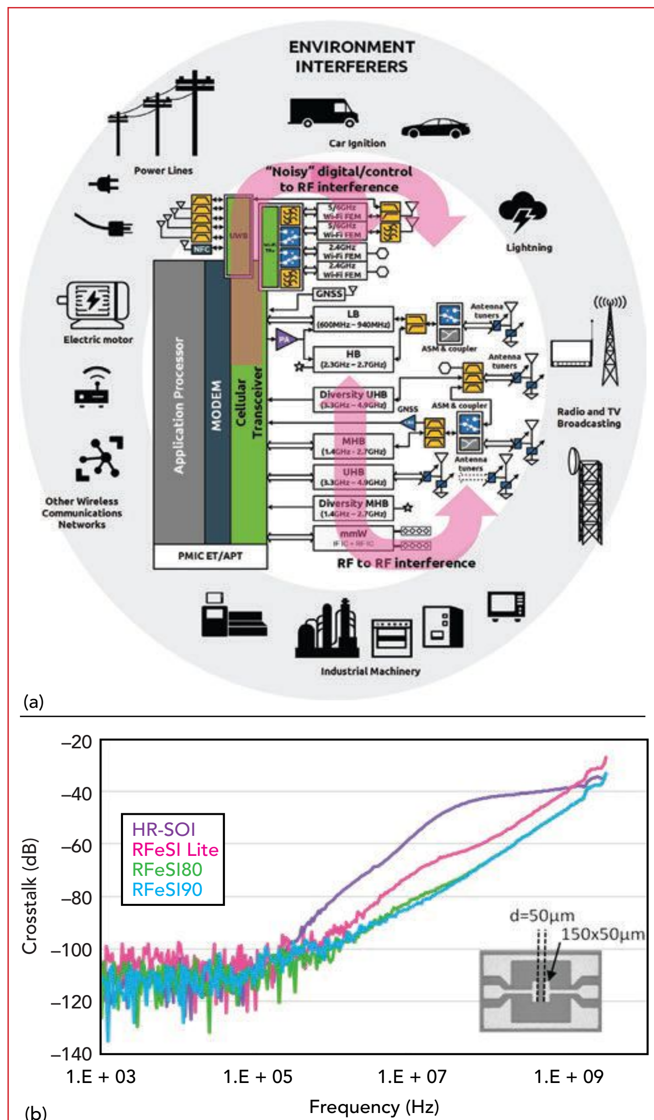

▲ Fig. 6 **(a) IoT device's coupled-noise and (b) Soitec's RF-SOI substrates crosstalk comparison.**

High Density Without Compromise!

- Test & Measurement
- Broadcast
- Medical

Learn More

High Density Enhances Efficiency with Improved Performance

Step into the next generation of RF performance and high density with the new PX and PRX connector families. Designed as a superior alternative to traditional coax connectors or as an upgrade for existing multi-pin solutions, these advanced connectors offer exceptional performance and scalability, available in configurations ranging from 13 to 53 pins.

Impedance	Frequency	Housing Contact #	Contact Size	Cable Types
50 Ohm	100 MHz to 67 GHz	13, 26, 28, 53	16	RG-178, 316, 405, M17/151(.047")
75 Ohm	100 MHz to 18 GHz	13, 23, 48	12	RG-179, SS75086

The PHOENIX Company of Chicago™

Leading Blindmate Microwave Contact Technology in mobile and IoT devices. Traditional SAW filters on bulk piezoelectric wafers suffer from significant signal leakage.

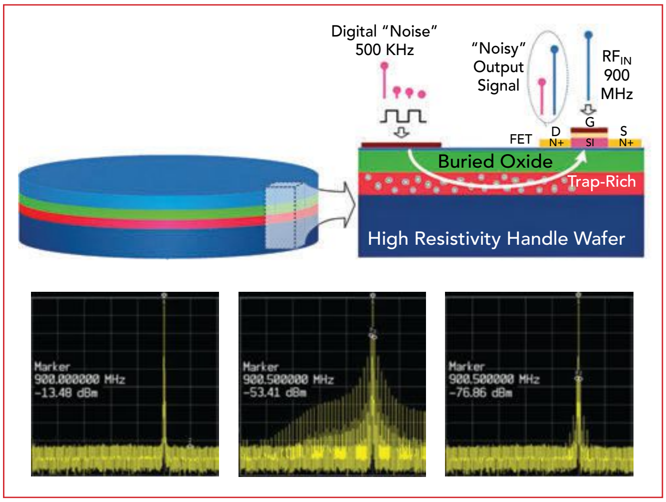

Fig. 7 Digital noise reduction of Soitec RF-SOI substrates.

Soitec's POI substrates confine acoustic energy both vertically and horizontally, as shown in ***Figure 8***. The POI layer stack also allows for thermal drift compensation without requiring extra processing steps. Filters on POI substrates support advanced configurations such as single-die multiplexers and antennaplexers,[8] enabling compact, efficient designs. Figure 8 illustrates the SAW on POI technology benchmark compared to other technologies, based on parameters including electromechanical coupling coefficient (K^2), quality factor (Q), phase velocity (v), thermal compensation factor (TCF) and power handling.

SAW on POI stands out as the most efficient solution among the technologies considered, offering an improved quality factor, TCF and coupling coefficient.

LOWERING RFFE POWER CONSUMPTION

A typical IoT device transmitter path can lose around 2.3 dB due to Tx path component insertion losses, as

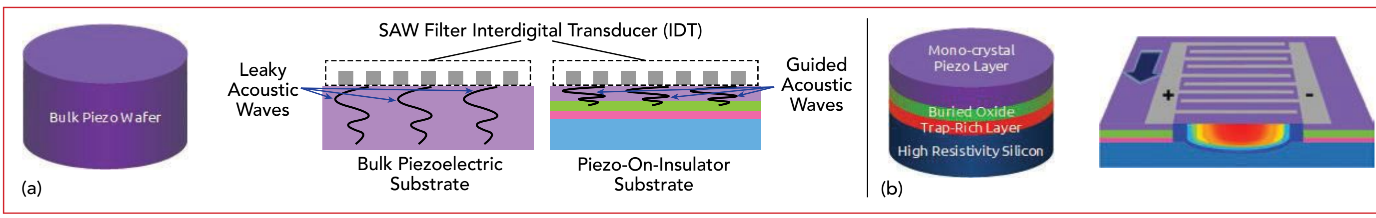

Fig. 8 SAW filters' (a) RF signal losses due to (b) confining acoustic energy.

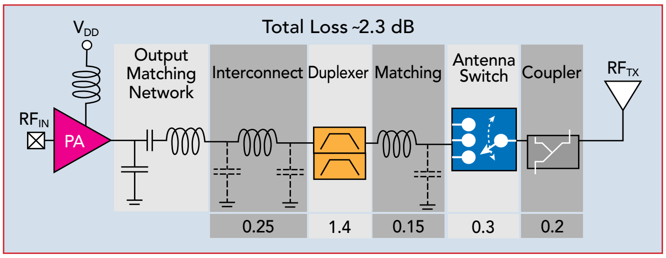

Fig. 9 4G/5G IoT transmitter path power loss budget.

shown in ***Figure 9***. Innovations in RF-SOI foundry processes and engineered substrates have reduced these losses by lowering transistor insertion loss (lower R_{ON}) and increasing its isolation (lower C_{OFF}), both without sacrificing power handling capabilities.[9,10]

The dense integration capabilities of CMOS on RF-SOI and SAW on POI enable direct matching between filters, switches and PAs/LNAs. This can reduce signal loss by up to 0.5 dB.[11]

INTEGRATION WITH FD-SOI

FD-SOI enables the co-integration of high performance transistors with low leakage and/or low power consumption, albeit lower performance transistors. This co-integration is achieved through CMOS processing, Soitec's FD-SOI substrates and body biasing techniques.[12] Through dynamic body biasing, FD-SOI can adapt threshold voltages to balance performance and power needs in real time.

Soitec's FD-SOI substrates support wider body-bias voltage ranges thanks to their ultra-thin buried oxide (BOX) layers, offering greater control over power consumption and system performance, as demonstrated in ***Figure 10***. Figure 10a shows a planar FET designed on a bulk substrate and Figure 10b shows that the Vth tuning capability is extended due to the use of body biasing enabled by using the FD-SOI substrate shown in Figure 10c. Figure 10b illustrates the threshold tuning range, with Vbias denoting the applied body-bias voltage and Vth representing the

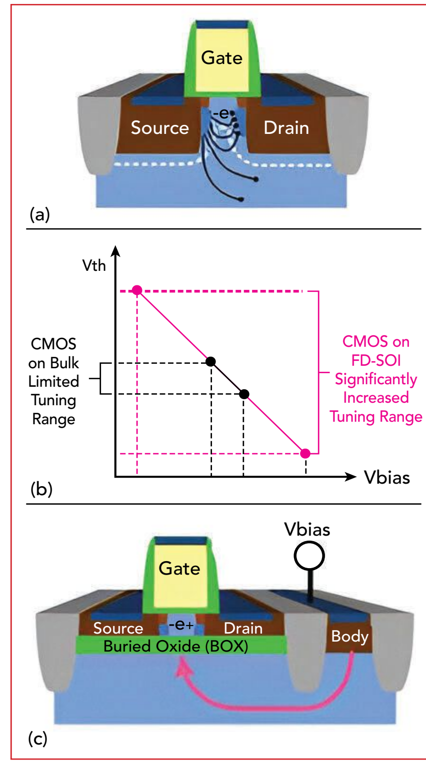

Fig. 10 Planar FET designed (a) on a bulk substrate with (b) Vth tuning capability increased by using (c) an FD-SOI substrate.

RF-LAMBDA

MADE IN USA

THE LEADER OF RF BROADBAND SOLUTIONS

EMC Broadband RF Power Amplifier

High Power Solid State

HUNDREDS IN STOCK

FAST SHIPPING

FREQUENCY UP TO 90GHZ

POWER UP TO 2KW CW

BENCHTOP AND RACKMOUNT

REMC06G18GG 6-18GHZ 400W

- AUTOMATIC BUILT IN SELF CALIBRATION AND BIAS ADJUSTMENT.
- OVER TEMPERATURE, CURRENT, INPUT POWER PROTECTION.
- VSWR MEASUREMENT AND OPEN CIRCUIT PROTECTION.
- USER FRIENDLY CONTROL INTERFACE.
- REMOTE ETHERNET CONTROL AND FIRMWARE UPDATE.
- HIGH POWER EFFICIENCY AND LIGHTWEIGHT.

RAMP42G47GA 42-47GHZ 8W

REMC02G06GE 2-6GHZ 500W

RAMP18G40GB-U 18-40G 20W

RAMP05M80GC 0.5-80GHZ

REMC18G40GQ 18-40GHZ 200W CW

resulting threshold voltage of the MOSFET.

Thanks to its compatibility with CMOS nodes down to 7 nm,[13] FD-SOI also enables integration of RFFE, analog/mixed-signal, memory and digital logic on one or a few dies, delivering significant area and power savings.

FD-SOI technology enhances performance in key RF blocks. PAs on FD-SOI offer 5 to 10 percent better power-added efficiency (PAE) than those on CMOS bulk, particularly above a few GHz.[14] Similarly, LNAs benefit from reduced parasitics and better linearity, resulting in lower noise figures and improved signal reception in crowded RF environments.

CONCLUSION

The complementary use of CMOS on RF-SOI, CMOS on FD-SOI and SAW on POI substrates addresses the most pressing RFFE challenges in IoT: interference, power efficiency, integration and performance. Each technology contributes to a modular, scalable and robust design framework adaptable to evolving IoT use cases. ■

References

1. A. R. Prasad and S. Dixit, "Wireless World in 2050 and Beyond: A Window into the Future!" *Springer Series in Wireless Technology*, Springer, Cham, July 2016.
2. 3rd Generation Partnership Project, "Technical Specification Group Radio Access Network; Study on support of reduced capability NR devices," *Mars*, Release 17, 2023.
3. C. Hetting, "Non-linear FEM technology critical for optimized Wi-Fi 6E, Wi-Fi 7 designs & performance, says Qorvo," January 2024, Web: https://wifinowglobal.com/news-and-blog/non-linear-fem-technology-critical-for-optimised-wi-fi-6e-wi-fi-7-designs-performance-says-qorvo-2/.
4. M. Kato et al., "Digital Envelope Tracking Benefits for 5G, 6G, and Wi-Fi 7 Mobile Devices," *2023 Asia-Pacific Microwave Conference (APMC)*, Taipei, Taiwan, 2023, pp. 673–675.
5. L. Andia, "System Technology Co-Optimization for High Performance RF and mmWave Front Ends," Workshop, *2023 Asia-Pacific Microwave Conference (APMC)*, Taipei, Taiwan, 2023.
6. L. Andia, Y. Morandini and J-M. Le Meil, "RF-SOI Engineered Substrates at the Heart of Modern RF & mmW Front-ends - Part 1: 5G," *Soitec*, Whitepaper, November 2020.
7. L. Andia, Y. Morandini and J-M. Le Meil, "RF-SOI Engineered Substrates at the Heart of Modern RF & mmW Front-ends - Part 2: Wi-Fi," *Soitec*, Whitepaper, February 2021.
8. "Qualcomm Thin-Film SAW Filter Technology in Diversity Module," *Yole Group*, February 2022.
9. J. Costa, "RFSOI Enabling the RF Mobile Front-End History, Future and Challenges," *semi International RF-SOI Workshop*, Shanghai, China, September 2018.
10. M. Jaffe et al., "Advances in SOI Technologies for RF and mmWave Applications," *IEEE Radio Wireless Week (RWW)*, Orlando, Fla., U.S., 2019.
11. D. Schnaufer, "Power Class 2: What You Need to Know," *Qorvo*, March 2017, Web: https://www.qorvo.com/design-hub/blog/power-class-2-what-you-need-to-know.
12. "Enabling Artificial Intelligence with Engineered Substrates," *Soitec*, January 2024, Web: https://www.soitec.com/docs/default-source/financial-reports/2024-2025/en/soitec-ai---dec-2024.pdf?Status=Master&sfvrsn=c906d0d0_1.
13. "FD-SOI Next Generation 10-7 nm," *CEA-Leti*, June 2022, Web: https://www.leti-cea.fr/cea-tech/leti/Documents/d%C3%A9monstrateurs/Flyer_FD-SOI_num.pdf.
14. W. Hua et al., "Power Amplifiers Performance Survey 2000-Present," *ETH*, September 2024, Web: https://ideas.ethz.ch/Surveys/pa-survey.html.

RF Amplifiers and Sub-Assemblies for Every Application

Delivery from Stock to 2 Weeks ARO from the catalog or built to your specifications!

- Competitive Pricing & Fast Delivery
- Military Reliability & Qualification
- Various Options: Temperature Compensation, Input Limiter Protection, Detectors/TTL & More
- Unconditionally Stable (100% tested)

ISO 9001:2000 and AS9100B CERTIFIED

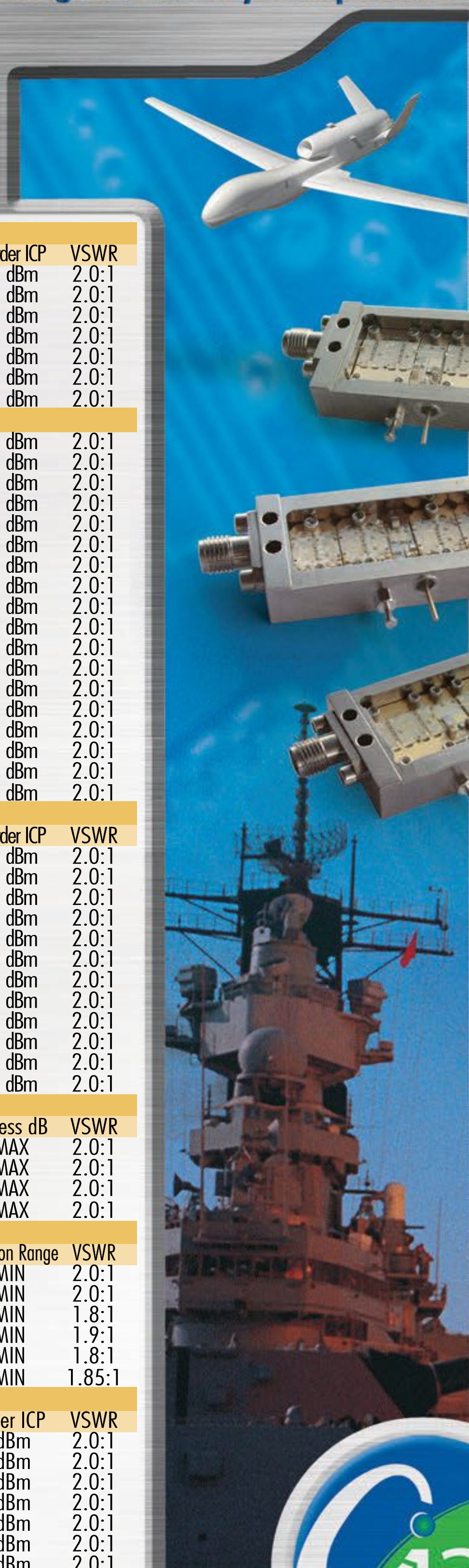

OCTAVE BAND LOW NOISE AMPLIFIERS

Model No.	Freq (GHz)	Gain (dB) MIN	Noise Figure (dB)	Power-out @ P1-dB	3rd Order ICP	VSWR
CA01-2110	0.5-1.0	28	1.0 MAX, 0.7 TYP	+10 MIN	+20 dBm	2.0:1
CA12-2110	1.0-2.0	30	1.0 MAX, 0.7 TYP	+10 MIN	+20 dBm	2.0:1
CA24-2111	2.0-4.0	29	1.1 MAX, 0.95 TYP	+10 MIN	+20 dBm	2.0:1
CA48-2111	4.0-8.0	29	1.3 MAX, 1.0 TYP	+10 MIN	+20 dBm	2.0:1
CA812-3111	8.0-12.0	27	1.6 MAX, 1.4 TYP	+10 MIN	+20 dBm	2.0:1
CA1218-4111	12.0-18.0	25	1.9 MAX, 1.7 TYP	+10 MIN	+20 dBm	2.0:1
CA1826-2110	18.0-26.5	32	3.0 MAX, 2.5 TYP	+10 MIN	+20 dBm	2.0:1

NARROW BAND LOW NOISE AND MEDIUM POWER AMPLIFIERS

Model No.	Freq (GHz)	Gain (dB) MIN	Noise Figure (dB)	Power-out @ P1-dB	3rd Order ICP	VSWR
CA01-2111	0.4 - 0.5	28	0.6 MAX, 0.4 TYP	+10 MIN	+20 dBm	2.0:1
CA01-2113	0.8 - 1.0	28	0.6 MAX, 0.4 TYP	+10 MIN	+20 dBm	2.0:1
CA12-3117	1.2 - 1.6	25	0.6 MAX, 0.4 TYP	+10 MIN	+20 dBm	2.0:1
CA23-3111	2.2 - 2.4	30	0.6 MAX, 0.45 TYP	+10 MIN	+20 dBm	2.0:1
CA23-3116	2.7 - 2.9	29	0.7 MAX, 0.5 TYP	+10 MIN	+20 dBm	2.0:1
CA34-2110	3.7 - 4.2	28	1.0 MAX, 0.5 TYP	+10 MIN	+20 dBm	2.0:1
CA56-3110	5.4 - 5.9	40	1.0 MAX, 0.5 TYP	+10 MIN	+20 dBm	2.0:1
CA78-4110	7.25 - 7.75	32	1.2 MAX, 1.0 TYP	+10 MIN	+20 dBm	2.0:1
CA910-3110	9.0 - 10.6	25	1.4 MAX, 1.2 TYP	+10 MIN	+20 dBm	2.0:1
CA1315-3110	13.75 - 15.4	25	1.6 MAX, 1.4 TYP	+10 MIN	+20 dBm	2.0:1
CA12-3114	1.35 - 1.85	30	4.0 MAX, 3.0 TYP	+33 MIN	+41 dBm	2.0:1
CA34-6116	3.1 - 3.5	40	4.5 MAX, 3.5 TYP	+35 MIN	+43 dBm	2.0:1
CA56-5114	5.9 - 6.4	30	5.0 MAX, 4.0 TYP	+30 MIN	+40 dBm	2.0:1
CA812-6115	8.0 - 12.0	30	4.5 MAX, 3.5 TYP	+30 MIN	+40 dBm	2.0:1
CA812-6116	8.0 - 12.0	30	5.0 MAX, 4.0 TYP	+33 MIN	+41 dBm	2.0:1
CA1213-7110	12.2 - 13.25	28	6.0 MAX, 5.5 TYP	+33 MIN	+42 dBm	2.0:1
CA1415-7110	14.0 - 15.0	30	5.0 MAX, 4.0 TYP	+30 MIN	+40 dBm	2.0:1
CA1722-4110	17.0 - 22.0	25	3.5 MAX, 2.8 TYP	+21 MIN	+31 dBm	2.0:1

ULTRA-BROADBAND & MULTI-OCTAVE BAND AMPLIFIERS

Model No.	Freq (GHz)	Gain (dB) MIN	Noise Figure (dB)	Power-out @ P1-dB	3rd Order ICP	VSWR
CA0102-3111	0.1-2.0	28	1.6 Max, 1.2 TYP	+10 MIN	+20 dBm	2.0:1
CA0106-3111	0.1-6.0	28	1.9 Max, 1.5 TYP	+10 MIN	+20 dBm	2.0:1
CA0108-3110	0.1-8.0	26	2.2 Max, 1.8 TYP	+10 MIN	+20 dBm	2.0:1
CA0108-4112	0.1-8.0	32	3.0 MAX, 1.8 TYP	+22 MIN	+32 dBm	2.0:1
CA02-3112	0.5-2.0	36	4.5 MAX, 2.5 TYP	+30 MIN	+40 dBm	2.0:1
CA26-3110	2.0-6.0	26	2.0 MAX, 1.5 TYP	+10 MIN	+20 dBm	2.0:1
CA26-4114	2.0-6.0	22	5.0 MAX, 3.5 TYP	+30 MIN	+40 dBm	2.0:1
CA618-4112	6.0-18.0	25	5.0 MAX, 3.5 TYP	+23 MIN	+33 dBm	2.0:1
CA618-6114	6.0-18.0	35	5.0 MAX, 3.5 TYP	+30 MIN	+40 dBm	2.0:1
CA218-4116	2.0-18.0	30	3.5 MAX, 2.8 TYP	+10 MIN	+20 dBm	2.0:1
CA218-4110	2.0-18.0	30	5.0 MAX, 3.5 TYP	+20 MIN	+30 dBm	2.0:1
CA218-4112	2.0-18.0	29	5.0 MAX, 3.5 TYP	+24 MIN	+34 dBm	2.0:1

LIMITING AMPLIFIERS

Model No.	Freq (GHz)	Input Dynamic Range	Output Power Range Psat	Power Flatness dB	VSWR
CLA24-4001	2.0 - 4.0	-28 to +10 dBm	+7 to +11 dBm	+/- 1.5 MAX	2.0:1
CLA26-8001	2.0 - 6.0	-50 to +20 dBm	+14 to +18 dBm	+/- 1.5 MAX	2.0:1
CLA712-5001	7.0 - 12.4	-21 to +10 dBm	+14 to +19 dBm	+/- 1.5 MAX	2.0:1
CLA618-1201	6.0 - 18.0	-50 to +20 dBm	+14 to +19 dBm	+/- 1.5 MAX	2.0:1

AMPLIFIERS WITH INTEGRATED GAIN ATTENUATION

Model No.	Freq (GHz)	Gain (dB) MIN	Noise Figure (dB)	Power-out @ P1-dB	Gain Attenuation Range	VSWR
CA001-2511A	0.025-0.150	21	5.0 MAX, 3.5 TYP	+12 MIN	30 dB MIN	2.0:1
CA05-3110A	0.5-5.5	23	2.5 MAX, 1.5 TYP	+18 MIN	20 dB MIN	2.0:1
CA56-3110A	5.85-6.425	28	2.5 MAX, 1.5 TYP	+16 MIN	22 dB MIN	1.8:1
CA612-4110A	6.0-12.0	24	2.5 MAX, 1.5 TYP	+12 MIN	15 dB MIN	1.9:1
CA1315-4110A	13.75-15.4	25	2.2 MAX, 1.6 TYP	+16 MIN	20 dB MIN	1.8:1
CA1518-4110A	15.0-18.0	30	3.0 MAX, 2.0 TYP	+18 MIN	20 dB MIN	1.85:1

LOW FREQUENCY AMPLIFIERS

Model No.	Freq (GHz)	Gain (dB) MIN	Noise Figure dB	Power-out @ P1-dB	3rd Order ICP	VSWR
CA001-2110	0.01-0.10	18	4.0 MAX, 2.2 TYP	+10 MIN	+20 dBm	2.0:1
CA001-2211	0.04-0.15	24	3.5 MAX, 2.2 TYP	+13 MIN	+23 dBm	2.0:1
CA001-2215	0.04-0.15	23	4.0 MAX, 2.2 TYP	+23 MIN	+33 dBm	2.0:1
CA001-3113	0.01-1.0	28	4.0 MAX, 2.8 TYP	+17 MIN	+27 dBm	2.0:1
CA002-3114	0.01-2.0	27	4.0 MAX, 2.8 TYP	+20 MIN	+30 dBm	2.0:1
CA003-3116	0.01-3.0	18	4.0 MAX, 2.8 TYP	+25 MIN	+35 dBm	2.0:1
CA004-3112	0.01-4.0	32	4.0 MAX, 2.8 TYP	+15 MIN	+25 dBm	2.0:1

CIAO Wireless can easily modify any of its standard models to meet your "exact" requirements at the Catalog Pricing.

Visit our web site at www.ciaowireless.com for our complete product offering.

Ciao Wireless, Inc. 4000 Via Pescador, Camarillo, CA 93012
Tel (805) 389-3224 Fax (805) 389-3629 sales@ciaowireless.com

Big Radar Power for Small Aircraft

Ten minutes into the test flight, it was time to see what the new radar could do.

A member of the mission crew pressed the button and pilot Rob Swaringen glanced at the display. While he's not allowed to describe in detail what he saw on the screen, he made one thing clear: this little, lightweight radar was doing some seriously heavy lifting.

The engineers and program representatives on board couldn't help but sneak into the cockpit for a peek. "It's the first time this thing is flying, and it worked like a champ," said Swaringen, a former F-16 pilot who went by the call sign Houdini.

The test, conducted aboard a modified commercial jet Raytheon uses as a flying test bed, marked an important milestone for the business' new PhantomStrike® radar. The radar puts the power of active electronically scanned array in a package compact and light enough for just about any aircraft — even small UAVs — and, in doing so, opens up a world of capabilities to a rapidly changing fleet.

The PhantomStrike radar is cooled entirely with air pulled straight from the platform. This means fewer lines to run and systems to connect, so installation took only a matter of hours, Swaringen said.

Swaringen, Raytheon's chief test bed pilot, knows firsthand the importance of superior situational awareness in every mission scenario — whether it's in combat with hostile aircraft buzzing from every angle or in a high-stakes test flight. He said technology like PhantomStrike would have come in handy when he was logging hours on the F-16.

"It [shows] 10x what I could see with previous capabilities," he said. "Just having that excellent air picture in your own cockpit — regardless of what's coming across the radio, what's on the link display — to have that in your own ship is a real game changer."

Larry Martin is a senior technology fellow at Raytheon and the technical lead for the PhantomStrike radar. Years ago, he and his team had set out to develop a system like nothing else on the market. Now it was airborne.

"It was the cherry on top to see it work," Martin said. Program teams, working on an accelerated schedule, had done the legwork to install the radar on Raytheon's Multi-Program Testbed aircraft, a Boeing 727 modified to carry, integrate and test sensors and electro-optical/infrared systems. "Once we were integrated on the plane, it was a big relief," he said. "A lot of questions were answered on our initial flights." The result, he said, is a radar that is truly the first of its kind.

PhantomStrike (Source: RTX)

Rafael & Israel MOD: Iron Beam 450 Development Completed

The R&D Unit within the Israel Ministry of Defense (IMOD) Directorate of Defense Research & Development (DDR&D), the Israeli Air Force and Rafael Advanced Defense Systems have successfully completed a series of tests lasting several weeks, demonstrating the capabilities of the Iron Beam high-power laser system, with Elbit Systems serving as a project partner manufacturing the laser source.

The test series, conducted at a facility in southern Israel, concludes the development phase and represents the final milestone before delivering the system to the IDF for operational deployment. The system proved its effectiveness in a complete operational configuration by intercepting rockets, mortars, aircraft and UAVs across a comprehensive range of operational scenarios.

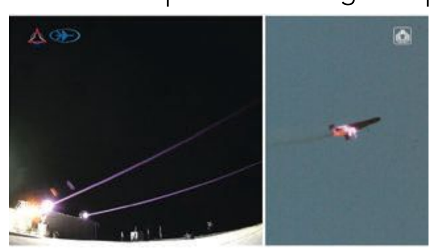

Iron Beam (Source: Rafael)

The successful trials mark a critical milestone toward operational deployment, with the first systems set to be integrated into the IDF air defense arrays by year-end.

Iron Beam is a ground-based high-power laser air defense system designed to counter aerial threats, including rockets, mortars and UAVs. It features an advanced targeting system that enables enhanced operational range, high precision and superior efficiency while maintaining its unique advantage of rapidly neutralizing threats using laser technology at negligible cost. The R&D Unit within the Ministry's DDR&D has spearheaded the system's development, working alongside primary developer Rafael.

The Iron Beam system represents a global technological and engineering breakthrough, expected to integrate into Israel's multi-layered defense array as a complementary capability to the Iron Dome, David's Sling and Arrow air defense systems. The system uses Rafael's unique "adaptive optics" technology, enabling a stable, focused and precise beam.

As announced last May, operational prototypes of Rafael's short-range tactical laser systems have been deployed throughout the current war and have successfully intercepted and defeated dozens of threats. Now that the Iron Beam's performance has been proven, we anticipate a significant leap in air defense capabilities through the deployment of these long-range laser weapon systems.

For More Information Visit mwjournal.com for more defense news.

IMOD Director General, Maj. Gen. (Res.) Amir Baram said, "Today marks the completion of our high-power laser system development — a historic milestone for Israel's defense establishment and defense industries. This is the first time in the world that a high-power laser interception system has reached full operational maturity, completing numerous interceptions across various simulated operational scenarios. The high-power laser system will integrate within Israel's multi-layered defense array, further enhancing multi-layered integration with additional missile interceptors through optimal cost-effectiveness and leveraging relative advantages against threat types, ranges and environmental conditions."

RTX's Collins Aerospace Awarded NATO Contract for Electromagnetic Warfare Command and Control System

Collins Aerospace has been awarded a contract by the NATO Communications and Information Agency to provide its Electronic Warfare Planning and Battle Management (EWPBM) solution to NATO. This integrated software tool is designed to plan, direct, coordinate, synchronize and assess EW activities.

> Provides common operating picture of electronic warfare threats.

The EWPBM solution will deliver a recognized electromagnetic picture, combining data from operations, intelligence systems and other sources, as well as an electronic order of battle, detailing the location and function of electronic devices. This comprehensive overview will enhance the understanding of both friendly and enemy EW capabilities.

EWPBM advances traditional battle management by incorporating situational awareness of the electromagnetic environment, aiding commanders in navigating complex multi-domain warfare. The software solution creates an electromagnetic operating picture, manages EW tactics, processes data for action plans and monitors sensors and jammers.

Collins Aerospace will collaborate closely with NATO to rigorously test, validate and integrate the system, significantly boosting NATO's EW capabilities and contributing to the collective defense and security of member nations.


Reactel, Inc.
Reacting First to All Your Filter Needs.
Filter Solutions For Mission Critical Applications
High Performance, Rugged Packaging, Small Size and Weight
Great things *can* come in small packages. Reactel filters are ideally suited for the demanding environments that unmanned vehicles encounter.
Many manufacturers rely on Reactel to provide units which are:
High performance - Lightweight - Low profile
Contact a Reactel engineer with your filter or multiplexer requirements. We can create a unit which will be the perfect fit for your applications.
REACTEL, INC.
RF & Microwave Filters - Multiplexers - Multifunction Assemblies
REACTEL, INC.
REACTEL, INC.
REACTEL, INC.
8031 Cessna Avenue • Gaithersburg, Maryland 20879 • (301) 519-3660 • reactel@reactel.com • reactel.com
Intertek
RoHS
MADE IN MD
Since 1979

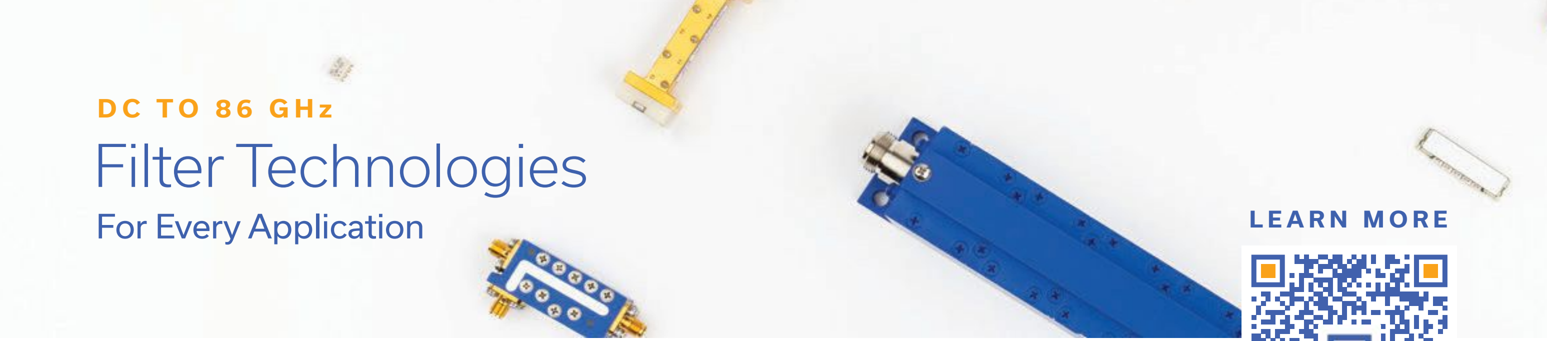

DC TO 86 GHz

Filter Technologies

For Every Application

LEARN MORE

CAVITY

- Passbands to 43.5 GHz
- Stopbands to 57 GHz
- Bandwidths as narrow as 1%
- 100+ dB rejection

CERAMIC RESONATOR

- Fractional bandwidths from 0.5 to 40%
- Excellent power handling, up to 20W
- High Q in miniature SMT package

LUMPED L-C

- Wide catalog selection
- Several package options including aqueous washable
- Variety of filter topologies

LTCC

- Tiny size, as small as 0202
- Industry's widest selection of mmWave LTCC filters
- Proprietary designs with stopband rejection up to 100 dB

MICROSTRIP

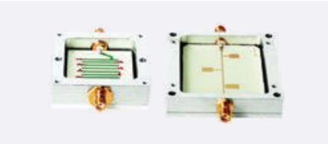

- Connectorized designs with 4 to 40% fractional bandwidth
- Power handling up to 10W
- Flat group delay

MMIC REFLECTIONLESS

- Patented topology absorbs and internally terminates stopband signals
- Perfect for pairing with amplifiers, mixers, multipliers, ADC/DACs & more

RECTANGULAR WAVEGUIDE

- WR-12, WR-15 and WR-28 interfaces
- Passbands up to 87 GHz
- High stopband rejection, 40 dB

SUSPENDED SUBSTRATE

- Ultra-wide passbands up to 26 GHz
- Wide stopbands up to 40 GHz
- High Q

THIN FILM ON ALUMINA

- Passbands from DC to 40 GHz
- High rejection with wide passband
- Miniature SMT package

Mini-Circuits®

RF Front-End Modules for Mobile

The RF front-end market is undergoing a massive transformation, says Yole Group in its new report, "RF Front-End Module for Mobile 2025." The RF front-end module market for mobile devices is at a critical juncture. Valued at $15.4 billion in 2024, the market is characterized by a delicate balance of growth drivers, including continued 5G expansion and new 5G bands and headwinds such as architectural simplification, intense cost pressure and declining ASPs. Yole Group forecasts that despite a flat trend through 2027, the market will reach over $17 billion by 2030.

The RF front-end module market is entering a new era of competition. Many Chinese OEMs and suppliers are no longer followers. They are now setting the pace, driving innovation with an expanding domestic ecosystem of foundries and IDMs and technological capabilities. This rising pressure is forcing historical leaders to adapt quickly, streamline their architectures and protect their market shares.

Chinese OEMs are the engine of this transformation. In 2024, the Chinese smartphone market grew by 6 percent year-on-year, fueled by surging demand and AI-driven innovation. Huawei's comeback has been spectacular, posting 25 percent year-over-year growth and reclaiming the premium segment, while Vivo captured the number one spot with a 17 percent share. Xiaomi, Oppo and Honor maintained solid positions with 15 percent each, creating a highly competitive domestic landscape.

These market dynamics have empowered Chinese RF suppliers to propose innovative solutions and develop a vertically integrated supply chain, particularly at the filter level and including SAW and BAW. This ecosystem is supported by government incentives and positions Chinese players to challenge long-established suppliers. Filters are the second-largest RF front-end market segment, and despite the rise of SiP modules, some applications still require discrete filters, creating a strong opportunity to assess BAW technologies across players, applications and costs.

> How Chinese OEMs are driving innovation and disruption

Traditional leaders such as Qualcomm, Broadcom, Qorvo, Skyworks and Murata still control over 70 percent of the global market but are facing increasing competition. Qualcomm leads with a 21 percent share, thanks to its end-to-end platform strategy, followed by Broadcom with 18 percent, due to its FBAR filter solutions for Apple. Pricing pressure and Chinese OEM preferences are reshaping design wins and margins.

For example, one Chinese player, Maxscend, leads among Chinese suppliers with a 4 percent share, dominating in discrete devices and growing its module business through vertical filter integration. Other Chinese companies such as Lansus, Vanchip, OnMicro, SmarterMicro and HiSilicon are also gaining traction, benefiting from Huawei's domestic supply chain realignment and its push to secure local design wins.

The next battlefield will be 6G, starting with 6 GHz band front-end modules and progressing to FR3 modules by the end of the decade. Unlike during the 5G rollout, Chinese companies are expected to enter 6G with full domestic capabilities, supported by strong government backing and an evolving foundry ecosystem — a shift that could redefine the global RFFE market balance.

The release of the "RF Front-End Modules for Mobile 2025" report from Yole Group marks a turning point for the industry. This comprehensive report provides market forecasts, competitive landscape analysis and technology roadmaps, helping industry players anticipate disruptions, prepare for 6G and capture new opportunities in a rapidly evolving ecosystem.

170 NTN Operator-Satellite Partnerships in 80 Countries and Territories, GSA Data Shows

The Global Mobile Suppliers Association (GSA) recently published its most up-to-date report on the global status of "Non-Terrestrial 5G Networks and Satellite Connectivity." By August 2025, there were 170 publicly announced operator-satellite partnerships in 80 countries and territories, with 34 operators in 25 markets having launched commercial services. The report also confirms that Starlink leads the provider landscape with 44 partnerships, followed by AST SpaceMobile and Lynk. In spectrum, Ka-Band remains the most widely used frequency range, supporting both feeder and service links. L- and S-Bands are increasingly important for direct-to-cell applications.

From rural broadband to direct-to-cell, the GSA data confirms satellite connectivity is moving from niche to mainstream. Rural and enterprise broadband remains the dominant application, accounting for half of all partnerships. Satellite-to-cellphone services are expanding quickly, with 12 launches and 24 trials or licensed projects, driven by players like SpaceX, AST SpaceMobile and Lynk, enabling unmodified smartphones to connect in remote areas.

Joe Barrett, president of GSA, commented, "Today there are a limited but growing number of smartphones supporting satellite connectivity. Overall, the findings in the GSA's latest NTN market report point to an evolv-

For More Information Visit mwjournal.com for more commercial market news.

ing landscape where satellite services are moving from niche to mainstream, with strong growth expected in broadband and direct-to-cell offerings, and slower but steady expansion in IoT applications. From spectrum usage to satellite-operator partnerships, our latest report examines how the satellite connectivity landscape is set to evolve in the rest of 2025 and beyond. And in such a dynamic market, access to this latest data can be critical to business planning and success."

Full and unlimited access to the detailed data behind this report is available to all employees of GSA Member and GSA Associate organizations subscribing to the GAMBoD database.

5G Growth Hits 2.6B Connections Worldwide

According to new data from 5G Americas and Omdia, global 5G connections climbed past 2.6 billion in Q2 2025, a 37 percent year-over-year surge, and are projected to reach nearly 9 billion by 2030, representing 60 percent of all wireless connections worldwide.

In parallel, global cellular data consumption grew by 15 percent year-over-year, reaching 384 million TB in Q2 2025, signaling accelerating demand for next-generation connectivity that powers everything from streaming and gaming to smart factories and autonomous vehicles.

North America continues to outpace the globe in 5G adoption and data consumption. As of Q2 2025, the region reached:

- 339 million 5G connections — covering 88 percent of the population and on track to surpass 100 percent coverage before the end of 2025
- 43 million TB of cellular traffic during the quarter, averaging 111 GB per user per month — nearly double the next highest region (Oceania, Eastern and Southeast Asia at 67 GB per user).

Beyond subscriber growth, 5G is fueling the IoT. Global IoT connections hit 3.8 billion in Q2 2025 and are expected to reach 5 billion by 2030. Increasingly, 5G is the backbone for mission-critical applications in:

- Smart factories optimizing production
- Autonomous logistics improving supply chain efficiency
- Energy distribution enabling smarter grids
- Healthcare powering telemedicine and remote monitoring.

Nxbeam

Ku/ Ka/ V/ E-Band Power Amplifier MMICs

Maximized performance for linear power applications

Ku/Ka-Band MMIC Die and Packaged MMICs

MMIC Die:

NPA1020-DE	12.5 - 14.5 GHz	15 W
NPA2020-DE	23.0 - 25.0 GHz	10 W
NPA2001-DE	26.5 - 29.5 GHz	35 W
NPA2002-DE	27.0 - 30.0 GHz	35 W
NPA2003-DE	27.5 - 31.0 GHz	35 W
NPA2004-DE	25.0 - 27.5 GHz	40 W
NPA2030-DE	27.5 - 31.0 GHz	20 W
NPA2040-DE	27.5 - 31.0 GHz	10 W

QFN Packaged MMICs:

NPQ2101-SM	27.5 - 31.0 GHz	5 W
NPQ2103-SM	27.5 - 31.0 GHz	8 W
NPQ2105-SM	27.5 - 31.0 GHz	12 W
NPQ2107-SM	27.5 - 31.0 GHz	17 W

Contact Nxbeam for Flange Packaged Options

V-Band MMICs

MMIC Die:

NPA4000-DE	47.0 - 52.0 GHz	1.5 W
NPA4010-DE	47.0 - 52.0 GHz	3.0 W

E-Band MMICs

MMIC Die:

NPA7000-DE	65.0 - 76.0 GHz	1.0 W

Around the Circuit

Barbara Walsh, Multimedia Staff Editor

IN MEMORIAM

Ronald E. Reedy, a pioneering scientist, visionary entrepreneur and beloved mentor, passed away September 9, 2025, at the age of 77. Ron dedicated his life to advancing science and technology. He graduated from the U.S. Naval Academy at Annapolis, where he cultivated the discipline, service and intellectual rigor that would guide his career. Following his naval service, he earned an MSEE from the Naval Postgraduate School and went on to earn his Ph.D. in Electrical Engineering & Applied Physics from the University of California, San Diego. After working in Point Loma, Calif., at the Naval Ocean Systems Laboratory developing silicon-on-sapphire (SOS) technology for the Navy, Ron co-founded Peregrine Semiconductor. Ron helped revolutionize the semiconductor industry by commercializing advances in SOS and CMOS technology. His leadership as the company's first CEO and later its CTO set the stage for innovations that powered the era of mobile communications. Later, as the founder of Skeyeon, a satellite systems company, he charted a bold path in very low Earth orbit satellites, contributing key patents and technologies that redefined how space systems can operate efficiently and reliably in very low orbits.

MERGERS & ACQUISITIONS

AAR CORP., a provider of aviation services, announced it has acquired **American Distributors Holding Co., LLC (ADI)**, a distributor of components and assemblies, for $146 million in an all-cash transaction funded using the company's existing revolving credit facility. The acquisition immediately expands AAR's new parts distribution activity with new additional product lines and extensive OEM relationships. The business will become part of AAR's Parts Supply segment. Founded in 1983, ADI distributes to a broad set of commercial and defense customers across the aerospace and defense industry.

COLLABORATIONS

Nokia and **Boldyn Networks** have deployed a private 5G network at the Callio FutureMINE site in Pyhäjärvi, Finland, transforming one of Europe's deepest mines into a next-generation testbed for mining innovation. Formerly a fully operational copper mine for over 60 years, Callio now provides a real-world mining environment where technology companies can test and validate their equipment. The private 5G solution designed by Boldyn to scale and adapt to the most demanding environments and delivered by Nokia Modular Private Wireless, provides seamless, high performance connectivity across multiple underground levels and a vast tunnel network stretching several kilometers and reaching depths of up to 1.5 km.

AccelerComm and **Radisys® Corporation** announced that a joint project to support the development of the next generation of non-terrestrial networks has been funded through the U.K. Space Agency's International Bilateral Fund (IBF). This project will tighten the integration of these technologies so that they can be offered as a complete package to satellite manufacturer and operator customers. The IBF supports ambitious partnerships between U.K. organizations and international space entities and this joint project will see the integration of the latest versions of AccelerComm's technology into Radisys' lab in India, providing a valuable resource for joint research and demonstrations to customers and partners around the world.

SWISSto12, together with **Astrum Mobile**, Asia-Pacific's only satellite-to-device (S2D) company, announced a major milestone in the development of the NEASTAR-1 geostationary satellite: the successful completion of the Preliminary Design Review. This marks a key step forward following the program's initial announcement earlier this year. NEASTAR-1 is being developed on SWISSto12's HummingSat platform, a new class of geostationary small satellites, up to 5x more compact than traditional counterparts. Purpose-built for Astrum Mobile, NEASTAR-1 will deliver satellite-to-device broadcasting and datacasting services directly to standard mobile phones and handheld devices across the Asia-Pacific region.

BAE Systems' FAST Labs™ research, development and production organization and the **U.S. Air Force Research Laboratory** have signed a three-year cooperative research and development agreement (CRADA) to advance quantum sensing and networking capabilities. This collaboration aims to refine and integrate cutting-edge technologies into quantum sensors, networks and distributed sensing research in an effort to revolutionize capabilities and enhance future security for defense and civilian applications. Under the CRADA, BAE Systems' FAST Labs will utilize its expertise in developing quantum RF sensors based on Rydberg atoms, which are highly excited atoms suitable for studying quantum mechanics and enabling new technologies. This approach allows for frequency-independent sensing, ideal for integration on smaller platforms.

For More Information

For up-to-date news briefs, visit mwjournal.com

Around the **Circuit**

NEW STARTS

Northrop Grumman's Microelectronics Center is now open for external aerospace and defense companies to access the company's three U.S. government-accredited semiconductor manufacturing facilities. This decision expands the secure production of defense microelectronics on U.S. soil. Northrop Grumman's Microelectronics Center is comprised of three manufacturing facilities — two U.S. government-accredited semiconductor foundries in California and Maryland and an advanced packaging facility in Florida. Northrop Grumman's advanced packaging facility is capable of 100 to 300 mm wafer bumping, probing and dicing, which allows multiple smaller, specialized chips to be combined into a single, more powerful electronics package.

Since its founding in 1989, **Spectrum Instrumentation** has grown from a small development team into a globally recognized manufacturer of PC-based high performance measurement technology. Founder and CEO Gisela Hassler has led the company for 36 years and is now bringing about the next milestone in the company's history. To accommodate the company's steady growth, a state-of-the-art headquarters is being built at the technology industrial park in Ahrensburg near Hamburg, Germany. The foundation stone was laid on September 9, 2025. The new company building will provide Spectrum Instrumentation with the opportunity to continue its steady growth. All company departments, including research and development, production, sales and administration, will have spacious, ultra-modern facilities.

ACHIEVEMENTS

Ericsson has been recognized as a Leader in the 2025 Gartner® Magic Quadrant™ for CSP 5G RAN Infrastructure Solutions, with the highest position on Ability to Execute axis. The report, released on September 10, 2025, gives a market overview of the critical 5G RAN infrastructure capabilities, based on how Gartner experts comprehensively and independently assessed vendors who offer 5G solutions for communications service providers across two indices: Completeness of Vision and Ability to Execute. Around half of the world's mobile 5G traffic outside China is carried over Ericsson-powered networks.

Collins Aerospace, an RTX business, has been awarded a contract by the **NATO Communications and Information Agency** to provide its Electronic Warfare Planning and Battle Management (EWPBM) solution to NATO. This integrated software tool is designed to plan, direct, coordinate, synchronize and assess EW activities. The EWPBM solution will deliver a Recognized Electromagnetic Picture, combining data from operations, intelligence systems and other sources, as well as an Electronic Order of Battle, detailing the location and function of electronic devices. This comprehensive overview will enhance the understanding of both friendly and enemy EW capabilities.

Charter Engineering Inc. has earned the AS9100D certification, joining parent company dB Control and sister companies Paciwave and TTT-Cubed in meeting this internationally-recognized aerospace quality management standard. This milestone underscores Charter Engineering's ongoing commitment to excellence in aerospace and defense manufacturing. AS9100D is the global benchmark for aerospace quality, requiring organizations to meet rigorous criteria in reliability, risk management and continuous improvement. By achieving this certification, Charter Engineering now joins a select group of manufacturers whose processes and quality systems meet the industry's most demanding standards.

CONTRACTS

Blighter has won a follow-on contract from a military customer in Southeast Asia to supply its Blighter B400 series radars for border surveillance. The radars will be installed by Blighter's local systems integration partner onto specialist army vehicles for rapid deployment to border infiltration hotspots. When required, the radars can also be trailer-mounted on a higher mast or dismounted and set up on a tripod for locations that are inaccessible by vehicle. Blighter's ultra-reliable low-power solid-state radars contain no moving parts, so they are easily transportable and can be quickly reconfigured to match the changing patterns and locations of border infiltration.

MBDA has signed a contract with the **National Directorate of Naval Armaments** for the production of the TESEO MK2/E anti-ship missile, which is currently under development for the Italian Navy. The contract covers the supply of new generation TESEO MK2/E anti-ship missiles, which will equip new units of the Italian Navy. This includes the FREMM EVO class frigates, the MPCS/PPA (Multi-Purpose Combat Ship/Pattugliatori Polivalenti d'Altura) and the new generation DDX destroyers. The missile will also complement the previous MK2/A version, which is already in-service on the FREMM and Horizon class naval units.

PEOPLE

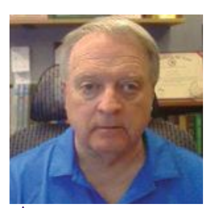

▲ *Richard L. Powers*

Aerospace BD announced the appointment of **Richard L. Powers** of Wakefield, N.H., as its chief technology officer. His first action in this new role was published in the *Microwave Journal* September Military Supplement discussing "Countering High Frequency Surface Wave Radar." Powers considers himself privileged to have the opportunity to support the warfighter, working with brilliant and dedicated industrial and government colleagues over the past 47 years. He earned his B.S.E.E. from the University of Lowell in 1978 and M.S.E.E. from Northeastern University in 1984. He joined Sanders Associates in Nashua, N.H., in 1978 as an antenna and microwave engineer.

SMASHING
Performance BARRIERS
ADM 0001
ADM 0002
ADM 0003
ADM 0004
ADM 0005

Around the **Circuit**

▲ *Jingya Huang*

With its commitment to innovation and growth through employee development, **Indium Corporation** announced the promotion of **Jingya Huang** to senior manager of Marketing Communications, to continue to lead the company's branding and promotional efforts. In her new role, Huang is responsible for the strategic direction of Indium Corporation's global marketing communications initiatives, focusing on innovation and maximizing impact in markets worldwide. She will continue to lead the Marketing Communications team with an emphasis on fostering innovation, ownership and collaboration. Huang will also provide strategic support to other internal teams and lead high-priority special projects that advance the company's mission and global presence.

▲ *Alberto Gironi*

EMIS, an electromagnetic interference (EMI) and electromagnetic compatibility (EMC) solutions company, has appointed **Alberto Gironi** as business development manager for Southern Europe. The appointment reflects EMIS' commitment to strengthening OEM sales and expanding its distributor network to deliver advanced EMC solutions across the region. With over 30 years of industry experience, Gironi brings deep expertise in passive electronic components, EMC compliance and power quality. His background includes senior positions with global EMC component suppliers and collaborations with OEMs, distributors and certification bodies. Gironi has supported clients in industrial automation, electric vehicle (EV) charging, medical equipment, robotics and energy management, giving him strong insight into high-growth markets.

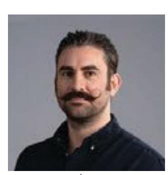

▲ *Yiannis Metallinos*

▲ *Gary Langridge*

Intelliconnect (Europe) has strengthened its senior leadership team with the appointment of **Yiannis Metallinos** as managing director and **Gary Langridge** as engineering manager. Intelliconnect is a market-leading provider of interconnects, cable assemblies and subsystems for applications in RF, microwave, defence, space, medical, test and measurement, education, research, quantum computing and other emerging low-temperature computing markets. Metallinos brings extensive leadership and operational experience gained across PE, private and PLC environments, spanning industries including electronics, precision engineering, FMCG, EV, automotive and marine. Langridge offers over 30 years of engineering and product development experience. His career spans industries where technical innovation must balance with cost, quality and time-to-market.

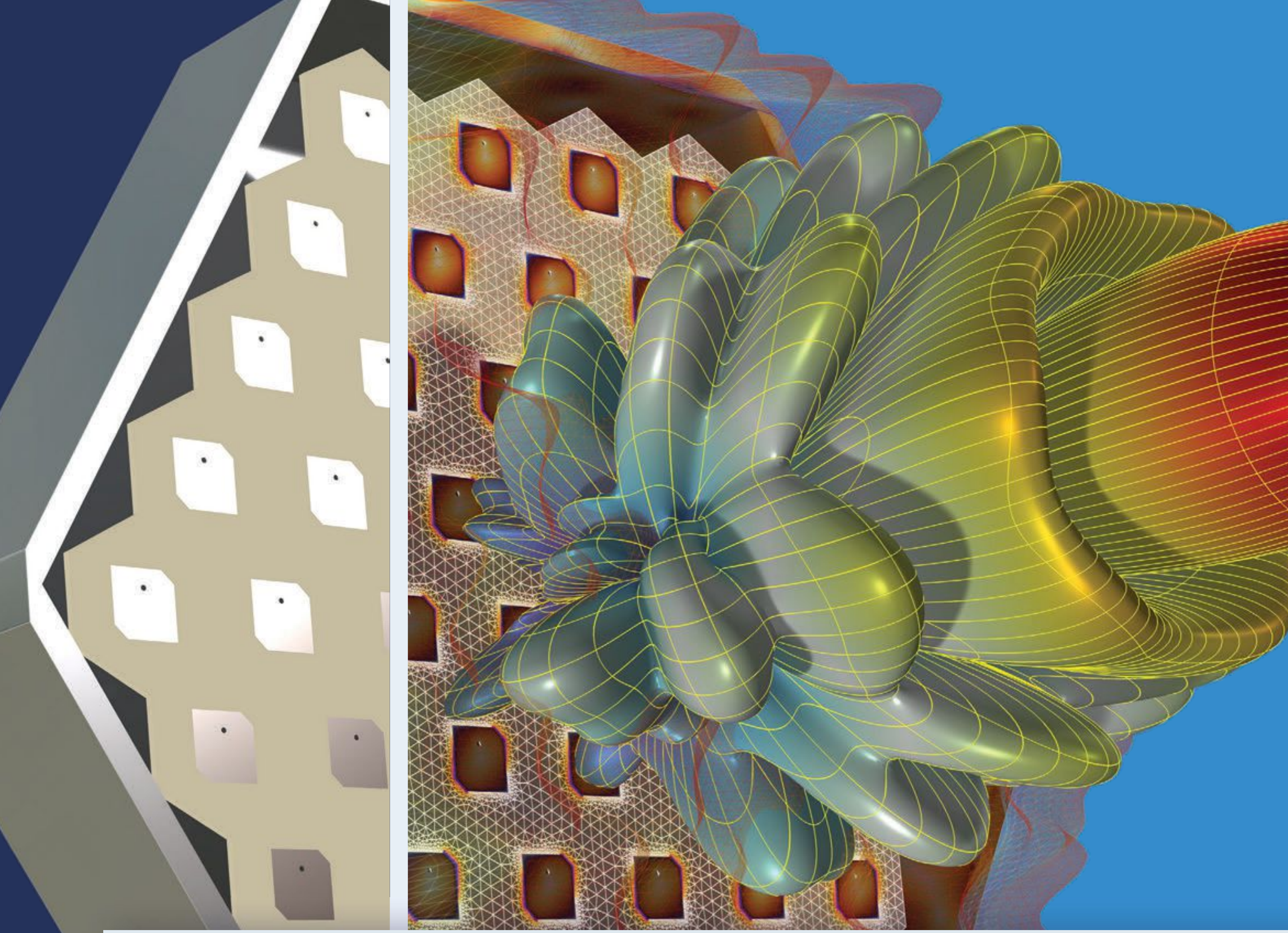

A Compact Single-Fed Wideband Circularly Polarized Patch Antenna

Lingbu Kong, Hui Zhang, Yi-Bo Wang, Jin-Ju Zhang, Guo-Ren Li, Zhi-Zhong Jiang, Xue Li and Sheng-Qing Li
School of Electronic Science and Engineering, Hunan University of Information Technology, China

A single-feed patch antenna with circular polarization (CP) and slot loading is introduced, featuring an I-shaped slot etched on the radiating patch, which introduces mutually orthogonal modes. A crossed slot on the ground plane, coupled with an annular ring microstrip feed line, forms the feed structure. This mechanism simultaneously excites two orthogonal modes with a 90-degree phase difference, resulting in CP radiation. Measurements demonstrate a 25.56 percent 3 dB axial ratio bandwidth and a 32.5 percent 10 dB impedance bandwidth. Gain reaches 9.2 dBi at 3.58 GHz. The antenna's size is 0.84 × 0.65 × 0.067 λ_o^3 with λ_o defined as the wavelength at 3.48 GHz.

Due to its compact size and simple structure, the patch antenna is commonly used in various wireless communication systems, such as satellite and aviation communications.[1-3] Conventional design methods for CP patch antennas typically achieve an operational bandwidth of only around 0.7 percent, which limits their use in practical applications.[4]

To broaden the operational bandwidth, parasitic components or etched slots are incorporated into the antenna structure.[5-9] Wu et al.[5] proposed a CP patch antenna using a capacitively coupled feed and four parasitic strips, resulting in an enhanced axial ratio bandwidth (ARBW). Ding et al.[6] employed parasitic elements and a feed ring placed on the same plane, achieving a broad ARBW. Lin and Chu[7] significantly improved antenna ARBW from 1.3 to 3.3 percent by incorporating parasitic structures. Hao et al.[8] generated CP in a single-feed antenna through an etched slot on the patch, yielding a 5.4 percent ARBW. Wang et al.[9] used a ground plane with four slots, which further extended the ARBW compared to a fully grounded plane.[6]

CP can be achieved with power dividers.[10,11] Chen et al.[10] used a power divider to extend the ARBW of a patch antenna, yielding an impedance bandwidth of approximately 10.6 percent (from 870 to 967 MHz) and an ARBW of about 6 percent (from 893 to 948 MHz). Despite the improved bandwidth, however, the antenna was relatively large (220 × 220 × 14 mm^3). Kim and Kim[11] used a ring structure to achieve a 90-degree phase shift and employed a Gysel power divider, resulting in 71.7 percent impedance bandwidth and 29.7 percent ARBW. A metal reflector was placed underneath the antenna to enhance its overall gain; however, using a thicker substrate introduced additional difficulties in the manufacturing process.

Multilayer designs have been widely used to improve the performance of single-fed CP patch antennas.[12-20] Deng et al.[14] used a corner-truncated ring to simplify the feed structure. It achieved a 20.6 percent impedance bandwidth and an ARBW of approximately 6.94 percent by incorporating corner truncations and L-shaped branches on the radiating patch. Liu et al.[16] introduced a high gain CP patch antenna by adopting a stacked patch structure with pin loading. Li et al.[17] demonstrated significant performance improvements by incorporating an L-shaped stub. The antenna achieved an impedance bandwidth of approximately 42.1 percent and an ARBW of about 26.0 percent with a maximum gain of 8.6 dBiC.

Multiple feed techniques are effective in extending ARBW.[21,22] Lin et al.[21] proposed a wideband tri-fed CP antenna achieving a 47.88 percent ARBW with three symmetric feed points 120 degrees apart. Tamjid et al.[22] described a quad-fed CP antenna achieving 32.5 percent impedance bandwidth and a peak gain of 7.33 dBic using two coupled-line power dividers. However,

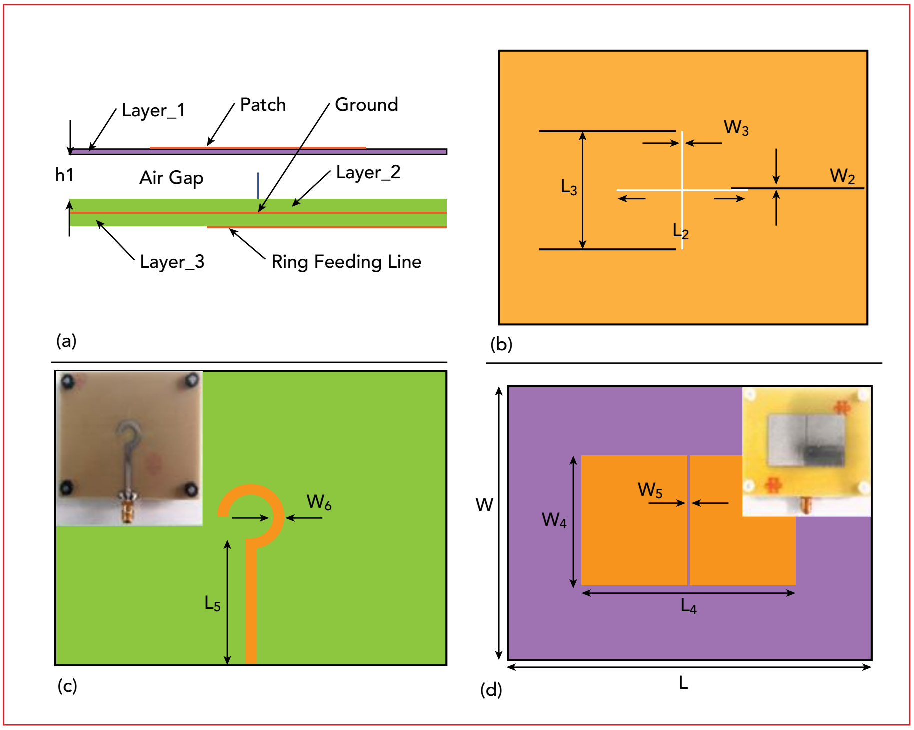

Fig. 1 **Antenna structure: (a) side view, (b) lower view of the second layer, (c) lower view of the third layer and (d) upper view of the first layer.**

the feeding network design was complex.

A single-feed CP patch antenna with a compact structure and wide bandwidth is proposed in this work. The design incorporates a slotted radiating patch, an annular ring microstrip feed line and a ground plane with a crossed slot, resulting in a simplified structure. The annular ring microstrip feed line is aperture-coupled to the radiating patch through a cross-shaped slot, which enables CP radiation. Measurements yield a 32.5 percent impedance bandwidth (from 3.45 to 4.79 GHz) with $|S_{11}|$ below -10 dB, and a 25.56 percent ARBW (from 3.48 GHz to 4.5 GHz), with the AR below 3 dB.

ANTENNA DESIGN

Figure 1a shows a side view of the antenna, consisting of Layer_1, an air gap, Layer_2 and Layer_3, with the height of the air gap between Layer_1 and Layer_2 denoted as h1. The bottom of Layer_2 features a ground plane with a crossed slot (see ***Figure 1b***). ***Figure 1c*** shows the annular microstrip feed line at the bottom of Layer_3. ***Figure 1d*** shows the rectangular patch on Layer_1, which is etched with an I-shaped slot.

The annular ring microstrip feed line is aperture-coupled to the patch through the crossed slot, enabling the generation of CP radiation. The ε_r value of Layer_1 is 2.32, with a thickness of 0.5 mm. Layer_2 and Layer_3 have ε_r values of 3.55, each with a thickness of 1 mm. The optimized geometrical parameters are (in mm): W_4 = 26, L_4 = 42, W_5 = 0.4, W = 56, L = 72, W_3 = 0.9, L_3 = 24, W_2 = 0.5, L_2 = 26, h_1 = 3.2, W_6 = 2.2 and L_5 = 24.2.

Figure 2 shows the surface current distributions of the two orthogonal modes (Modes 1 and 2) introduced by the I-shaped slot. The red arrows indicate the directions of the surface currents associated with these modes. Mode 1 corresponds to the TM_{01} mode, while Mode 2 is a new mode introduced by the I-shaped slot.

Generating CP requires exciting two orthogonal modes with equal amplitudes and a 90-degree phase difference. According to the magnetic field coupling excitation method, excitation is applied to regions

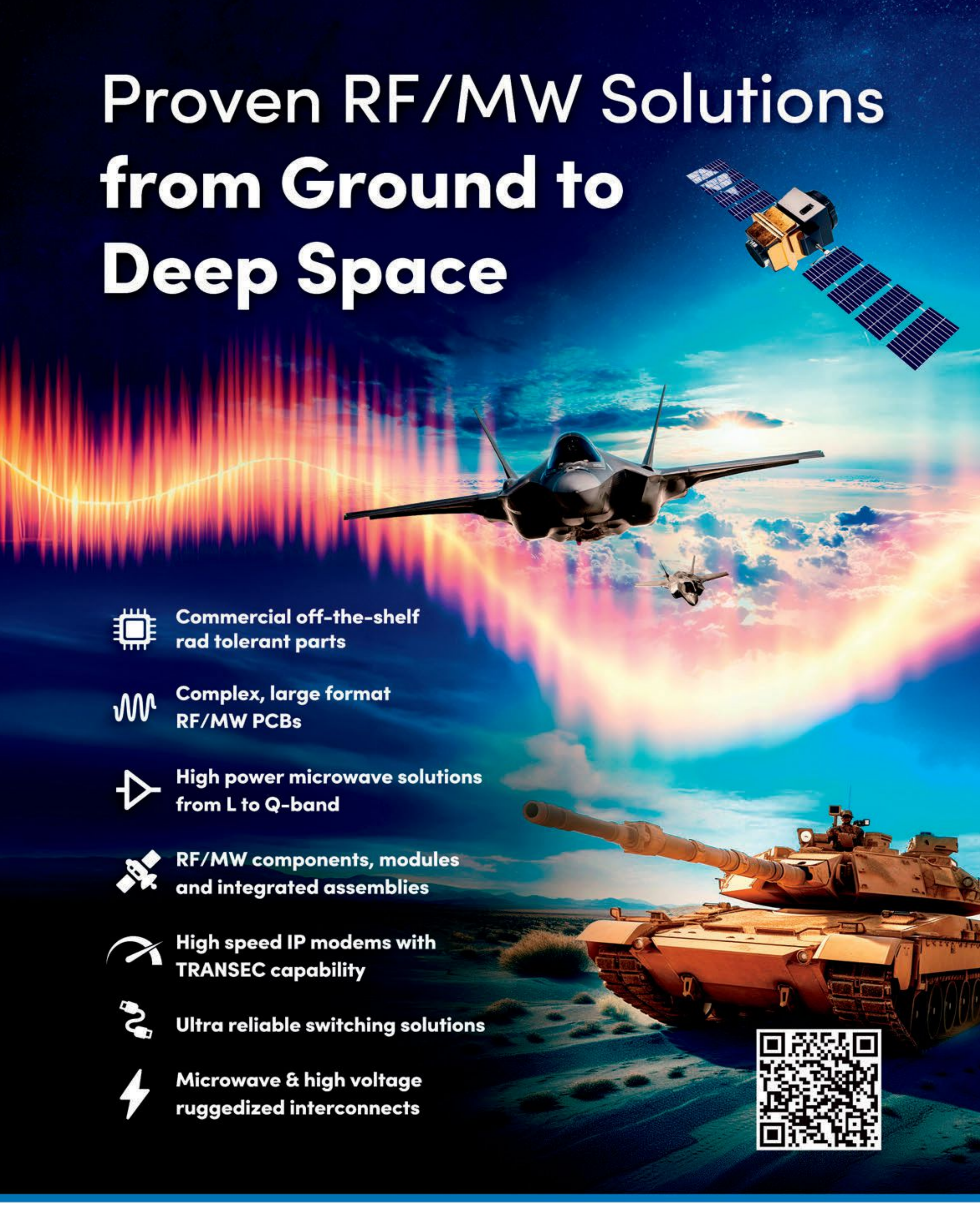

Proven RF/MW Solutions from Ground to Deep Space
Commercial off-the-shelf rad tolerant parts
Complex, large format RF/MW PCBs
High power microwave solutions from L to Q-band
RF/MW components, modules and integrated assemblies
High speed IP modems with TRANSEC capability
Ultra reliable switching solutions
Microwave & high voltage ruggedized interconnects

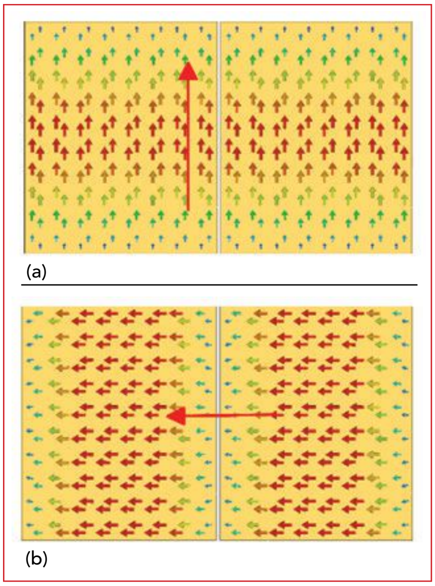

▲ **Fig. 2** **Modal surface current distribution: (a) Mode 1 and (b) Mode 2.**

with stronger currents.[23] Therefore, a cross-shaped slot is etched on the ground plane, and both modes are simultaneously excited using an annular microstrip feed line. By appropriately adjusting the length of the cross-shaped slot, the phase difference of radiation in the far-field can be tuned to approximately 90 degrees.

To better understand the CP radiation mechanism, simulation over time is performed at 4 GHz (see ***Figure 3***). In ***Figures 3a*** and ***3b***, the current directions are orthogonal to each other. In ***Figures 3c*** and ***3d***, the current magnitudes remain unchanged, but their directions are reversed with respect to Figures 3a and 3b. This clockwise rotation of the surface current over time results in left-handed circular polarization (LHCP) radiation.

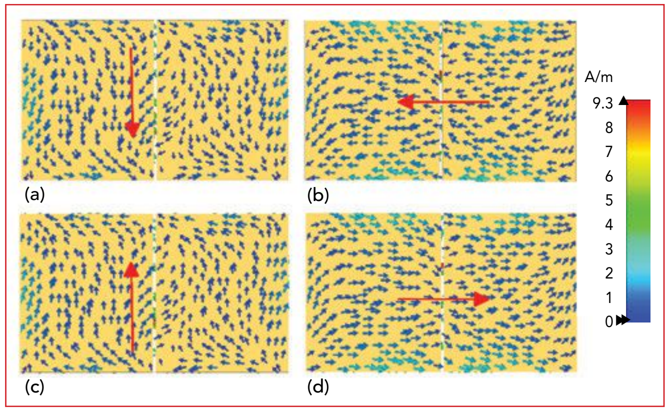

▲ **Fig. 3** **Patch surface current distribution as a function of time: (a) t=0, (b) t=T/4, (c) t=T/2 and (d) t=3T/4. (T = period at 4 GHz).**

PARAMETRIC STUDIES

When L_2 is increased from 25 mm to 27 mm, $|S_{11}|$ decreases at higher frequencies and increases at lower frequencies, with the resonant frequency shifting to lower values. This is due to the slot altering the current distribution and effective electrical length of the antenna. As L_2 increases, the AR minimum points also shift to lower frequencies, with optimal performance at L_2 = 26 mm (see ***Figure 4a***).

As W_2 increases from 0.4 mm to 0.6 mm, $|S_{11}|$ in the high frequency band increases, where $|S_{11}|$ in the low frequency band shows almost no change (see ***Figure 4b***). Additionally, the AR is almost unaffected as W_2 increases. To optimize the impedance bandwidth, the width of the slot is determined to be 0.5 mm.

Increasing L_4 from 41 mm to 43 mm reduces $|S_{11}|$ at low frequencies but has little effect at high frequencies, with the 3 dB ARBW narrowing (see ***Figure 5a***). The optimal performance is achieved at L_4 = 42 mm.

As W_4 increases from 25 to 27 mm, $|S_{11}|$ is above -10 dB at 4.13 GHz for W_4 = 25 mm and at 3.5 GHz for W_4 = 27 mm. Optimal CP performance is for W_4 = 26 mm (see ***Figure 5b***).

The analysis of these four parameters indicates that the AR is primarily influenced by the slot length and the length of the radiating patch. When the lengths of the slot and patch are suitably adjusted, the phase difference between the two orthogonal modes is altered, which in turn affects the AR. By adjusting the lengths of the cross-shaped slot and the radiating patch, the phase

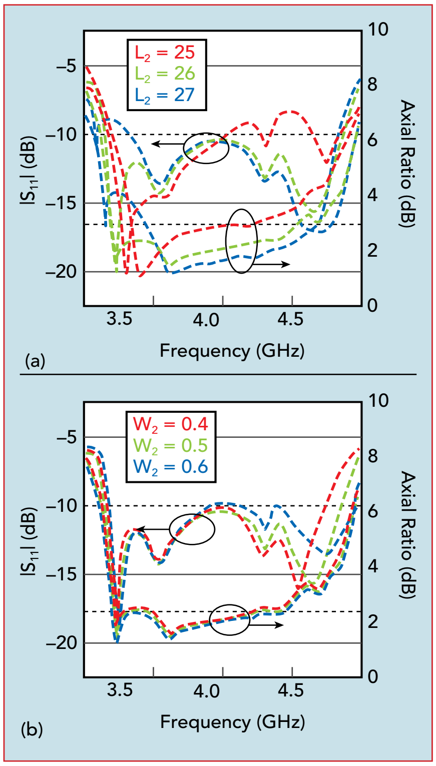

Fig. 4 Effect of (a) slot length (L_2) and (b) slot width (W_2) on $|S_{11}|$ and AR.

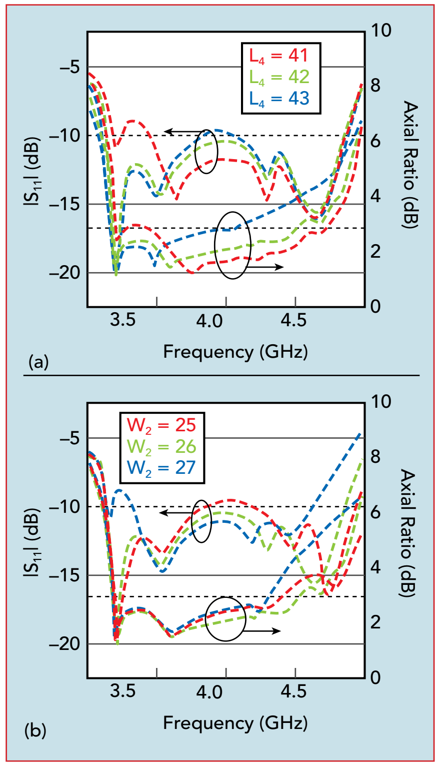

Fig. 5 Effect of (a) patch length (L_4), and (b) patch width (W_4) on $|S_{11}|$ and AR.

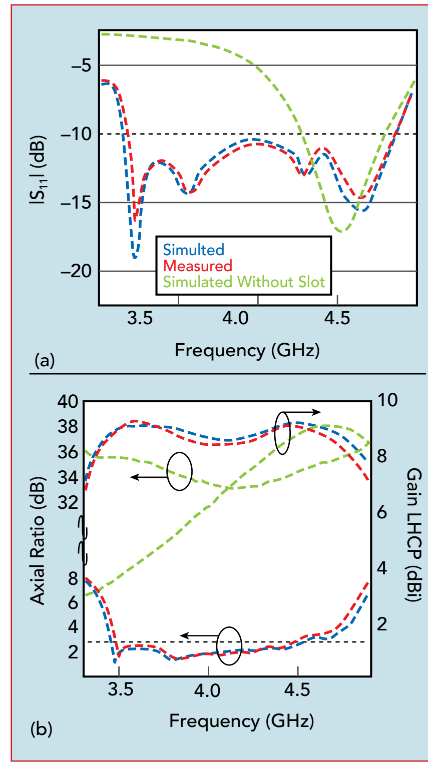

Fig. 6 Simulated and measured results: (a) $|S_{11}|$ and (b) AR and gain.

difference in the far-field is effectively tuned to approach 90 degrees, thereby enhancing the generation of CP radiation.

EXPERIMENTAL RESULTS

The antenna resonates only at 4.51 GHz when the radiating patch is not etched with slots (see ***Figure 6***). The introduction of an I-shaped slot at the center of the patch leads to the emergence of three additional resonant frequencies at 3.5, 3.75 and 4.32 GHz, resulting in broadband performance. Measured values of $|S_{11}|$, AR and gain show close agreement. The measured -10 dB impedance bandwidth is approximately 32.5 percent (from 3.45 to 4.79 GHz). Similarly, the measured 3 dB ARBW is approximately 25.56 percent (from 3.48 GHz to 4.50 GHz). The antenna demonstrates excellent gain performance across the operating band, with a peak gain of approximately 9.2 dBi at 3.58 GHz.

Figure 7 shows normalized radiation patterns obtained from both measurements and simulations. The designed CP patch antenna radiates LHCP, in accordance with the current distribution shown in Figure 3. Cross-polarization levels are be-

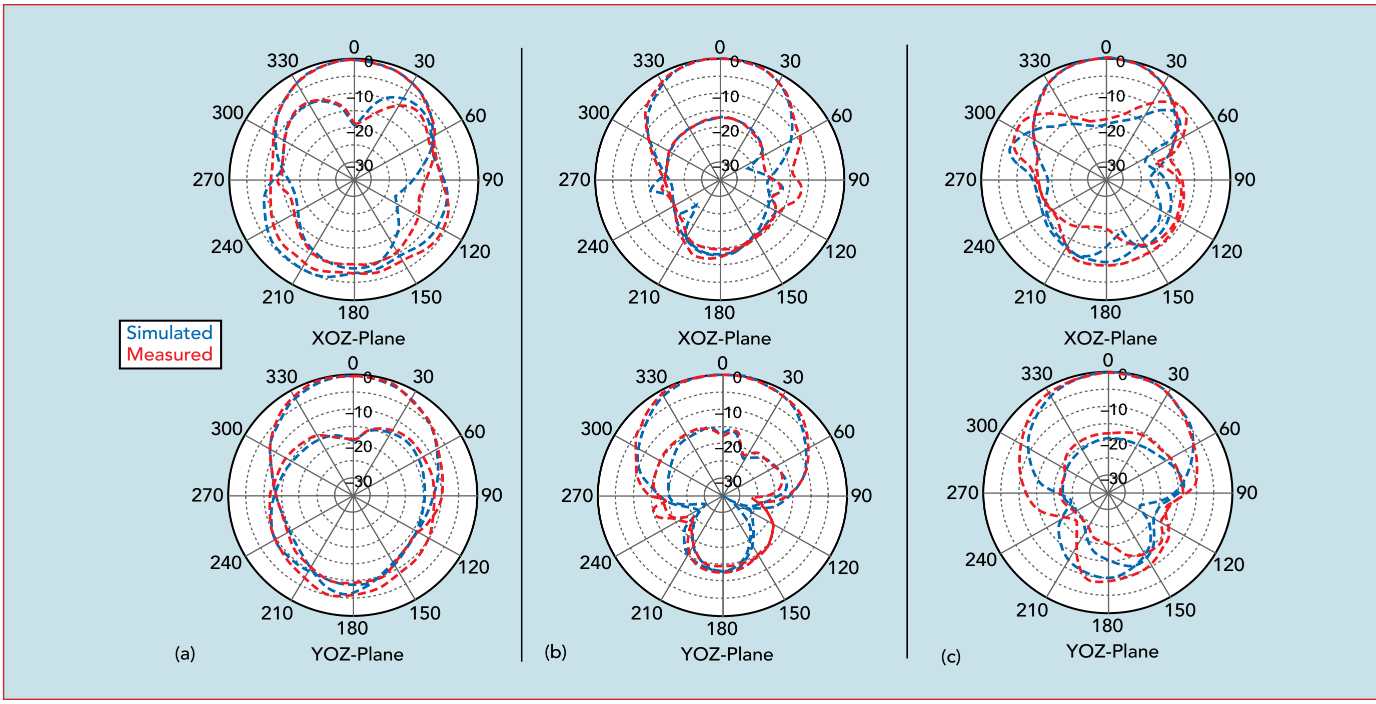

Fig. 7 Normalized radiation patterns from both simulation and measurement: (a) 3.5, (b) 3.9 and (c) 4.4 GHz.

low -15.0 dB.

The performance of the CP patch antenna is summarized in ***Table 1***, where it is compared with those of other CP patch antennas.[15-20] This antenna demonstrates superior ARBW, impedance bandwidth and gain in a simple and compact structure.

CONCLUSION

A single-feed CP patch antenna with compact and wideband characteristics uses an annular ring microstrip feed line aperture-coupled to the patch through a crossed slot. This results in four resonant frequency points on the $|S_{11}|$ curve and three minimum points on the AR curve. This configuration achieves an impedance bandwidth of 32.5 percent (from 3.45 GHz to 4.79 GHz) and an ARBW of 25.56 percent (from 3.48 GHz to 4.50 GHz). This antenna features a simple structure, a low profile and a wide ARBW, making it suitable for broadband wireless communication applications.

ACKNOWLEDGMENT

This work was supported in part by the Key Laboratory of Intelligent Monitoring on Navigation Safety and in part by the Key Scientific Research Project of the Hunan Provincial Department of Education under Grant 24A0748. ■

References

1. C. -M. Su and K. -L. Wong, "A Dual-Band GPS Microstrip Antenna," *Microwave and Optical Technology Letters*, Vol. 33, No. 4, May 2002, pp. 238-240.
2. H. H. Tran and I. Park, "Wideband Circularly Polarized Cavity-Backed Asymmetric Crossed Bowtie Dipole Antenna," *IEEE Antennas and Wireless Propagation Letters*, Vol. 15, June 2015, pp. 358-361.
3. M. F. Farooqui and A. Kishk, "3-D-Printed

Telonic Berkeley

1080 La Mirada Court
Vista, CA 92081

Phone
(760) 744-8350

Fax
(760) 744-8360

Web Address
www.telonicberkeley.com

email
info@telonicberkeley.com

TELONIC BERKELEY INC.
AS9100D AND ISO 9001:2015 CERTIFIED AND AN ITAR CONTROLLED COMPANY

A Pioneer of RF & Microwave Filters

…employing proven design elements (Lumped, Combline/Cavity, and Tubular) to produce high-quality Passband, Lowpass, Highpass, and Bandstop Microwave Filters… including Diplexers, Multiplexers, Filter Banks, Switches, Multipliers… also Rotary Attenuators

Telonic Berkeley **Fixed Filters** are known and used worldwide. Our impressive array of fixed filter types has evolved over the years in responding to the demanding needs of the electronic industry while offering performance parameters tailored specifically to each customer's unique requirements.

Telonic Berkeley Engineers are ready and anxious to provide innovative solutions for your RF multi-channel or **Multiplexer** needs. Our Diplexer, Triplexer or Quadraplexer designs in lumped element or combline/cavity designs may be the solution you are looking for.

Telonic Tubular Bandpass Filters are available in 2 to 12 sections. Three different and frequency sizes ranges allow for the selection of an optimal design for each requirement. Almost any type of input or output connection is available as a standard item.

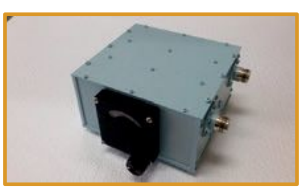

Tunable Filters including Manually Tuned Bandpass Filters, Manually Tuned Bandstop Filters, Digitally Tuned Bandstop Filters, and Multi-Octave Digitally Tuned Filters up to 36 Gigahertz are available.

Telonic Berkeley offers a full range of **RF Cable Assemblies,** Flat Ribbon Cables, Grounding Cables, Wire Harnesses, Discrete Harnesses, and Power Cords

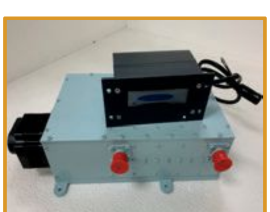

Network Managed Tunable RF Filters provide remote management, monitoring and diagnostic capabilities. High Power Tunable BSF and BPF are available

TABLE 1

COMPARISON OF CP PATCH ANTENNAS

Reference	Layers	Size (λ_0^3)	3-dB ARBW (%)	-10 dB IBW (%)	Gain (dBi)
15	2	4.89 × 4.89 × 0.14	16	>24.4	18.8
16	2	1.32 × 1.32 × 0.05	6	11.5	11
17	4	1 × 1 × 0.122	26	42.1	8.6
18	2	0.88 × 0.88 × 0.12	26.5	43.2	8.5
19	2	0.7 × 0.7 × 0.03	10.2	20.48	8.8
20	2	0.46 × 0.46 × 0.15	21.1	48.75	8.15
This Work	3	0.84 × 0.65 × 0.067	25.56	32.5	9.2

Tunable Circularly Polarized Microstrip Patch Antenna," *IEEE Antennas Wireless Propagation Letters*, Vol. 18, No. 7, July 2019, pp. 1429-1432.

4. Z. N. C. Nasimuddin and X. Qing, "A Compact Circularly Polarized Cross Shaped Slotted Microstrip Antenna," *IEEE Transactions on Antennas and Propagation*, Vol. 60, No. 3, March 2012, pp. 1584-1588.
5. J. J. Wu, Y. Z. Yin, Z. D. Wang and R. Lian, "Broadband Circularly Polarized Patch Antenna with Parasitic Strips," *IEEE Antennas and Wireless Propagation Letters*, Vol. 14, November 2015, pp. 559-562.
6. K. Ding, C. Gao, D. X. Qu and Q. Yin, "Compact Broadband Circularly Polarized Antenna with Parasitic Patches," *IEEE Transactions on Antennas and Propagation*, Vol. 65, No. 9, September 2017, pp. 4854-4857.
7. J. -F Lin and Q. -X. Chu, "Enhancing Bandwidth of CP Microstrip Antenna by Using Parasitic Patches in Annular Sector Shapes to Control Electric Field Components," *IEEE Antennas and Wireless Propagation Letters*, Vol. 17, No. 5, May 2018, pp. 924-927.
8. S. Hao, Q. Chen, J. Li and J. Xie, "A High-Gain Circularly Polarized Slotted Patch Antenna," *IEEE Antennas and Wireless Propagation Letters*, Vol. 19, No. 6, June 2020, pp. 1022-1026.
9. L. Wang, Z. M. Zhu and Y. F. En, "Performance Enhancement of Broadband Circularly Polarized Slot-Microstrip Antenna Using Parasitic Elements," *IEEE Antennas and Wireless Propagation Letters*, Vol. 20, No. 12, December 2021, pp. 2255-2259.
10. X. Chen, G. Fu, S. -X. Gong, Y. -L. Yan and W. Zhao, "Circularly Polarized Stacked Annular-Ring Microstrip Antenna with Integrated Feeding Network for UHF RFID Readers," *IEEE Antennas and Wireless Propagation Letters*, Vol. 9, June 2010, pp. 542-545.
11. S. Kim and J. -I. Kim, "A Circularly Polarized High-Gain Planar 2x2 Dipole-Array Antenna Fed by a 4-way Gysel Power Divider for WLAN Applications," *IEEE Antennas and Wireless Propagation Letters*, Vol. 18, No. 5, May 2019, pp. 1051-1055.
12. S. Shekhawat, P. Sekra, D. Bhatnagar, V. K. Saxena and J. S. Saini, "Stacked Arrangement of Rectangular Microstrip Patches for Circularly Polarized Broadband Performance," *IEEE Antennas and Wireless Propagation Letters*, Vol. 9, September 2010, pp. 910-913.
13. W. Yang, J. Zhou, Z. Yu and L. Li, "Single-Fed Low Profile Broadband Circularly Polarized Stacked Patch Antenna," *IEEE Transactions on Antennas and Propagation*, Vol. 62, No. 10, November 2014, pp. 5406-5410.
14. C. Deng, X. Lv and Z. Feng, "Low-Profile Circularly Polarized Patch–Ring Antenna with Compact Feeding Network," *IET Microwaves, Antennas and Propagation*, Vol. 12, No. 3, November 2017, pp. 410-415.
15. Z. Gan, Z. -H. Tu, Z. -M. Xie, Q. -X. Chu and Y. Yao, "Compact Wideband Circularly Polarized Microstrip Antenna Array for 45 GHz Application," *IEEE Transactions on Antennas and Propagation*, Vol. 66, No. 11, November 2018, pp. 6388-6392.
16. Z. -X. Liu, L. Zhu and X. Zhang, "A Low-Profile and High-Gain CP Patch Antenna with Improved AR Bandwidth via Perturbed Ring Resonator," *IEEE Antennas and Wireless Propagation Letters*, Vol. 18, No. 2, February 2019, pp. 397-401.
17. W. Li, X. Wei, Y. S. Li, X. Xiong, K. L. Chung and Z. X. Huang, "Wideband Single-Fed Circularly Polarized Stacked Patch Antenna with L-Shaped Stub," *Applied Computational Electromagnetics Society Journal*, Vol. 37, No. 12, December 2022.
18. K. Ding, Y. Wu, K. -H. Wen, D. -L. Wu and J. -F. Li, "A Stacked Patch Antenna with Broadband Circular Polarization and Flat Gains," *IEEE Access*, Vol. 9, February 2021, pp. 30275-30282.
19. T. Shi, R. Chai, X. Chen, M. Li, T. Zhang and M. C. Tang, "A Low-Profile, Circularly Polarized, Metasurface-Based Antenna with Enhanced Bandwidth and Stable High Gain," *IEEE Antennas and Wireless Propagation Letters*, Vol. 22, No. 2, February 2023, pp. 253-257.
20. Y. Cheng and Y. Dong, "Wideband Circularly Polarized Split Patch Antenna Loaded with Suspended Rods," *IEEE Antennas and Wireless Propagation Letters*, Vol. 20, No. 2, February 2021, pp. 229-233.
21. C. Lin, F. Zhang, Y. Jiao, F. Zhang, Y. C. Jiao, F. Zhang and X. Xue, "A Three-Fed Microstrip Antenna for Wideband Circular Polarization," *IEEE Antennas and Wireless Propagation Letters*, Vol. 9, April 2010, pp. 359-362.
22. F. Tamjid, F. Foroughian, C. M. Thomas, A. Ghahreamani, R. Kazemi and A. E. Fathy, "Toward High-Performance Wideband GNSS Antennas – Design Tradeoffs and Development of Wideband Feed Network Structure," *IEEE Transactions on Antennas and Propagation*, Vol. 68, No. 8, August 2020, pp. 5796-5806.
23. R. Martens, E. Safinn and D. Manteuffel, "Inductive and Capacitive Excitation of the Characteristic Modes of Small Terminals," *Loughborough Antennas & Propagation Conference*, November 2011.

INVITED PAPER

Using Power Sensors for Manufacturing Test

Orwill Hawkins
LadyBug Technologies, LLC, Boise, Idaho

Power sensors, such as LadyBug's LBSF09A compact RF power sensor, are widely used in manufacturing test systems across industries, including communications equipment, RF component validation, printed circuit board testing, military and aviation hardware, wearables and medical devices.

These cost-effective tools allow manufacturers to verify product performance either directly or within a test chamber, ensuring compliance and quality. Power sensors add value throughout the manufacturing process; by identifying defective subassemblies or components before integration, they prevent inventory build-up of faulty parts and reduce wasted time and resources.

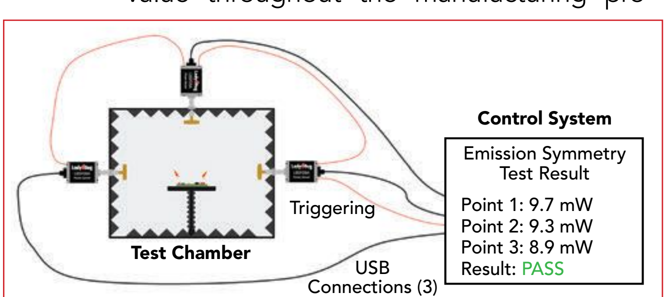

Fig. 1 **Test chamber with a DUT and three power sensors equipped with antennas.**

Figure 1 depicts a test chamber with three power sensors connected to a test system. The three power sensors are connected by USB-C connections and linked with daisy-chained triggering, allowing the test system to synchronize and evaluate all measurements simultaneously. During testing, the device under test (DUT) can be rotated inside the chamber, enabling the collection of comprehensive RF radiation data.

With their frequency coverage, accuracy and measurement flexibility, power sensors are well-suited for testing devices that incorporate new signal formats, high-power components or emerging technologies. Integrated into automated test equipment (ATE), they deliver rapid analysis during early manufacturing stages and after final assembly. This allows engineers to devote more effort to product design and process optimization.

▲ Fig. 2 LadyBug LBSF09A RF power sensor.

FROM TRADITIONAL TEST SYSTEMS TO MODERN SENSORS

Test equipment has evolved over the past several decades. Early systems relied on bulky power meters paired with external sensors and required frequent manual calibration steps, such as zeroing and input isolation. These procedures often interrupted the test process and slowed throughput.

Modern power sensors, by contrast, are compact, self-contained instruments with interfaces such as USB, HiSLIP LAN, SPI and I^2C. LadyBug's patented NoZero technology eliminates re-zeroing, ensuring uninterrupted operation. The result is faster, more reliable testing with higher overall efficiency, see ***Figure 2***.

APPLICATION EXAMPLE: DEVELOPMENT TO PRODUCTION

In early product development and initial manufacturing runs, companies often build small-scale test systems tailored to their specific device. These setups allow engineers to validate performance, explore design tradeoffs and confirm regulatory compliance before investing in large-scale automated equipment.

Compact USB or LAN-connected power sensors are particularly valuable at this stage. They integrate with laboratory PCs, require minimal support hardware and can be controlled through common software environments such as Python, MATLAB or LabVIEW. This flexibility reduces setup time and keeps development costs low.

When a product succeeds in the market and production volumes increase, testing requirements evolve from small, single-station setups to fully integrated production test systems. Power sensors support this transition by enabling engineers to establish validated measurement routines during early development and then carry those same routines into scaled manufacturing. This continuity ensures consistent results across stages, minimizes re-engineering efforts and accelerates the path from product concept to high volume deployment.

TECHNICAL EXAMPLE: MEASURING RETURN LOSS

Return loss (RL) is a common parameter used to verify device performance. ***Figure 3*** shows a compact test setup using two LadyBug LBSF09A 9 GHz power sensors and directional couplers. A signal source drives the DUT, while one sensor measures forward power and the other measures reflected power.

To minimize measurement uncertainty, the coupler monitoring reflected power is placed closest to the DUT. This placement improves directivity (forward/reverse isolation), reducing error across all power levels. At very low signal levels, where noise dominates, the sensor's dynamic range, exceeding 86 dB, enables detection of small reflections.

Formula and Calculation

RL is defined in ***Equation 1*** as:

$$RL\,(dB) = -10\log_{10}\left(\frac{P_r}{P_i}\right) \qquad (1)$$

where:

- P_i = incident (forward) power into the DUT
- P_r = reflected power from the DUT

Power values are measured in linear units (e.g., mW) and then converted to decibels. Since the ratio is dimensionless, any consistent linear unit can be used. In practice, engineers often prefer to work directly in dB for convenience, but the underlying calculations are performed in the linear domain to maintain accuracy.

Correction Factor

To account for coupler loss and coupling factors, a tracking correction factor T is applied, as shown in ***Equation 2***:

$$RL\,(dB) = -10\log_{10}\left(\frac{P_{rev}}{P_{for}} \times T\right) \qquad (2)$$

A typical method for determining T is to measure with a known full reflection (shorted port), as demonstrated in ***Equation 3***:

$$T = \frac{P_{for}}{P_{rev}} \qquad (3)$$

For higher accuracy, measurements are taken with both open and short terminations. Averaging these results yields a correction factor, Tave, which removes most system source match errors. This correction factor is then applied in the RL calculation in ***Equation 4***:

$$RL\,(dB) = -10\log_{10}\left(\frac{P_{rev}}{P_{for}} \times T_{ave}\right) \qquad (4)$$

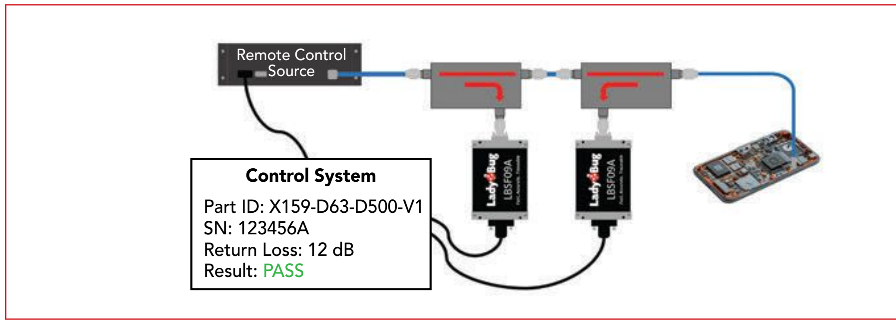

Fig. 3 Example simple system for automated return loss measurement.

Practical Considerations

The system can automatically detect conditions such as reflected power near the noise floor, indicating insufficient signal, unexpected RL values, DUT faults, DUT mismatches, measurement inconsistencies due to component defects or poor connections. By logging and flagging such events, defective devices can be identified before they enter final assembly or shipment, improving yield and reducing costs.

While RL can also be measured with a one-port network analyzer, such instruments are more expensive and less flexible than a power-sensor-based setup. In a manufacturing line, multiple RL measurements are often required at different assembly stages or test stations. Outfitting each point with a network analyzer would be cost-prohibitive, whereas deploying additional power sensors is both practical and economical. This makes power-sensor-based systems attractive for scalable manufacturing, where accuracy, throughput and cost control are all critical.

Note on VSWR

Some engineers prefer to express a mismatch in terms of voltage standing wave ratio (VSWR). VSWR can be derived directly from RL using the relationships in ***Equations 5*** and ***6***:

$$\rho = 10^{\left(-\frac{RL}{20}\right)} \tag{5}$$

$$\text{VSWR} = \frac{(1+\rho)}{(1-\rho)} \tag{6}$$

Only the magnitude of the reflection is measured ($\rho = |S11|$). Phase information is not measured and is not required for the RL or VSWR calculations. This approach allows automated test systems to report both RL and VSWR at each station without additional hardware or measurements.

BROADER APPLICATIONS

While RL is a representative example, power sensors also support compliance testing, EMC assessments, calibration of other RF equipment and verification of production test systems. Their cost-effectiveness and interoperability make them suitable for a wide range of manufacturing environments.

SOFTWARE AND INTERFACE INTEGRATION

Modern manufacturing test systems are no longer isolated benches with a few dedicated instruments. Instead, they are complex networks of sensors, sources, controllers and databases, all coordinated by software. Power sensors fit into this environment because they provide standardized communication protocols and flexible connectivity options.

STANDARDIZED COMMAND AND CONTROL

LadyBug LBSF and LB5900 series power sensors support the standard commands for programmable instruments (SCPI) protocol, a widely adopted standard defined by IEEE 488.2. SCPI enables consistent control and data acquisition across different programming environments, including Python, C, C++, C#, MATLAB and LabVIEW. This interoperability ensures that engineers can integrate power sensors into almost any automated test framework without the need for specialized drivers.

For example, in Python, engineers can communicate with sensors over USB or LAN using libraries such as pyvisa, sending SCPI commands to configure measurements, retrieve power levels and log results. In larger test environments, virtual instrument software architecture abstracts the hardware connection so that the same code can operate over USB in the lab or LAN in production without modification.

Multi-Sensor Coordination

A key advantage of compact power sensors is their ability to operate in parallel. A single PC or industrial controller can manage multiple sensors simultaneously, each addressing a different test point or station. This scalability is key in manufacturing, where several measurements must be taken at different points along an assembly line. Coordinating multiple sensors through a centralized control program provides synchronized data collection and simplifies pass/fail decisions.

Data Management and Traceability

In modern factories, measurement results are rarely used only for real-time verification. Instead, they are stored in databases, linked to product or subassembly identification numbers and analyzed for trends. Power sensors can stream results directly into manufacturing execution systems or statistical process control software.

Remote and Distributed Testing

Remote Interfaces extend the reach of power sensors beyond the local workstation. This allows test stations to be monitored remotely or aggregated across multiple production sites. In some deployments, data is collected and analyzed in near real-time at a central location, providing global oversight of distributed manufacturing lines. USB, meanwhile, remains valuable for single-station setups where simplicity and low cost are paramount.

NEXT-GENERATION TEST SYSTEMS

The increasing complexity of RF products and the rising demand for higher throughput are reshaping the design of automated test systems. While today's power sensors integrate seamlessly with software frameworks and production databases, the next generation of systems may extend this integration further — leveraging Industry 4.0 concepts, cloud connectivity and advanced data analytics where appropriate.

In many deployments, measurement data may not remain confined to the local test station. Instead, results can be aggregated in centralized or cloud-based platforms, where advanced statistical methods and machine learning may be applied to identify subtle shifts in device performance before they cause yield degradation. This predictive capability gives manufacturers the option to act proactively, whether by adjusting processes, recalibrating equipment or isolating component lots.

Similarly, power measurements are increasingly being used as active triggers in automated workflows. Depending on system design, they can initiate equipment calibration, quality alerts or supply chain adjustments in real-time. Interfaces such as LAN, HiSLIP, SPI and I²C provide the flexibility to embed sensors into both legacy systems and emerging IoT-enabled architectures.

Together, these trends suggest the direction of next-generation test systems: distributed, data-driven and highly adaptive. Within this framework, compact and thermally stable power sensors are well-positioned to remain a key enabler of future test systems, delivering accuracy, scalability and cost-effectiveness while supporting the transition to future manufacturing models.

CONCLUSION

Power sensors have become indispensable in modern manufacturing test systems. They offer lower cost and reduced complexity compared to other options, scalability to integrate at every stage of assembly verification and flexibility through multiple interfaces and standardized SCPI commands. As assemblies grow more compact and complex, the role of power sensors will continue to expand. Their accuracy, adaptability and seamless software integration make them a cornerstone of next-generation ATE. ■

Microwave Journal

SPECIAL FOCUS

Table of Contents

Cover Feature

Technical Features

Product Feature

Tech Briefs

Departments

RF Modeling and Simulation For 6G System Design Using Digital Twins

Sassan Ahmadi
Keysight Technologies, Inc., Santa Clara, Calif.

VIRTUAL SYSTEM DESIGN IN 6G

6G represents a transformative leap in wireless, focused on sustainability, intelligence and global connectivity. Building on 5G expertise, 6G researchers are advancing enablers such as sub-THz communications, AI-native architectures and RF digital twins to improve performance and energy efficiency, targeting applications like immersive extended reality (XR) and autonomous systems. Realizing this vision requires overcoming challenges in sub-THz propagation, hardware complexity and the co-design of communication, sensing and AI, alongside the harmonization of regulations and the pursuit of sustainability imperatives. Digital twin technologies address these hurdles by enabling high-fidelity modeling, early validation and energy-aware design, ensuring that 6G evolves into a scalable, flexible and environmentally responsible connectivity platform.

MODELING AND SIMULATION OF 6G

As 6G advances from concept to realization, realistic modeling and simulation are vital for designing, validating and optimizing networks that span sub-THz frequencies, AI-native architectures, integrated sensing and non-terrestrial platforms. Traditional methods fall short of capturing nonlinearities, channel dynamics, interference and hardware impairments, making high-fidelity, cross-domain digital twins particularly useful. SystemVue, a system-level RF simulation software, provides such an environment, delivering near-circuit-level co-simulation of RF, baseband and antenna domains with hardware-in-the-loop integration to assess trade-offs, detect bottlenecks and validate reliability under real-world conditions. With advanced engines for time, frequency and phased-array analysis, integration with measurement tools and built-in libraries for algorithm testing, SystemVue bridges design and testing workflows, accelerating development, reducing risk and ensuring robust, compliant 6G system deployment.

PROMINENT 6G TECHNOLOGIES

Among the most transformative enablers of 6G are AI-native radio access networks (AI-RAN), integrated sensing and communication (ISAC), reconfigurable intelligent surfaces (RIS) and non-terrestrial networks (NTNs). AI-RAN introduces intelligence and self-optimization into the RAN, where machine learning (ML) manages spectrum, power, beamforming and mobility to enhance efficiency and quality of service in ultra-dense, heterogeneous environments. ISAC enables communication and sensing to share the same waveform and infrastructure, supporting applications such

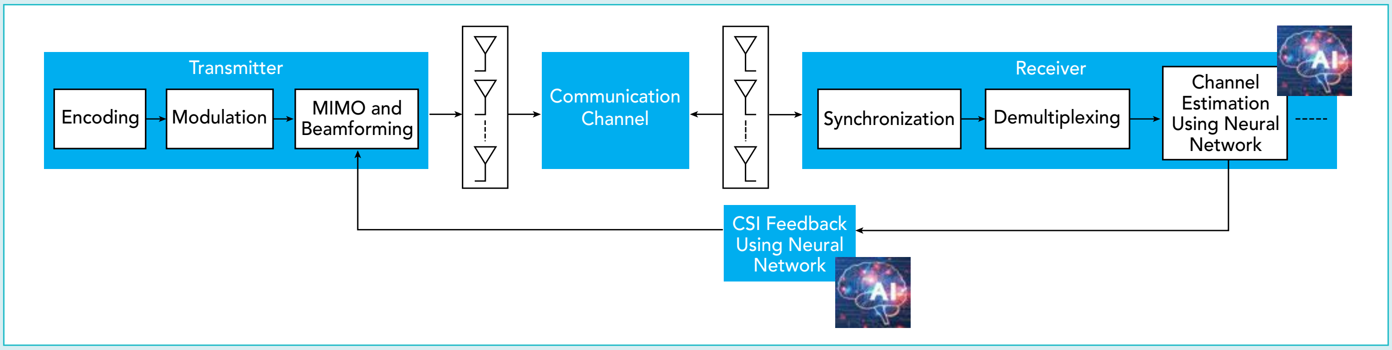

Fig. 1 **Example of a signal processing chain.**

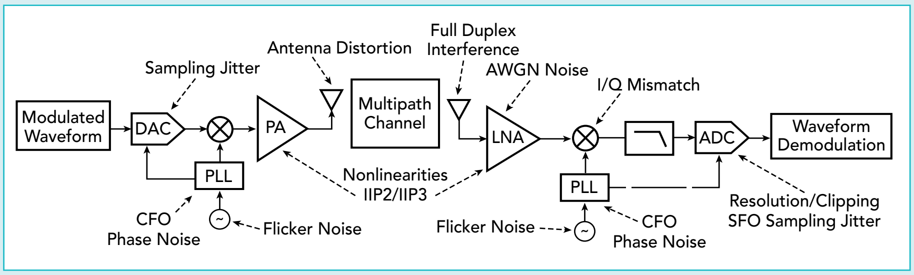

Fig. 2 **Modeling RF impairments in an ISAC system.**

as autonomous vehicles and smart factories. RIS utilizes programmable surfaces to shape wave propagation, enhancing coverage, energy efficiency and connectivity without requiring active transmission. Complementing these terrestrial advances, NTNs, including LEO satellites, high-altitude platforms and UAVs, extend 6G services to remote and underserved regions globally. Together, these technologies form the backbone of a highly adaptive and universally accessible 6G ecosystem.

AI and ML

AI and ML will be integral to 6G RAN, enabling proactive, self-optimizing networks that manage spectrum, beamforming and modulation in real-time across ultra-dense, high frequency environments. By leveraging techniques such as reinforcement learning and federated learning, AI extends intelligence for latency-sensitive use cases, including autonomous driving and industrial automation, while also enhancing security, anomaly detection and energy efficiency. SystemVue supports this evolution by generating high-fidelity training data from realistic RF and channel models, to train AI models using TensorFlow or PyTorch frameworks and reimporting the trained models for evaluation and benchmarking. This workflow enables techniques such as adaptive beamforming, CSI feedback compression and link adaptation, accelerating the design, validation and deployment of AI-native 6G RANs.

Figure 1 depicts an ML–enhanced wireless communication system focused on channel state information feedback and channel estimation. It shows a typical transmitter-receiver chain, where the source block includes encoding, modulation and beamforming. The signal propagates through a multipath channel, reaching the receiver, which performs synchronization, demultiplexing and channel estimation. This approach integrates AI/ML-based functions at both the receiver and feedback paths; one neural network is responsible for channel estimation at the receiver, while another neural network optimizes CSI feedback to the transmitter. This AI-assisted feedback loop enables adaptive beamforming at the source, improving link reliability and spectral efficiency by leveraging learned channel characteristics.

ISAC

ISAC is a key 6G enabler that fuses data transmission with environmental awareness, supporting applications such as autonomous driving, robotics, smart infrastructure and XR. By sharing waveforms and hardware for both communication and sensing, ISAC transforms networks into perceptive systems while introducing trade-offs between sensing accuracy and low-latency data delivery. SystemVue addresses these chal-

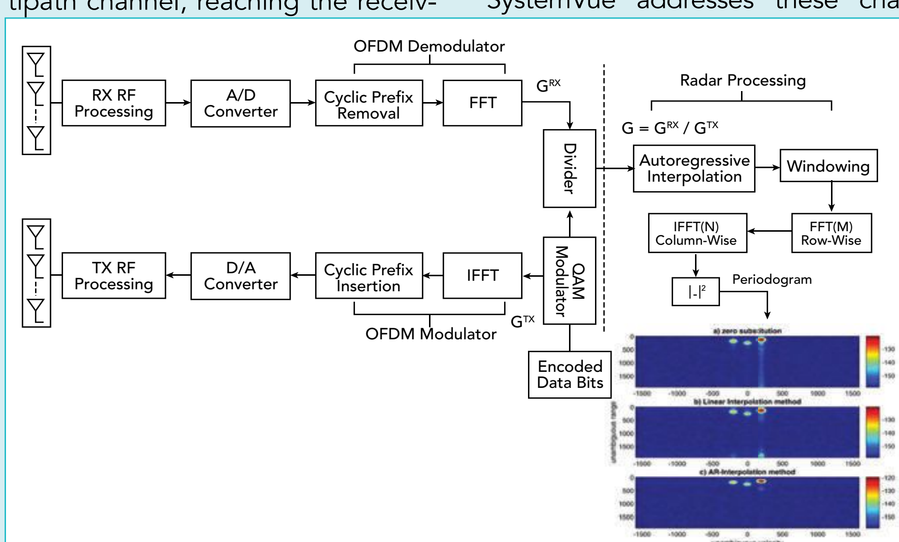

Fig. 3 **Example of sensing functionality by reusing 5G NR waveforms.**

lenges by unifying RF, baseband and antenna modeling with impairment simulation and hardware-in-the-loop workflows, enabling realistic evaluation of algorithms, beamforming and waveform reuse. By bridging digital twin simulation with over-the-air (OTA) testing, researchers and architects can accelerate ISAC prototyping and ensure the development of scalable and commercially viable 6G deployments.

Figure 2 shows a generic transceiver signal chain for ISAC systems, annotated with critical RF impairments across both the analog and digital domains. These include phase noise, carrier frequency offset (CFO), sampling jitter, flicker noise, antenna distortion, nonlinearities (IIP2/IIP3) and I/Q mismatch, all of which degrade fidelity and sensing accuracy. Channel effects, such as multipath and full-duplex interference in monostatic scenarios, are also highlighted. These emphasize the need for realistic modeling to evaluate simultaneous communication and sensing performance.

Figure 3 illustrates an example of an ISAC system that utilizes 5G New Radio (NR) waveforms for both communication and sensing functions. In this example, the 5G NR OFDM waveform is post-processed to extract relative range, Doppler and direction information of the hypothetical targets in the environment.

RIS

RIS is a 6G innovation that enables programmable wireless environments by using passive or semi-passive elements to dynamically reflect, focus or scatter signals, improving coverage, throughput and energy efficiency while overcoming non-line-of-sight conditions and blockages. Unlike traditional fixed infrastructure, RIS introduces a software-controlled paradigm but requires accurate modeling to account for factors such as beamforming gain, phase control, element layout and mobility at high frequencies. A digital twin provides a robust environment for RIS design, supporting custom array topologies, phase quantization errors and element-level impairments, while enabling co-simulation with RF and baseband parameters. By evaluating beam steering, side lobes and system-level trade-offs, engineers can optimize RIS placement and control strategies, ensuring the practical and scalable deployment of RIS in 6G networks.

Figure 4 shows the characterization of the RIS beamforming for various reflection angles θ_d at 5.8 GHz, showing a comparison between computed and measured radiation patterns using one-bit phase shifters. It presents measured and simulated radiation patterns of an RIS at various reflection angles $0 \le \theta_d \le 60$ degrees, along with the corresponding one-bit quantized phase distributions. The radiation patterns compare simulation (black) with physical measurements (red), demonstrating directional beam steering through discrete phase control. The quantized phase distributions show the one-bit phase quantization pattern (values of 0 and 180 degrees), applied across the RIS elements to steer the beam. These visualizations highlight the importance of accurately modeling antenna element phase, element spacing and angular response to understand the spatial behavior and control requirements of RIS.

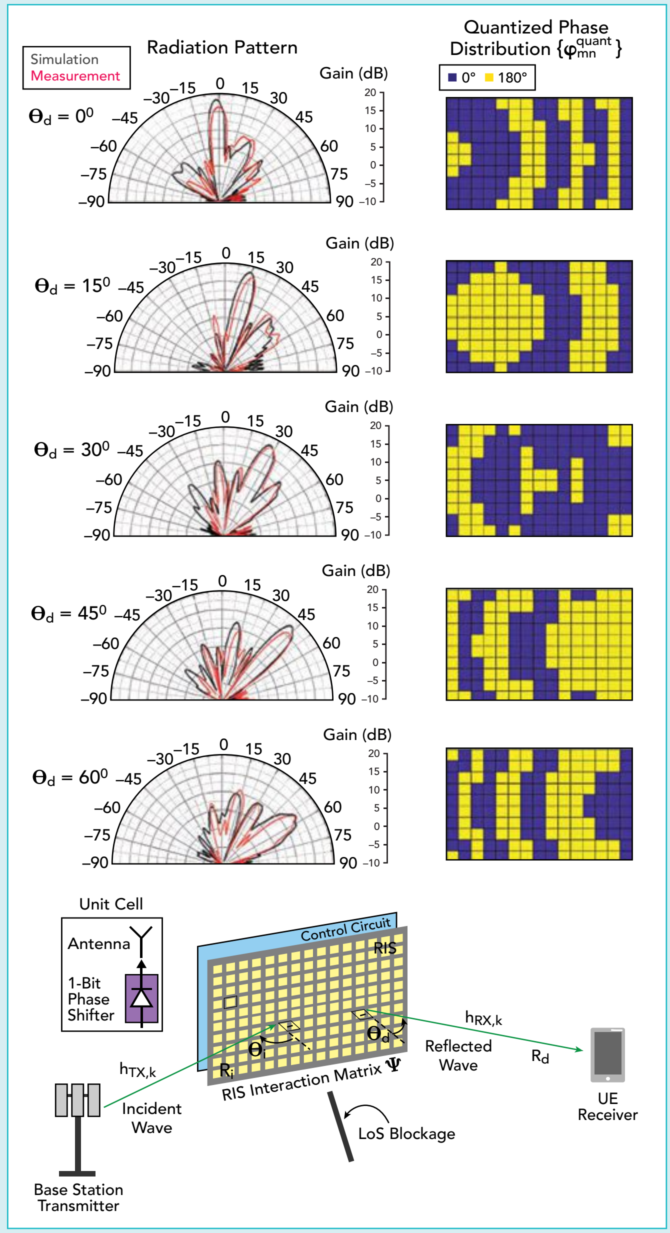

Fig. 4 **Characterization of RIS beamforming for various reflection angles.**

Integrating Terrestrial Networks and NTNs

The integration of terrestrial networks and NTNs is a key 6G advancement, combining satellites (LEO, MEO, GEO), HAPS, drones and airborne base stations with cellular infrastructure to provide global connectivity. This hybrid architecture extends reliable service to rural, open sea and disaster-hit regions where terrestrial networks are impractical, enabling applications such as global IoT, aviation and maritime communication and resilient emergency connectivity. By unifying the terrestrial and satellite domains, 6G aims to deliver persistent broadband access and support new services through scenarios ranging from transparent and regenerative satellite payloads to direct UE-to-UE relays.

Integrating NTNs introduces challenges, including long propagation delays, Doppler shifts, link intermittency and atmospheric impairments, as well as the need for seamless handovers and cross-domain resource management. A digital twin addresses these challenges by offering high-fidelity modeling of satellite payloads, gateways and user equipment under realistic conditions, incorporating impairments such as power amplifier (PA) nonlinearity, phase noise, I/Q imbalance and fading. It supports phased-array design, 3D satellite trajectory visualization and nonlinear PA modeling with digital predistortion (DPD), as well as error vector magnitude (EVM) analysis for performance validation. By bridging simulation with measured data and hardware-in-the-loop workflows, a digital twin also enables engineers to evaluate beam management and link robustness, ensuring NTN systems meet the reliability, scalability and interoperability requirements of 6G. ***Figure 5*** illustrates an example of SystemVue's comprehensive NTN modeling capabilities, representing both transparent and regenerative payload scenarios.

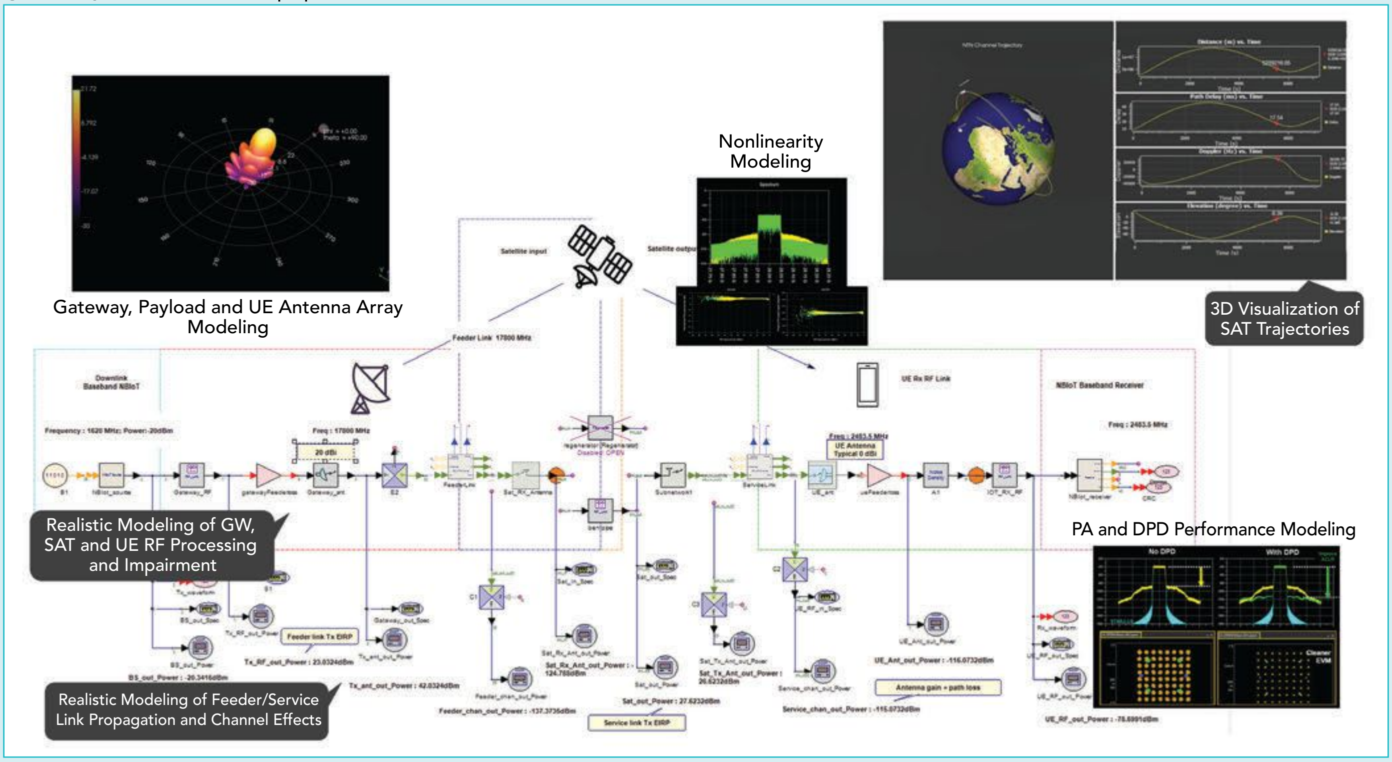

Fig. 5 **Example illustration of NTN link modeling with satellite trajectories.**

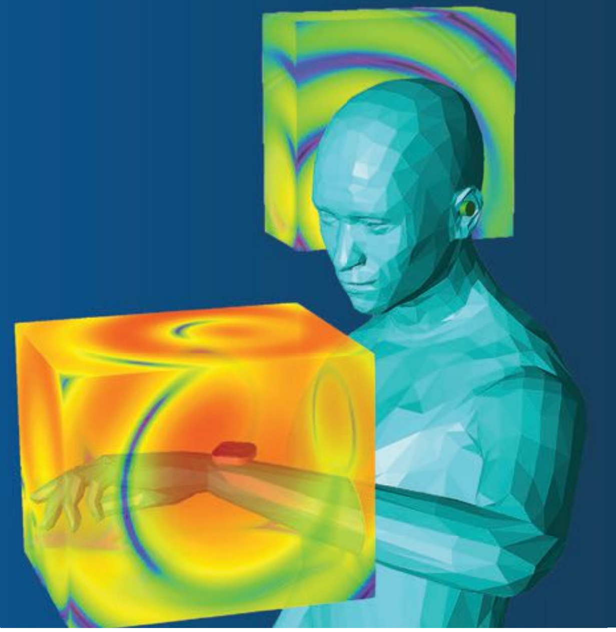

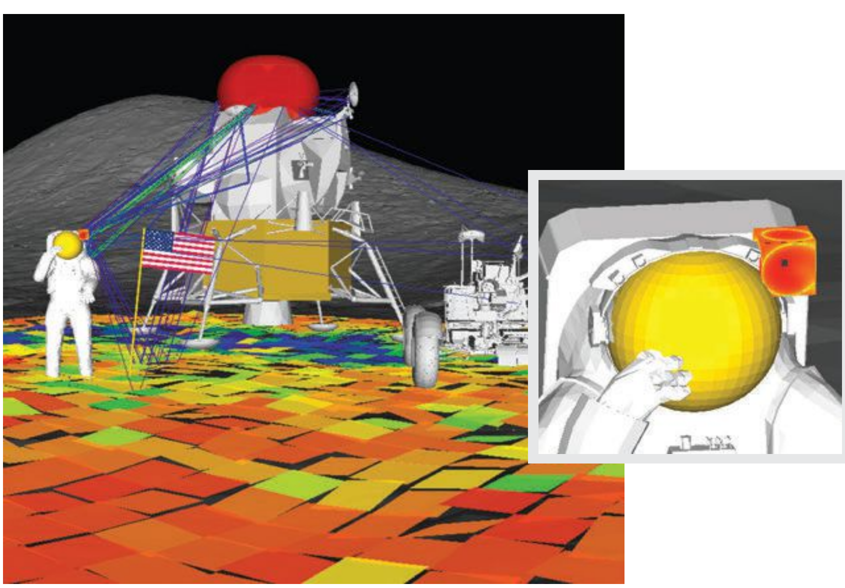

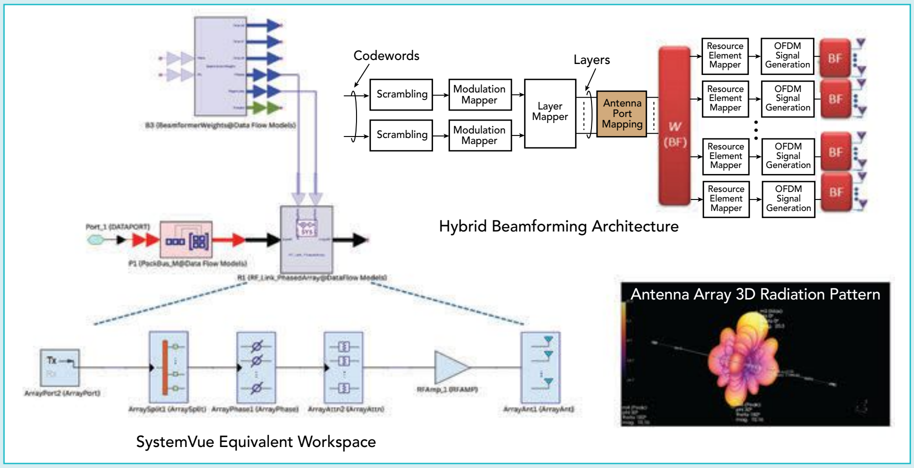

Fig. 6 **Virtual modeling of massive MIMO RF and antenna systems.**

New Spectrum

The frequency range 3 (FR3) band (7.125 to 24.25 GHz), positioned between 5G's FR1 and FR2 frequency ranges, is emerging as a vital spectrum for 6G, offering a balance of coverage, penetration and capacity. It provides broader bandwidth than FR1 while maintaining better propagation properties than FR2 and sub-THz, lending itself to applications such as ultra-reliable low-latency communication, XR and integrated sensing. However, challenges such as higher attenuation, interference and more stringent RF front-end requirements demand innovations in beamforming, antenna design and radio architecture. Teams can address these complexities by enabling high-fidelity modeling of propagation, hardware impairments and phased-array systems, while supporting waveform generation, coexistence studies and hardware-in-the-loop validation. By bridging simulation with test and measurement tools, a digital twin accelerates prototyping and ensures robust, cost-effective design for 6G systems that leverage the FR3 spectrum.

New RF and Antenna Technologies

The evolution toward 6G is driving advances in RF and antenna technologies to support sub-THz operation, ultra-high data rates and integrated sensing. Emerging semiconductor technologies such as InP HEMTs, GaN-on-SiC, SiGe BiCMOS and CMOS-SOI enable efficient high frequency amplification, while architectures like Doherty and distributed amplifiers, as well as digitally controlled beamforming PAs, enhance efficiency and scalability in massive arrays. At the same time, advanced CMOS nodes and packaging innovations such as antenna-in-package and system on chip (SoC) integration are enabling tighter RF digital integration, reduced losses and agile beamforming for applications such as low-latency links and holographic communication. To design these systems, workflows increasingly combine circuit, electromagnetic (EM) and system-level modeling with AI/ML and digital twins.

SystemVue, integrated with EM solvers and test instruments, supports accurate modeling of RF chains, phased arrays and impairments, accelerating convergence, improving performance prediction and enabling 6G designs. Teams can accelerate 6G RF and antenna development by creating a unified RF digital twin that bridges circuit-level accuracy with system-level validation. It supports advanced transistor and amplifier technologies through integration with Keysight ADS and EM tools, such as RFPro, while enabling array-aware modeling for complex antennas and RIS, including beamforming, phase/gain quantization and coupling analysis. ***Figure 6*** illustrates an example of this in the modeling of a hybrid beamforming transmitter. With capabilities such as DPD, phased-array calibration, AI-assisted optimization and hardware-in-the-loop workflows, teams can streamline co-design of RF front-ends and control logic. Its scalable phased-array engine simplifies massive architectures by automatically abstracting single-chain models into thousands of paths, paired with 3D beam visualization and predefined metrics for rapid insight. By combining measured data, EM models and high performance computing processing, teams can create workflows essential for designing and validating next-generation RF systems.

Full-Duplex Systems

Early progress in full-duplex and sub-band full-duplex (SBFD) schemes shows promise to increase spectral efficiency and reduce latency by enabling simultaneous transmission and reception on the same channel. While full-duplex requires extremely robust self-interference cancellation (over 100 dB), SBFD offers a practical alternative by separating uplink and downlink into different sub-bands, easing interference cancellation requirements while still supporting bidirectional or joint sensing-communication operations. SBFD becomes especially valuable in dense deployments and monostatic ISAC scenarios where transmitter leakage can block weak sensing signals. SystemVue provides an environment for modeling and validating duplexing schemes under realistic impairments, including PA nonlinearity, phase noise and I/Q imbalance, while supporting sub-band partitioning, SIC algorithm simulation and hardware-in-the-loop validation. These capabilities enable engineers to evaluate trade-offs and optimize full-duplex and SBFD designs for practical 6G deployment (see ***Figure 7***).

RF Digital Twin

A digital twin is a dynamic, virtual replica of a physical system that mirrors real-world behavior using high-fidelity models informed by live or measured data, enabling predictive analysis, optimization and early fault detection. For 6G RF and antenna systems, effective digital twins must capture nonlinearities, noise, coupling and channel impairments

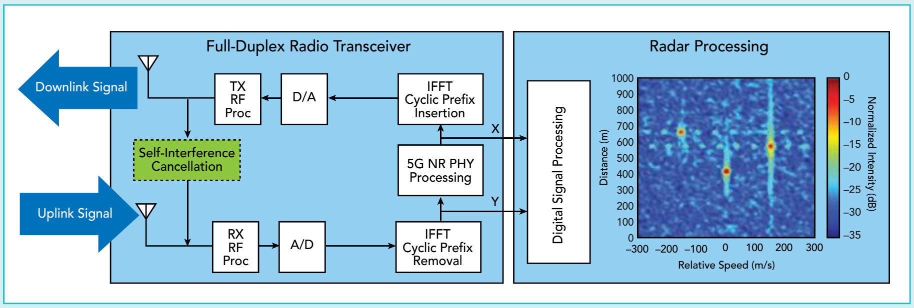

Fig. 7 **Full-duplex monostatic sensing at a base station.**

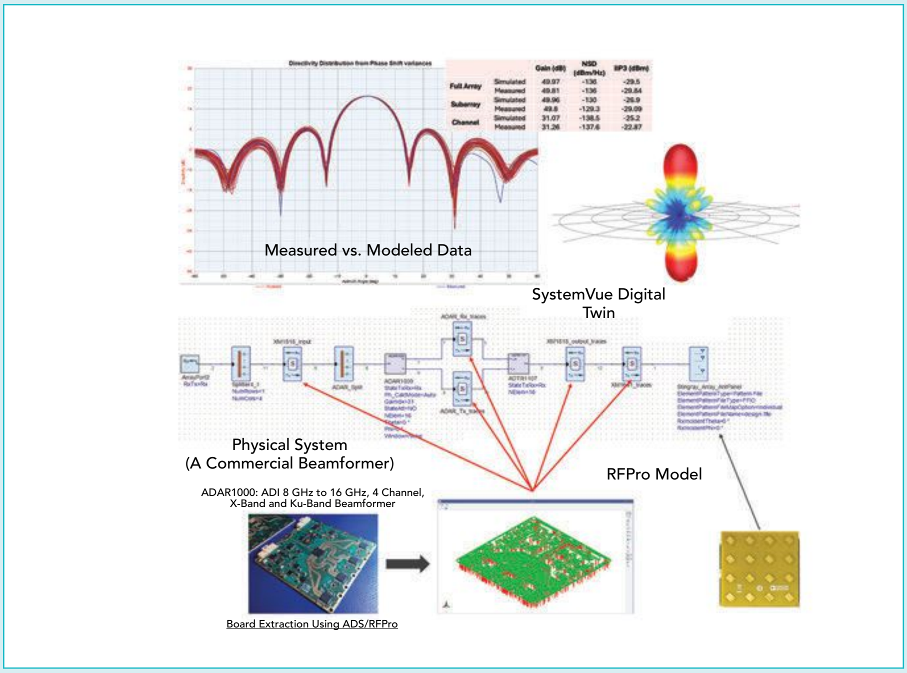

Fig. 8 **Example comparison of a physical circuit and its digital replica.**

such as Doppler and interference, while supporting co-simulation across circuit, system and propagation domains. SystemVue offers a robust environment for implementing RF digital twins, delivering near-circuit-level accuracy for signal chains, phased arrays and propagation effects. It integrates with EM tools and test instruments to ensure simulated results align with measured performance. By bridging design and hardware-in-the-loop validation, a digital twin enables engineers to accelerate prototyping, enhance energy efficiency and confidently optimize complex 6G technologies, including sub-THz operation, massive MIMO and RIS. ***Figure 8*** provides an example of a 6G digital twin workflow, which includes the accurate modeling of beamformers, splitters, PCB trace layouts and commercial RFICs. These virtual designs are validated using measured data, such as radiation patterns, gain, EVM and noise density, ensuring that simulation results closely correlate with physical performance.

AI-Based PA Modeling and Linearization

Artificial neural network (ANN)-based PA modeling and DPD provide an advanced method for modeling and linearizing RF PAs in 5G/6G, surpassing traditional approaches like memory polynomials or Volterra series in handling wide bandwidths, memory effects and dynamic impairments. By training on input–output signal pairs from measured or simulated PA data, ANNs learn the inverse nonlinear behavior of the amplifier and apply real-time predistortion on FPGA or DSP hardware, compensating for gain compression, AM/AM and AM/PM distortion and environmental variations through adaptive learning. AI also helps crest factor reduction intelligently suppress peaks while preserving spectral integrity, and AI-enhanced envelope tracking (ET) improves efficiency by dynamically adjusting the PA supply voltage, with ANN models compensating for the added nonlinearities of ET-enabled PAs. A digital twin integrates these AI-based methods with co-simulation, hardware-in-the-loop validation and closed-loop training, enabling spectrally clean transmitter designs for next-generation wireless systems.

LEADING THE TRANSITION TO 6G

Through simulation, testing and collaboration with global partners and 3GPP, Keysight is helping shape 6G for commercial readiness around 2030. The transition to 6G demands holistic, end-to-end system design, where advanced simulation tools bridge the gap between concept and deployment. Keysight's SystemVue provides a system design platform, delivering high-fidelity modeling, AI-assisted optimization and hardware-in-the-loop validation to accelerate innovation while reducing risk and cost. By supporting key 6G technologies such as ISAC, RIS, NTN and sub-THz RF front-ends, SystemVue serves as a powerful RF digital twin that captures real-world performance. With circuit-level accuracy, impairment modeling and AI/ML-driven workflows, it empowers designers to make informed trade-offs, enabling the development of scalable, reliable and sustainable 6G systems. ■

References

1. "6G System Design: Realistic Modeling, Simulation and Verification of Next Generation Wireless Systems," *Keysight*, Whitepaper, June 2025, Web: https://www.keysight.com/us/en/assets/3125-1338/white-papers/6G-System-Design.pdf.
2. SystemVue System-Level Baseband and RF Modeling Product Page, Web: https://www.keysight.com/us/en/products/software/pathwave-design-software/pathwave-system-design-software.html.

...And OTA Became Mainstream: How Innovations in OTA Testing Drive Next-Gen Wireless

Benoit Derat
Rohde & Schwarz GmbH & Co. KG, Munich, Germany

Over-the-air (OTA) testing, once confined to specialist labs, is now the backbone of modern wireless system validation. As 5G, connected vehicles and IoT become everyday realities, the industry's challenge is no longer just technical — it is pragmatic: deliver reliable system-level validation, keep costs and chamber size down and adapt to new scenarios.

The accelerating evolution of 5G and 6G wireless, coupled with the explosive growth of smarter IoT devices and applications that are now increasingly driven by embedded AI, is fundamentally reshaping both the scope and demands of OTA testing. Where traditional approaches once focused on isolated device evaluation, test technologies must now be developed to assess integrated wireless systems interacting within compact form factors, with real-time adaptation and context-aware intelligence reflecting the complexities of actual deployment environments.

TESTING BEYOND THE ANTENNA AND INTO COMPACT FAR-FIELD

Classic antenna measurements provide part of the story, evaluating radiated performance in isolation. But as radios morph into integrated "black boxes" radiating modulated signals, engineers need OTA methodologies that test the whole transceiver chain, not just for gain and directivity, but for how antenna impedance, hardware coupling and adjacent systems impact real-world connectivity.

Traditional near-field measurement is impractical for such system-level tests, hence the reliance on direct and indirect far-field approaches.[1] The rise of 5G, 6G, vehicle-integrated radio systems and electrically larger devices with respect to the wavelength, created a new imperative and drive for innovation: design OTA chambers to be as compact as possible, often by merging multiple functionalities within a single setup to maximize efficiency.

RETHINKING FAR-FIELD DISTANCE: THE EFFD

Here, innovation starts with the question: how close is "far enough" for reliable far-field OTA measurement? The long-held Fraunhofer or Rayleigh distance, dictating huge test chambers, does not fit today's reality. The introduction of the effective far-field distance (EFFD) approach reshaped best practices. This practical approach enables engineers to select a test range for a desired maximum error.[2]

The EFFD approach is based on quantifying the maximum allowed deviation, ϵ, on key metrics such as equivalent isotropic radiated power (EIRP) or antenna gain, as a function of measurement distance "R," device under test (DUT) size "D" (diameter of the minimum sphere containing the DUT) and frequency "f." The set of equations published by the IEEE[2] establishes the deviation as a predictable function, enabling the design of substantially smaller chambers for controlled accuracy loss. ***Figure 1*** shows the maximum

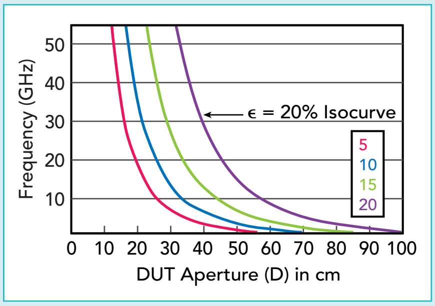

Fig. 1 Maximum deviation from EIRP at 3 m.

Fig. 2 ATS1800C ultra compact CATR (center), with additional side chambers (ATS1800M) for multi-angle-of-arrival tests.

deviation from EIRP at 3 m as a function of DUT size and frequency, showcasing how smaller chambers yield predictable errors.[2]

For example, instead of an 18 m Fraunhofer-distance based chamber for testing a 30 cm, 30 GHz device, 3 m of range length could be accepted if a 15 percent error can be tolerated. The price to pay for such distance reduction is the inflation of specific uncertainty contributors. Yet coupling a priori knowledge of the DUT with dedicated error compensation algorithms may support the mitigation of such effects. A relevant example is the parallax compensation algorithm, which allows limiting the uncertainty associated with the DUT phase center offset from the center of measurement system coordinates.[3]

ANTENNA TEST RANGES: SMALLER AND SMARTER

5G's mainstream adoption sparked the demand for compact antenna test ranges (CATRs), the gold standard for user equipment and base station validation. The ATS1800C CATR, as shown in ***Figure 2***, exemplifies this trend: small enough for a standard doorway (1.53 (L) × 0.90 (W) × 1.99 m (H)), yet able to deliver a 40 cm "quiet zone" meeting 3GPP RF conformance requirements from 6 to 90 GHz for user equipment testing.[4] This quiet zone is achieved through a 71 × 69 cm parabolic reflector with rolled edges mounted at the ceiling, offset fed by a corrugated choke horn with an orthomode transducer located at the chamber backwall center (light blue area). The chamber base includes a roll-over-elevation positioner with a maximum accumulated positioning error of 0.1 degree on both axes for an 8 kg DUT.

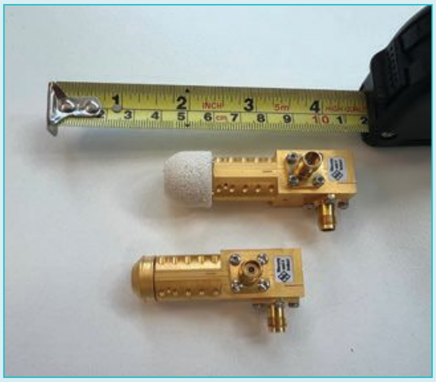

Fig. 3 New broadband CATR-FE60B wideband feed.

Reaching a quiet zone of this size in such a tight anechoic chamber required thousands of simulations for a co-optimization of the reflector and feeder system. Some details on the design process are presented by A. Tankielun et al.[5], where even further optimization was achieved through a new broadband design CATR feed covering a 3:1 bandwidth (22 to 64 GHz), a 2x to 3x wider frequency coverage than classical feeds (see ***Figure 3***). This CATR-FE60B wideband feed has a high field uniformity variant with a diffusing lens and a low path loss variant without.

Figure 2 also illustrates how the vertical CATR in the center can be complemented with two side chambers, adding three more reflector-feed systems. This unique and patented multi-CATR setup was invented to support 3GPP radio resource management testing with two angles of arrival, supporting all relevant 3GPP mmWave OTA tests in one single anechoic environment. Key design and validation aspects for this setup are detailed by C. Rowell, B. Derat and A. Cardalda-García.[6]

A "thermal bubble" can surround the DUT, permitting controlled OTA testing at temperatures from -40°C to +85°C, pivotal for automotive, aerospace and industrial applications.[4] The description of the design of a thermal testbed for metrology of active antennas outlined by B. L. Schoenholz, J. M. Downey and M. T. Piasecki[7] provides insights into how the performance of state-of-the-art mmWave arrays (here for connected objects used in space applications) is critically affected by temperature. In this example, there is more than 4 dB of gain over temperature (G/T) variation across a 60 K range, which must be qualified and potentially compensated in the device.

PLANE-WAVE SYNTHESIS: PRECISION AT THE SMALLEST SPACE COST

Plane-wave synthesis (PWS) prompted another leap forward. This technology uses arrays of controlled sources to create uniform electromagnetic illumination over a "quiet zone" at a fraction of the classic range size. Rohde & Schwarz was the first to bring this methodology to market with the R&S PWC200 test system, shown in ***Figure 4***.

PWS arrays achieve uniformity by digitally controlling amplitude and phase at each element, synthesizing wave fronts with deviations from an ideal plane-wave with possibly less

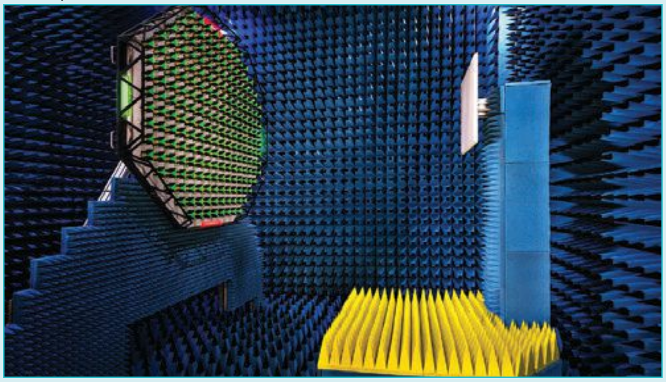

Fig. 4 R&S PWC200 PWS system.

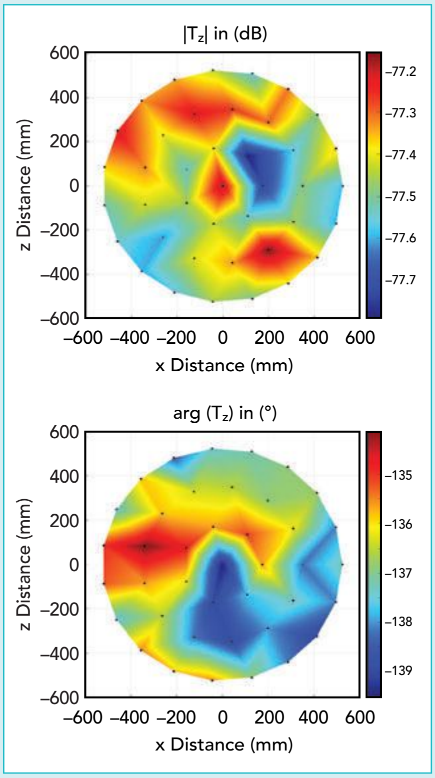

Fig. 5 **Field magnitude and phase variation in the quiet zone, 1.05 m disc at 2 m and 3.3 GHz.**

than ±0.3 dB in amplitude and ±2 degrees in phase across meter-scale zones (see ***Figure 5***). This is particularly advantageous for evaluating large 5G/6G antenna panels employed for massive MIMO.

Detailed studies[8] demonstrated quiet zone quality and PWS uncertainty more systematically. They established that PWS systems rival compact ranges in accuracy while reducing spatial footprint by a factor of 2 to 5, depending on the configuration. Indeed, where a CATR requires a reflector twice the quiet zone diameter D at 5 D distance, PWS achieves similar test fidelity at 1.8 D aperture and just 2 D range. The concept's limitation is bandwidth, typically bound by the capabilities of the beamforming circuitry. Yet, when the frequency range is suitable for the tests, PWS likely provides the most space and cost-effective OTA test alternative, at least in the sub-6 GHz frequency range.

BEYOND MEASUREMENT: AUGMENTED OTA AND DIGITAL TWINS

Some RF performance scenarios are too complex or cost-prohibitive for exhaustive measurement. Here, hybrid approaches, blending measured near-field data and numerical modeling in an augmented OTA approach, are the new standard.[9,10]

For example, validation of in-vehicle connectivity[9] can be solved through spherical scans of the antenna under test, where those measured data are then transformed to numerically "excite" a detailed model (a vehicle interior with passengers, etc.), or true "digital twin" workflow. For 5G/6G vehicular and IoT deployments, digital twin methods offer a crucial pathway to mapping dynamic, real-world scenarios onto repeatable lab procedures. By linking measurement to simulation, engineers can systematically explore device performance over thousands of conditions with statistical rigor and at scales impossible via hardware alone.

Figure 6a shows a car middle console with antennas measured in a spherical scanning OTA range, ***Figure 6b*** represents a car model with passengers and ***Figure 6c*** displays the calculated in-cabin electric field distribution from measured data injected in IMST EMPIRE XPU simulation software.

These hybrid techniques also extend to complex exposure evaluations, where absorption rates in the human body are predicted via combined OTA measurements and real computation.[10] Recent advances in interfacing measurements and simulations and phase-retrieval of digitally modulated signals with no RF port access make these methods both practical and scalable.[11,12]

CHARACTERIZING RIS: THE MBET ADVANCE

The future of wireless includes smart, reconfigurable intelligent surfaces (RIS), but their bistatic radar cross section (RCS) evaluation would classically demand complex and costly lab setups. The development of a monostatic-bistatic equivalence theorem (MBET) addressed this: researchers can now transform monostatic CATR measurements into bistatic RCS data with a mean deviation over all angles better than -24 dB, as confirmed experimentally.[13]

Figure 7 shows RCS data, represented in this case with UV projections for a RIS configured for an incident angle of (EL - 30 degrees, AZ - 45 degrees) reflected towards (EL - 30 degrees, AZ - 285 degrees) at 28 GHz. Figure 7a shows the raw monostatic measurement, Figure 7b shows the simulated bistatic RCS and Figure 7c shows the MBET-reconstructed bistatic RCS.

RIS technology is projected as a breakthrough for next-generation network control, spectrum re-use and ultra-low power wireless de-

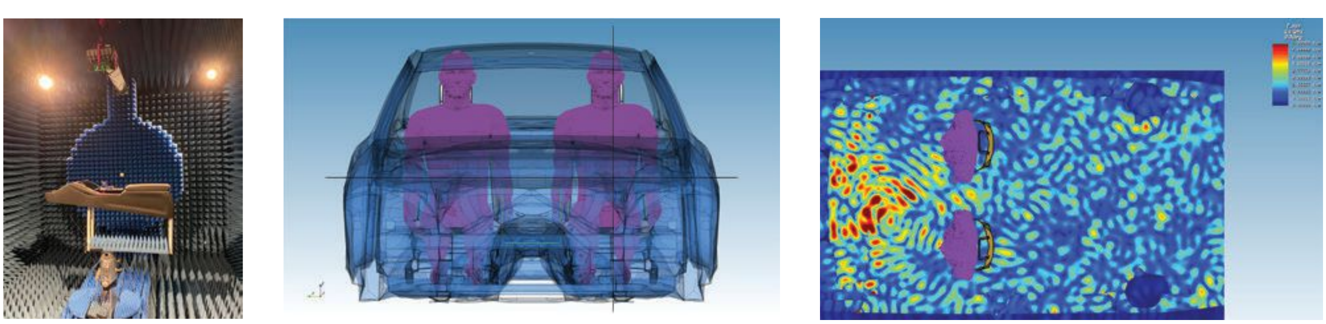

Fig. 6 **Digital twin workflow with (a) a car console in an OTA range, (b) a car model and (c) calculated in-cabin electric field distribution.**

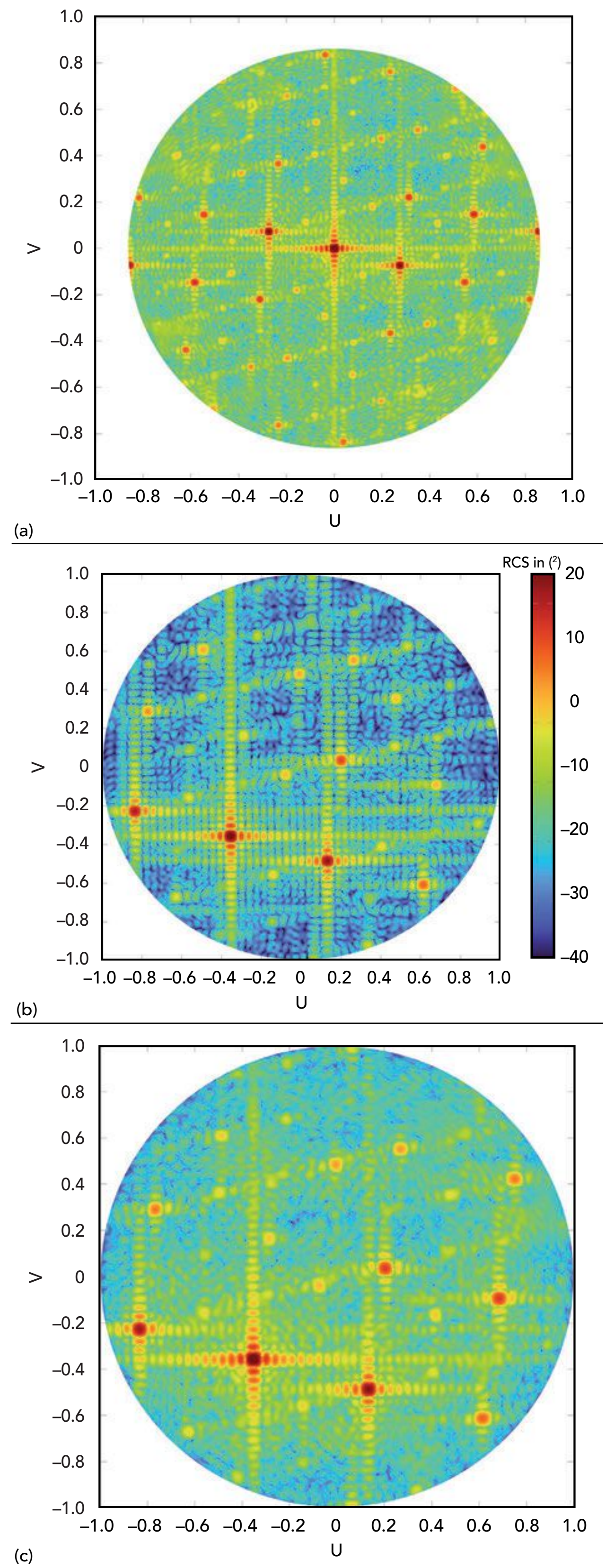

Fig. 7 RCS measurements in UV projections for a specific RIS and configuration.

sign. By enabling space-efficient and accurate lab-based RCS validation, the MBET technique could be key to unlocking testing capabilities for scaling up RIS deployment.

THE ROAD AHEAD FOR OTA: DIGITAL TWINS AND INSTRUMENTATION TECHNOLOGY

With fresh insight into far-field boundaries, continued refinement of compact ranges and PWS chambers and the rise of numerically augmented OTA, the wireless industry stands ready for rapid transformation. The next frontier could be the deeper integration of experimental measurement and simulation, moving OTA facilities toward true digital twin validation. Measurement will create and tune the digital twin, while simulation will open nearly unlimited possibilities for realistic and complex scenario testing.

On the instrumentation side, advancements are equally crucial. As the latest RF analyzers and calibration techniques become available, OTA measurement delivers more precise, complete results. Recent work, for example, on enhanced group delay measurements on devices with embedded mixers using a harmonic phase reference and two-step calibration[14] highlights just one example of how much progress is possible.

As 5G matures and 6G and IoT move from vision to reality, the sophistication and scale of required test solutions will only grow. The convergence of cutting-edge hardware and simulation tools promises a future where this scale can be reached, no challenge is too complex and no OTA test scenario is out of reach. ■

Acknowledgments

Special thanks to the unwavering engineering teams at Rohde & Schwarz, IMST GmbH and Prof. Keusgen at TU Berlin.

References

1. B. Derat, C. Rowell and A. Tankielun, "Promises of Near-Field Software and Hardware Transformations for 5G OTA," *IEEE Conf. on Antenna Meas. & Applications (CAMA)*, 2018, pp. 1–4.
2. "Discussion on Measurement Test Distance for Determining EIRP or TRP for Active Antenna Systems," *IEEE SA*, White Paper, ANSI C63, 31 Jan. 2024.
3. G. F. Hamberger et al., "Correction of Over-the-Air Transmit and Receive Wireless Device Performance Errors Due to Displaced Antenna Positions in the Measurement Coordinate System," *IEEE Trans. on Antennas and Propag.*, Vol. 68, No. 11, 2020.
4. B. Derat et al., "Acceleration of Over-The-Air Measurements Under Extreme Temperature Conditions Through Optimization of Air Flow and Thermal Efficiency," *Antenna Meas. Tech. Asso. Symp. (AMTA)*, 2022.
5. A. Tankielun et al., "A Novel Wide-Beam Broadband Feed Enabling Ultra-Compact Antenna Test Ranges," *Antenna Meas. Tech. Asso. Symp. (AMTA)*, 2025.
6. C. Rowell, B. Derat and A. Cardalda-García, "Multiple CATR Reflector System for Multiple Angles of Arrival Measurements of 5G Millimeter Wave Devices," *IEEE Access*, Vol. 8, 2020.
7. B. L. Schoenholz, J. M. Downey and M. T. Piasecki, "Design of a Thermal Testbed for Metrology of Active Antennas," *2022 Antenna Measurement Techniques Association Symposium (AMTA)*, 2022.
8. A. Tankielun et al., "Quiet Zone Verification of Plane Wave Synthesizer Using Polar Near-Field Scanner," *14th European Conf. on Antennas and Propag. (EuCAP)*, 2020.
9. B. Derat et al., "Optimization of In-Vehicle Connectivity through Simulation-Augmented Antenna Measurements," *Antenna Meas. Tech. Asso. Symp. (AMTA)*, 2022.
10. B. Derat et al., "Absorbed Power Density Assessment Using Simulation-Augmented Over-the-Air Measurement," *IEEE Access*, 2024.
11. D. Schaefer et al., "Power Normalization for Over-The-Air Augmented Exposure Assessment," *German Microwave Conf. (GeMIC)*, 2024.
12. B. Derat, M. Erkocevic and G. Hamberger, "Reconstruction of Near-Field Millimeter-Wave Power Density from Over-The-Air Measurements," *IEEE Conf. on Antenna Meas. & Applications (CAMA)*, 2021.
13. F. Bette et al., "Monostatic to Bistatic Equivalence Theorem for 2-Dimensional Reflection Pattern Measurements of Reconfigurable Intelligent Surfaces," *Antenna Meas. Tech. Asso. Symp. (AMTA)*, 2025.
14. B. Derat et al., "Over-The-Air Group Delay Measurements of Frequency-Converting Devices Using a Harmonic Phase Reference," *Antenna Meas. Tech. Asso. Symp. (AMTA)*, 2025.

Unclogging the Wireless Pipeline: Tackling Network Congestion with ISAC and RIS

Houman Zarrinkoub
MathWorks, Natick, Mass.

Network congestion is a constant challenge in wireless communications, from 1G to the forthcoming 6G. As the number of connected devices skyrockets, the limited available bandwidth must be allocated judiciously to allow for higher network capacity and speed. Recently, two advancements have emerged with the most promising ways to address this challenge: integrated sensing and communication (ISAC) and reconfigurable intelligent surfaces (RIS). Individually or combined, ISAC and RIS can enhance capacity, reduce congestion and provide improved user experiences, as demonstrated in ***Figure 1***.

Fig. 1 ISAC and RIS enable wireless signal paths to connect users across the urban landscape.

UNDERSTANDING ISAC AND RIS

ISAC provides the network operator with more intelligence about users. ISAC enables efficient reuse of resources, including hardware and waveforms, to combine the sensing and communication functions. The same equipment that offers communication services can also sense the environment, providing valuable data about user locations and movements. Access to this data enhances the user experience by allowing the network to communicate optimally with users.

RIS, on the other hand, addresses the problem of signal blockage and low signal power, especially in high-density urban settings. RIS allows RF signals' reflections to be reconfigured based on the location of the user. Once the user's location is determined, RIS manipulates the signals' phase, amplitude and polarization to direct them toward specific users. This capability en-

sures signals reach their intended audience, even in environments with obstacles, such as dense foliage, tall buildings in urban areas or indoor settings with multiple walls and partitions.

THE SYNERGY OF ISAC AND RIS

The real power of ISAC and RIS lies in their synergy. ISAC's sensing capabilities can inform RIS on how to best direct signals. RIS uses the data ISAC provides to minimize interference and ensure each user receives the strongest possible connection. Adjusting signal paths in real-time helps alleviate network congestion and optimize available bandwidth by steering signals around obstacles and directing them toward users.

One key advantage of coupling ISAC and RIS is their economic viability. These technologies do not require new base stations, with minimal new hardware and investment needed. Instead, engineers can integrate them into existing network setups and avoid major infrastructure changes. ISAC uses existing base station setups, simply enhancing their operation with sensing capabilities. While RIS requires some investment in metasurfaces, the overall hardware investment is significantly lower than deploying new base stations or overhauling existing network infrastructure.

POTENTIAL USE CASES FOR ISAC AND RIS

The combination of ISAC and RIS is promising for addressing network congestion and enhancing connectivity in a variety of applications, including broadband wireless communications, autonomous vehicles and smart manufacturing.

Broadband Wireless Communications

In urban environments where obstacles cause signal deterioration, ISAC and RIS overcome these challenges to enable robust, high speed internet access. ISAC gathers intelligence about user locations and movements to optimize signal delivery. RIS uses building surfaces with reconfigurable elements that alter signals to overcome blockages and enhance connectivity based on the user locations ISAC provides.

Autonomous Vehicles

In autonomous vehicle operation, ISAC offers customized communication services that enable precise and reliable communication for real-time decision-making. RIS allows engineers to manipulate the environment, ensuring the signal is focused only where needed. Using ISAC and RIS in autonomous vehicle communication supports safe and efficient operations by reducing accidents and improving traffic flow.

Smart Manufacturing

Smart manufacturing relies on efficient communication and sensing to optimize production processes and improve operational efficiency. ISAC and RIS technologies facilitate these goals by enabling real-time data exchange and environmental monitoring within manufacturing facilities. ISAC's sensing capabilities provide detailed insights into machine operations and environmental conditions, while RIS ensures reliable connectivity by dynamically adjusting signal paths to avoid interference. This combination enhances the flexibility and responsiveness of manufacturing systems, allowing for more efficient resource utilization and reduced downtime, even in highly congested industrial environments.

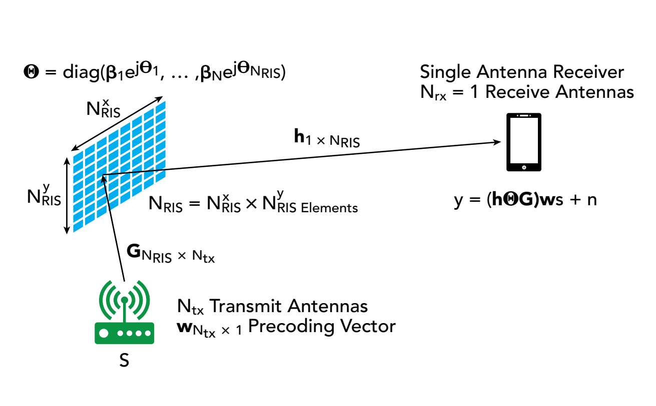

Fig. 2 **RIS scenario example.**

BEST PRACTICES IN ISAC AND RIS DEPLOYMENT

Engineers should employ various best practices, including environmental modeling, custom waveform development and advanced algorithm and hardware implementation, to effectively deploy ISAC and RIS into modern communication systems. Precise modeling and simulation of the propagation environment are crucial for successful ISAC deployment. Any errors during modeling propagate and affect the final design. Path loss, multipath and signal reflection must all be accurately modeled to optimize performance and system efficiency. Additionally, it is essential to use ray tracing to model the wireless channel by simulating the reflection, refraction and diffraction of electromagnetic waves in the environment. Ray tracing requires extreme precision as it is susceptible to atmospheric effects. Modeling and simulation are vital because the accuracy of the propagation environment directly affects waveform effectiveness.

RIS SYSTEM MODEL EXAMPLE

Here is an example using the MATLAB 6G Exploration Library for 5G toolbox that simulates a RIS channel using two concatenated clustered delay line (CDL) channel models and provides an iterative algorithm to control the phases of each RIS element. It then sends a 6G-like signal through the RIS channel and displays the constellation of the received signal. ***Figure 2*** models this scenario example. An Ntx-antenna transmitter sends a complex symbol s using a precoding vector w of size $Ntx \times 1$. The example assumes there is no line of sight between the transmitter and the receiver. An $NRIS = NxRIS \times NyRIS$-element RIS reflects the transmitted signal towards a single antenna receiver. $NyRIS$ and $NxRIS$ are the numbers of elements per row and column, respectively, in the RIS. The signal is affected by the channel matrix G of size $NRIS \times Ntx$, which models the channel between the transmitter and the RIS. The ith element of the RIS causes an amplitude and phase

change to the impinging signal, which is modeled by the complex number $\beta_i e^{j\theta_i}$. The reflected signal then travels towards the receiver through a channel modeled by a matrix h of size $1 \times N_{RIS}$. The received signal y is affected by noise n.

The example models both the channel between the transmitter and the RIS and the channel between the RIS and the receiver using CDL channels. To model the RIS, the example applies a phase rotation θ_i to each RIS element between both CDL channels. An iterative algorithm calculates the value of the phase shifts θ_i assuming knowledge of channel matrices G and h. This example also models path loss and RIS scattering loss. Where appropriate, the example uses parameters as defined in the group report from ETSI on RIS.[1] This example models the RIS with a stochastic channel model.

ISAC EXAMPLE USING 5G WAVEFORM

This example, using the MATLAB 5G Toolbox and Phased Array System Toolbox, simulates data frame transmissions through the physical downlink shared channel (PDSCH) of a 5G New Radio (NR) link and shows how the channel matrix estimates obtained from the received frames can be processed to extract radar measurements of moving scatterers present in the channel. Recent research has explored various ISAC approaches, ranging from the joint design of dual-function systems to enabling sensing capabilities within existing wireless networks.

The example illustrates how sensing can be effectively accomplished using a 5G NR waveform, as defined by the 3GPP NR standard. Channel matrix estimates obtained from received PDSCH frames inherently capture information about the time delays and Doppler shifts experienced by the transmitted waveform as it travels to the receiver. By processing this information, in a manner akin to standard radar data cube techniques, these time delays and Doppler shifts can be translated into the positions and velocities of the corresponding scatterers, thereby forming radar detections.

The example begins by defining an ISAC scenario with a single transmitter and a single receiver, where the transmitter represents a base station and the receiver models user equipment. It then configures the transmitted 5G NR waveform, illustrating that the selection of demodulation reference signal parameters is directly related to the desired sensing performance. The example proceeds by simulating the propagation of PDSCH frames through a scattering MIMO channel. For each received frame, the channel matrix is estimated and then processed to detect moving scatterers present in the channel. The example demonstrates that from the sensing perspective, the modeled 5G link is a bistatic radar capable of measuring bistatic range and angle-of-arrival of the targets. Finally, these measurements are passed to a tracking algorithm to form target tracks and

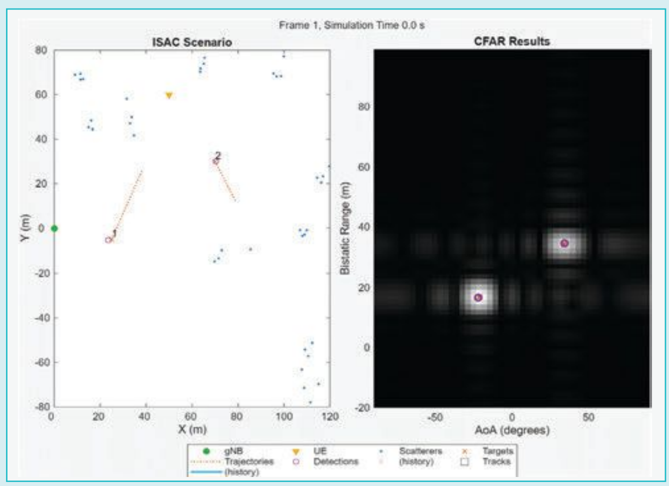

Fig. 3 ISAC example results.

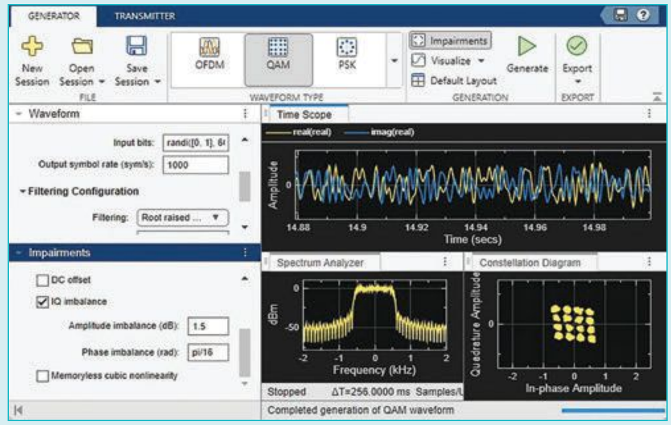

▲ Fig. 4 **Generating custom waveforms using the Waveform Generator app in MATLAB.**

estimate target positions and velocities in Cartesian coordinates, with the results shown in ***Figure 3***.

Wireless communication waveforms based on industry standards cannot be used in ISAC and RIS design. Instead, engineers must design custom waveforms to enable sensing and communication to work together seamlessly. Engineers can use the Wireless Waveform Generator app in MATLAB® to generate standards-based waveforms, as shown in ***Figure 4***. Carefully designed waveforms enable ISAC and RIS to achieve high-resolution sensing and maintain robust communication links. When it comes time to deploy ISAC and RIS systems, their success hinges on both the waveform design and the sophisticated algorithms and hardware solutions that manage the complex computations needed for accurate sensing and communication.

Deploying ISAC and RIS technologies requires developing efficient algorithms and advanced hardware solutions to ensure reliable real-time performance. Engineers must implement the algorithms primarily on field-programmable gate arrays (FPGAs) because of their high speed processing capabilities, but this puts a burden on the real-time performance of the FPGAs. Therefore, the algorithms implementing ISAC and RIS must be optimized using FPGA-ready IP blocks.

ISAC AND RIS IN 6G AND BEYOND

As the era of 6G wireless communications draws closer, the challenge that network congestion presents grows with every passing day. The integration of ISAC and RIS has the potential to transform many industries by enabling simultaneous sensing and communication while optimizing signal propagation and coverage. Their economic viability makes them even more attractive as they offer solutions that take advantage of existing infrastructure without extensive overhauls. As engineers push the boundaries of 6G wireless communications and beyond, the synergy of ISAC and RIS will play a central role in shaping tomorrow's wireless networks. ■

Reference

1. "Reconfigurable Intelligent Surfaces (RIS); Communication Models, Channel Models, Channel Estimation and Evaluation Methodology," *ETSI*, GR RIS 003 V1.1.1.

New Software for 5G Device Verification

Anritsu
Morgan Hill, Calif.

Developing and testing 5G devices in accordance with 3GPP standards and regulatory agencies is becoming increasingly complex. From multiple frequencies extending into mmWave and greater bandwidth requirements, to antenna arrays and high speed chipsets in compact packages, performance verification is essential. Anritsu has introduced two software solutions for its radio communication test station MT8000A to address the challenges associated with verifying the RF performance of 5G devices.

The new software options support key technologies specified in 3GPP Release 17, including 1024-QAM modulation for downlink (DL) and Tx switching 2Tx to 2Tx for uplink (UL), enabling accurate and flexible evaluation of 5G devices with enhanced transmit/receive (TRx) performance. They create a flexible solution to conduct necessary RF tests efficiently and accurately (see ***Figure 1***).

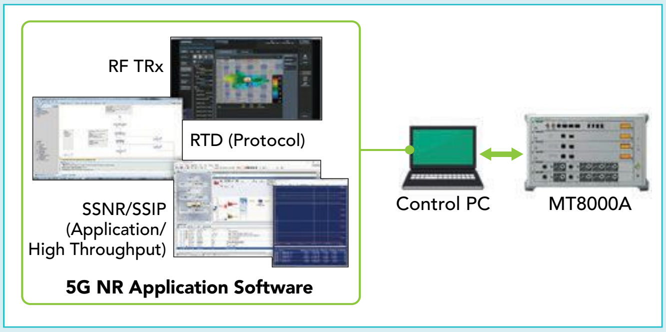

Fig. 1 **Anritsu software for verification of 5G devices.**

The NR DL 1024-QAM MX800010A-022 software enables RF testing for DL 1024-QAM modulation. It delivers significantly higher data rates and spectral efficiency than 256-QAM by encoding more bits per symbol, but it requires a much stronger signal-to-noise ratio and is more susceptible to interference and noise. The NR UL Tx switching 2Tx to 2Tx MX800010A-019 software supports RF testing for UL transmission switching technology.

Dynamic switching between multiple antennas based on communication conditions can be done through the software to ensure stable and high speed transmission performance. Easy-to-change parameter settings are also supported by the MX800010A software to simplify RF performance tests.

EMERGING 5G USE CASE SUPPORT

Anritsu has developed these two software options to address new 5G use cases, such as augmented/virtual reality (AR/VR), 8K video and live streaming, as they require a test environment that can evaluate the Tx and Rx performance of 5G devices. These technologies will utilize frequency range (FR) 1 sub-6 GHz frequency bands and pose complex design and test challenges.

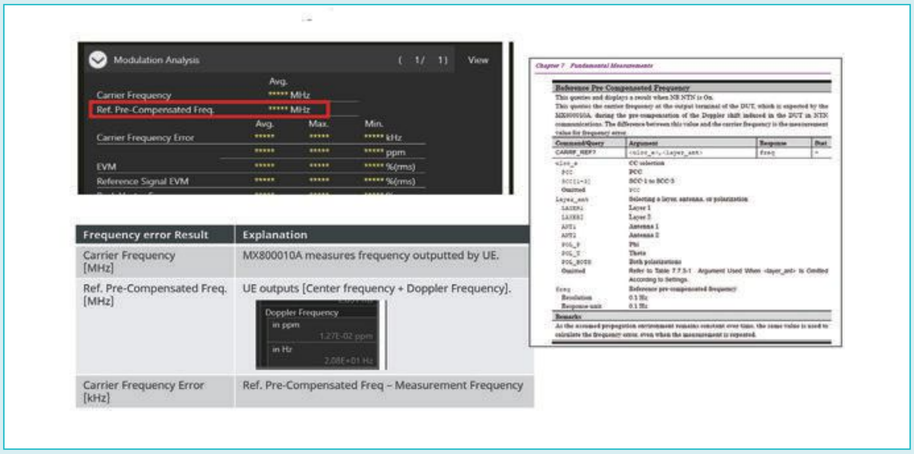

Fig. 2 **GUI for easy-to-understand results based on 3GPP NR NTN standards.**

Fig. 3 **The radio communication test station MT8000A.**

The MX800010A software now also supports 5G NR non-terrestrial network (NTN) measurements. Signals between low Earth orbit satellites used in NTNs are subject to propagation delays and the Doppler effect. The MX800010A measures the shifted frequency as carrier frequency to ensure 5G devices are performing according to 3GPP NR NTN standards using a simple GUI that creates straightforward displays, as shown in ***Figure 2***.

FLEXIBLE PLATFORM SUPPORT

The MX800010A expands the overall capability of the MT8000A, a modular platform that supports a wide range of RF, microwave and mmWave testing. It can be used for 5G, LTE and other wireless standard validations by providing all-in-one support for RF measurements, protocol tests and applications tests in FR1 and FR2 mmWave bands.

When the software is installed in the MT8000A, it can be used with an over-the-air (OTA) chamber to conduct mmWave RF measurements and beamforming tests using call connections specified by 3GPP. OTA tests are essential because the TRx performance of mobile devices is influenced by factors such as the terminal form and antenna characteristics.

Anritsu's compatible OTA solutions extend MT8000A capabilities across diverse use cases aligned with CTIA and 3GPP test specifications. The MT8000A is listed on CTIA's authorized equipment list for 5G FR2 OTA testing and validated for 3GPP FR2 OTA RF conformance testing.

In addition to mmWave 5G TRx tests, the MX800010A enabled MT8000A can evaluate antenna characteristics. The two OTA antenna tests that can be conducted in this configuration are total radiated power and total radiated sensitivity.

The software can also be used to conduct specific absorption rate tests to determine the amount of energy in the electromagnetic spectrum radiated from the 5G UE. The test helps protect mobile device users from electromagnetic waves based on national and regional regulations and standards.

CONTROLLING COST-OF-TEST

The MX800010A is part of Anritsu's software-based approach that helps control the cost-of-test of 5G devices. The MT8000A, as shown in ***Figure 3***, is a flexible hardware platform that allows for easy integration of software into the analyzer. Other key tests on various technologies can be integrated into the MT8000A with specific software and modules, allowing for a solution that addresses the need to test legacy technologies, as well as an efficient upgrade path to support future standard development and regulatory requirements.

For example, the new MX800010A software supports a 5G non-standalone (NSA) mode that can be used in conjunction with Anritsu's radio communication analyzer MT8821C as an LTE anchor or the LTE anchor can reside on the MT8000A. NSA call connection and RF tests can be performed in this configuration so that legacy tests can be done. The MT8821C can also operate standalone for NTN NB-IoT measurements.

EASE-OF-USE

The new MX800010A software comes with a GUI to create a comprehensive, user-friendly platform for RF signal testing and measurement. It provides an intuitive interface to simplify performing various measurements, analyzing RF signals and managing test results. MX800010A also integrates with specified OTA chambers, allowing scripting with third-party tools.

When used with the MT8000A, the MX800010A GUI enables streamlined and efficient testing of 5G devices. The GUI controls measurements and configures tests easily for all 3GPP and CTIA RF tests supported by the software, such as spectrum analysis, channel power measurement and modulation accuracy.

The platform supports the creation of test setups based on standards, allowing the MT8000A/MX800010A solution to comply with ever-changing test parameters. All tests can be automated for one-button testing and repeatable results, regardless of who is performing the tests.

Anritsu Company
Morgan Hill, Calif.
www.anritsu.com

67 GHz SPnT Coaxial Switch for Upper V-Band and Next-Gen Wireless

Teledyne Relays introduces the CCR/CCT-39V, a 67 GHz single-pole multi-throw (SPnT) coaxial switch designed for upper V-Band test and development. As networks add multi-Gbps fixed-wireless links and labs ramp mmWave research toward 6G, engineers need repeatable, low loss routing that preserves error vector magnitude and dynamic range across many automated paths.

The CCR/CCT-39V is outfitted with 1.85 mm-f connectors and is engineered for 1.70 dB maximum insertion loss at 67 GHz, 50 dB minimum isolation at 67 GHz and long-life repeatability of 2 million cycles. The switch has a characteristic impedance of 50 Ω and a switching time of 20 ms. These specs enable accurate measurements in over-the-air (OTA) chambers, link validation stands and high-throughput benches. The CCR/CCT-39V is offered in SP4T and SP6T configurations.

Positioned above Teledyne's widely used 18 to 52 GHz portfolio for 5G FR1/FR2, the 67 GHz SPnT switch extends coverage through the upper V-Band for applications such as V-Band backhaul/FWA link testing, harmonics and spur studies, WiGig/802.11ad/ay device characterization and OTA beam experiments. It also provides a practical on-ramp to early 6G mmWave research and development, aligning with ecosystems that sit adjacent to E-Band instruments and frequency-extender front-ends.

Teledyne complements the 39V with a broad switching portfolio that includes SPDT, SPnT, transfer and 2P3T devices, along with matrix boxes that consolidate multiple paths into compact, serviceable enclosures. Together, these solutions enable engineering teams to scale from today's 5G workflows to tomorrow's higher frequency experiments without compromising measurement fidelity.

Teledyne Relays
Hawthorne, Calif.
www.teledyne-ade.com/relays

A Dual Polarized 28 GHz Phased Array

As 5G/6G research accelerates worldwide, the demand for scalable, synchronized and versatile phased array platforms is increasing in turn. To address this need, TMYTEK introduces the BBox™ 8×8 Duo, a dual polarized (2-Pol) 28 GHz IF-ready phased array antenna system designed to empower innovation in advanced wireless testing and prototyping.

The BBox™ 8×8 Duo integrates 64 antenna elements with dual-orthogonal polarization, delivering up to 50 dBm EIRP. Its 1 µs beam switching capability and steering range of ±60 degrees azimuth and ±30 degrees elevation serve applications including real-time beamforming, mobility testing and dynamic research environments. With an IF input/output architecture, the phased array connects to software-defined radios (SDRs) and test instruments, bridging the gap between simulation and practical FR2 experimentation.

Synchronization has been optimized for multi-device MIMO configurations, ensuring precise timing across distributed setups. This capability makes the BBox™ 8×8 Duo suitable for applications in massive MIMO, hybrid beamforming and JCAS/ISAC research. Control flexibility is provided through a ready-to-use GUI and APIs for Python, MATLAB and LabVIEW.

Key applications include FR2 MIMO prototyping and validation, OAI and O-RAN-compatible SDR testbeds and 6G joint communication and sensing experiments. The phased array also supports NLOS beam tracking and RIS-enabled mobility testing.

By combining dual polarization, 50 dBm EIRP, sub-microsecond beam switching and FR2 band support (26 to 29 GHz), the BBox™ 8×8 Duo provides a robust and scalable building block for academia and industry. It accelerates the path from prototype to real-world deployment, enabling the wireless community to explore and realize the potential of 5G, 6G and beyond.

VENDORVIEW

TMY Technology, Inc.
New Taipei City, Taiwan
https://tmytek.com/

SN0916 16-PORT 9 GHZ ANALYZER

VENDORVIEW

SN0916 is a versatile 9 GHz multiport solution with excellent dynamic range (140 dB typical) and measurement speed (24 µs). This VNA enables dependable, accurate testing of various DUTs: multiport antennas, integrated circuits, switches, interconnects, cable assemblies, diplexers, etc. SN0916 has a streamlined calibration process for reduced test times. The hardware can fit 19 in. rack and utilizes robust, durable port connectors with ergonomic positioning for simplified cable connection. Additional models are available in 6-, 8-, 10-, 12- and 14-port configurations.

Copper Mountain Technologies
www.coppermountaintech.com

DUAL-RIDGED BROADBAND HORN ANTENNA

VENDORVIEW

Eravant's SAV-1431141129-1F-S1 is a dual-ridged broadband horn antenna with a 1.0 mm connector that covers 14 to 110 GHz with 11 dBi gain. It includes a bubble level for alignment and L-shaped bracket for tripod mounting. It is ideal for broadband gain and pattern measurements in antenna ranges.

Eravant
www.eravant.com

YOUR PARTNERS IN 6G TESTING

While 6G standards continue to evolve, ETS-Lindgren is already developing solutions to prepare customers for 2030 — and beyond. They are supporting early 6G research with advanced test environments, precision measurement systems and next-gen OTA validation tools. With a proven track record across every generation of wireless, ETS-Lindgren empowers researchers, developers and manufacturers to accelerate breakthroughs and stay ahead of the curve. ETS-Lindgren remains committed to a smarter, more connected future.

ETS-Lindgren
www.ets-lindgren.com

MMWAVE SURFACE-MOUNT CAPACITORS

KYOCERA AVX introduces the new 500 S Series Broadband Microwave Capacitor. This unique, patented component greatly exceeds both multilayer and single-layer capacitor performance. It delivers extremely low insertion loss with ultra-high self-resonance performance, in a rugged, laser-marked package compatible with automatic SMT manufacturing. Broadband mmWave functional applications include bypass, coupling/DC blocking, phase compensation, impedance matching and tuning.

KYOCERA AVX
www.kyocera-avx.com

HIGH SPEED MULTI-COAX CABLE ASSEMBLIES

VENDORVIEW

The MIcable 70/90 GHz high speed multi-coax cable assemblies feature a solderless spring-load contact design, effectively ensuring the connection reliability of multi-channel contacts, stability in electrical performance and ease of maintenance and replacement. The products have excellent electrical performance in low VSWR, low loss, high delay and phase matching accuracy and excellent amplitude consistency. With a single-row contact pitch of 2.5 mm and double-row pitch of 3.0 mm, it offers high density and space-saving. They're ideal choices for applications such as signal integrity measurement, differential signal measurement, SERDES development and automated testing.

MIcable Inc.
www.micable.cn

SERIES 955 – 5G BROADBAND POWER AMPLIFIER

The Series 955 is a high performance broadband power amplifier engineered for next-generation 5G, radar and advanced communication systems. Operating over a wide 20 to 54 GHz frequency range, it delivers exceptional performance with a typical gain of 45 dB, P1dB of +30 dBm and saturated output power (Psat) of +31.5 dBm across the band. Designed for reliability and efficiency, the Series 955 ensures high linearity and stable power output, making it ideal for demanding high frequency applications and high speed data transmission systems.

Millimeter Wave Products, Inc.
www.miwv.com

WIRELESS INSITE® 4.0

VENDORVIEW

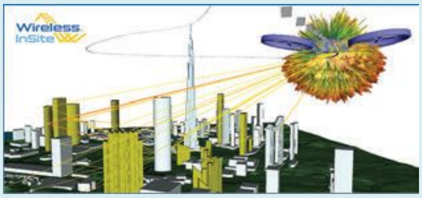

Remcom has introduced Wireless InSite® 4.0, the latest version of its 3D wireless prediction software. The release adds time-based mobility for modeling dynamic RF environments, lunar propagation capabilities supporting NASA's Artemis mission and advanced wideband ray-tracing with S-parameter outputs. Engineers can evaluate mobile scenarios with precision, simulate RF propagation on lunar terrain and analyze multi-technology systems with frequency-dependent accuracy. Wireless InSite 4.0 delivers high-fidelity performance insights for terrestrial, non-terrestrial and on-body communication systems.

Remcom
www.remcom.com

VOLTAGE-CONTROLLED SAW OSCILLATOR

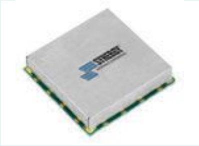

Model HFSO2000-5 is a unique ultra-low phase noise voltage-controlled SAW oscillator ideal for applications in high-quality phase locked sources for single frequency applications. This distinctive VCO product is a vital signal source for radar, test instruments and as clocks in high speed ADC and DDS. This free running VCO operates at 2000 MHz, with +5 V supply, typical tuning range of 500 kHz and phase noise -138 dBc/Hz at 10 kHz offset and operates from -20°C to +70°C.

Synergy
www.synergymwave.com

Miniaturized High-Power Broadband Tunable Harmonic Filter Bank

Tri-TeQ
Framingham, Mass.

Modern communication systems often need compact high-power filters to reject amplifier harmonic signals. Traditional fixed filter banks are large and bulky, as they frequently rely on multiple fixed filters and switches to cover the entire frequency range, which adds to the size and complexity. Tri-TeQ's patented tunable harmonic switched filter banks (THSFBs) address these issues by reducing the number of filters and switches through tunability. Power handling and performance are maintained while the unit footprint is reduced to less than a quarter the size of related products.

Tri-TeQ offers 10 W, 20 W, 50 W, 100 W and 125 W THSFBs, all of which feature proprietary techniques for power handling and size reduction. Tri-TeQ's flagship TH-112 unit, shown in ***Figure 1***, features 100 W CW power handling with 10 harmonic filter bands, in a package size that is 75 percent smaller than competing designs with similar power handling and electrical performance. A typical application for this THSFB is filtering transmit harmonics of the final power amplifier (PA) stage in broadband multi-octave military hopping radios.

Fig. 1 **TH-112 tunable harmonic switched filter bank (3.3 x 2.5 x 0.72 in.).**

MINIATURIZATION TECHNIQUES

The basis of the harmonic switched filter bank (HSFB) is a lowpass filter. The lowpass filter passes the fundamental frequency and rejects all the harmonic signals at a frequency of an octave and higher. If the PA operates over a multi-octave frequency range, then multiple lowpass filters will be required. The filters switch between each band corresponding to the frequency at which the PA is functioning.

Most traditional HSFBs use single-pole multiple-throw (SPnT) switches at the input and output of the unit. Often, they have at minimum a single-pole 6-way switch for a


iNRCORE®
FAMILY OF BRANDS
You CAN'T Build Without iNRCORE
01005
0201
0402
0603
0805
SIGNAL
Ethernet, Transceiver Modules, MIL-STD-1553, Data Bus Couplers, Baluns, Delay Lines
CAPACITORS
High-Q/Low ESR Multi-Layer Ceramic, Broadband, Single Layer, Thin Film, Variable
FILTERS
Bandpass, High Pass, Low Pass, Notch, EMI/RFI, Bias Tee, Amplitude Equalizer, Diplexers/Multiplexers
INDUCTORS
Conical, Ceramic Chip, High Frequency, High Q, Planar, Toroidal, CMC, THT, SMT, MIL-STD-981, MIL-PRF-27
PL8201
1925
PL10302
1925
100B-4009
1921
1000B-5012X
1921
1000B-5003X
1921
X-1644NL
1921
For more information
SCAN HERE!
ISO 9001 CERTIFIED
AS9100 CERTIFIED
ITAR Registered
www.iNRCORE.com
+1-215-781-6400

ProductFeature

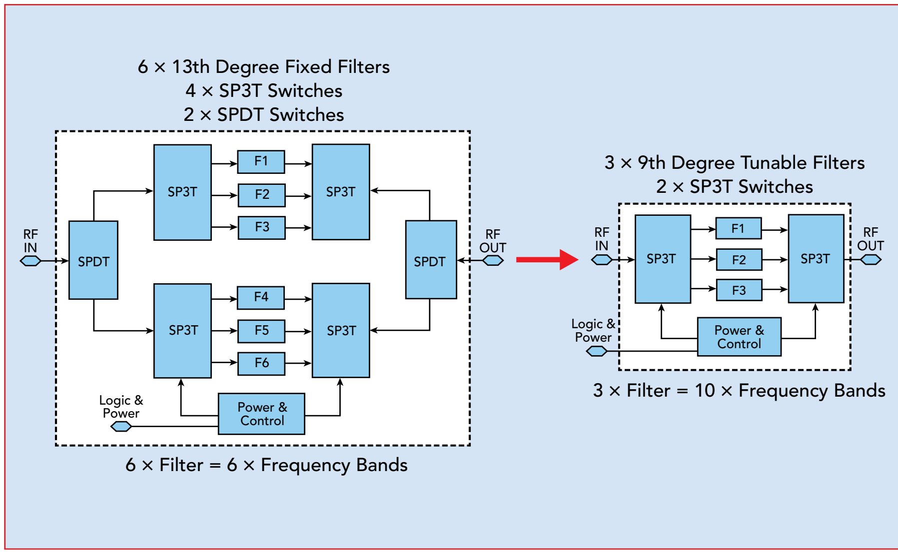

Fig. 2 Simplified depiction of size reduction implementation.

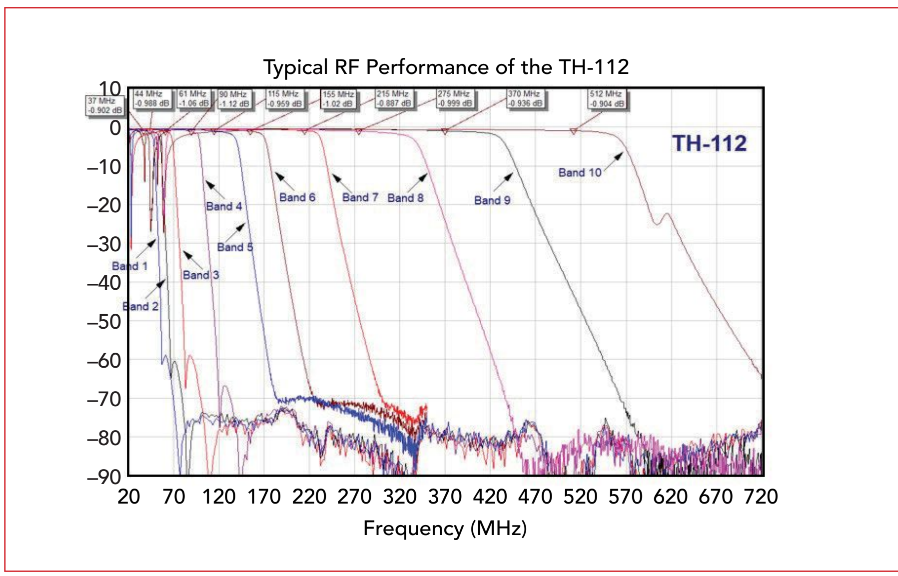

Fig. 3 Typical TH-112 performance.

30 to 512 MHz coverage, with a high-power lowpass filter in each of the six arms of the switch, as demonstrated in ***Figure 2***. These units are enclosed within a housing with heat sinks. Tri-TeQ's THSFB offers a reduced number of switches and filters by making each filter tunable. By reducing the number of filters from six to three, the three tunable filters are formed to create 10 bands. Fewer switches and filters make the filter topology simpler. Additionally, by having 10 bands rather than six, the selectivity required from each filter is reduced from 15 percent typical to 45 percent, allowing for lower-order filters, reducing the insertion loss (IL), particularly at the passband edge, shown in ***Figure 3***. A reduction in IL also leads to decreased power dissipation, which minimizes thermal challenges and eliminates the need for extensive heat sinking, further reducing size. The TH-112 has a greater than 75 percent reduction in footprint and a larger reduction in volume when compared to current parts of the same class, without sacrificing harmonic rejection and with improved IL (see ***Table 1)***. Additionally, THSFBs require fewer control lines and control schemes, making integration and operation easier.

Reducing switches and using lower degree filters significantly decreases the bill of materials. Fewer and lower degree filters also

TABLE 1

KEY TH-112 PERFORMANCE PARAMETERS

Parameter	Performance
Frequency Range	30 to 512 MHz
Input/Output Impedance	50 Ω
Insertion Loss	1.2 dB Maximum (0.9 dB Typical)
Number of Bands	10+ Off State
Stop Band Rejection	60 dB Minimum
Frequency Switching Time (Sub Bands)	< 15 µs
Frequency Switching Time (Between Sub Bands)	< 70 µs
In Band RF Power	100 W CW
Peak Power	200 W and 5% Duty Cycle with 1 ms Pulse Width
Peak Power (Off State)	+15 dBm
DC Power	+5.0 V +/- 0.5 V < 350 mA
Control	4-line TTL

TABLE 2

KEY ADVANTAGES OF THSFB OVER FIXED HSFBS

Parameter	Advantages of Creating THSFB for Harmonic Suppressions
Size and Weight	Size Reduction of 75% and > 50% weight reduction.
Performance	Lower degree filters, reduced switch count and filter selectivity lead to reduced IL, particularly at the passband edge.
Heat Dissipation	Improved IL allows for simpler thermal management. No complex and bulky heat sinking required.
Control Complexity	Simpler.
Cost	Reduced BOM count and faster tuning time equate to reduced unit cost.

reduce the build and tune time, equating to reduced hours spent working on the unit, all of which enables a reduction in the unit cost and lead time, while still enabling improved reliability and consistency over traditional methods.

TH-112 FILTER PERFORMANCE AND THSFB ADVANTAGES

The technology employed within the current range of Tri-TeQ's THSFBs can be adapted to other frequency ranges and numbers of bands for user-specific applications. The current units with power handling of 50 W or below are available in either SMA or surface-mount packages.

Converting a traditional HSFB into a tunable form reduces unit size, complexity and cost, while enhancing performance (see ***Table 2***). Tri-TeQ welcomes any questions regarding the products highlighted, as well as collaboration and inquiries for custom adaptations of these THSFBs.

Visit www.tri-teq.com or contact info@tri-teq.com for more information.

Tri-TeQ
Framingham, Mass.
www.Tri-Teq.com

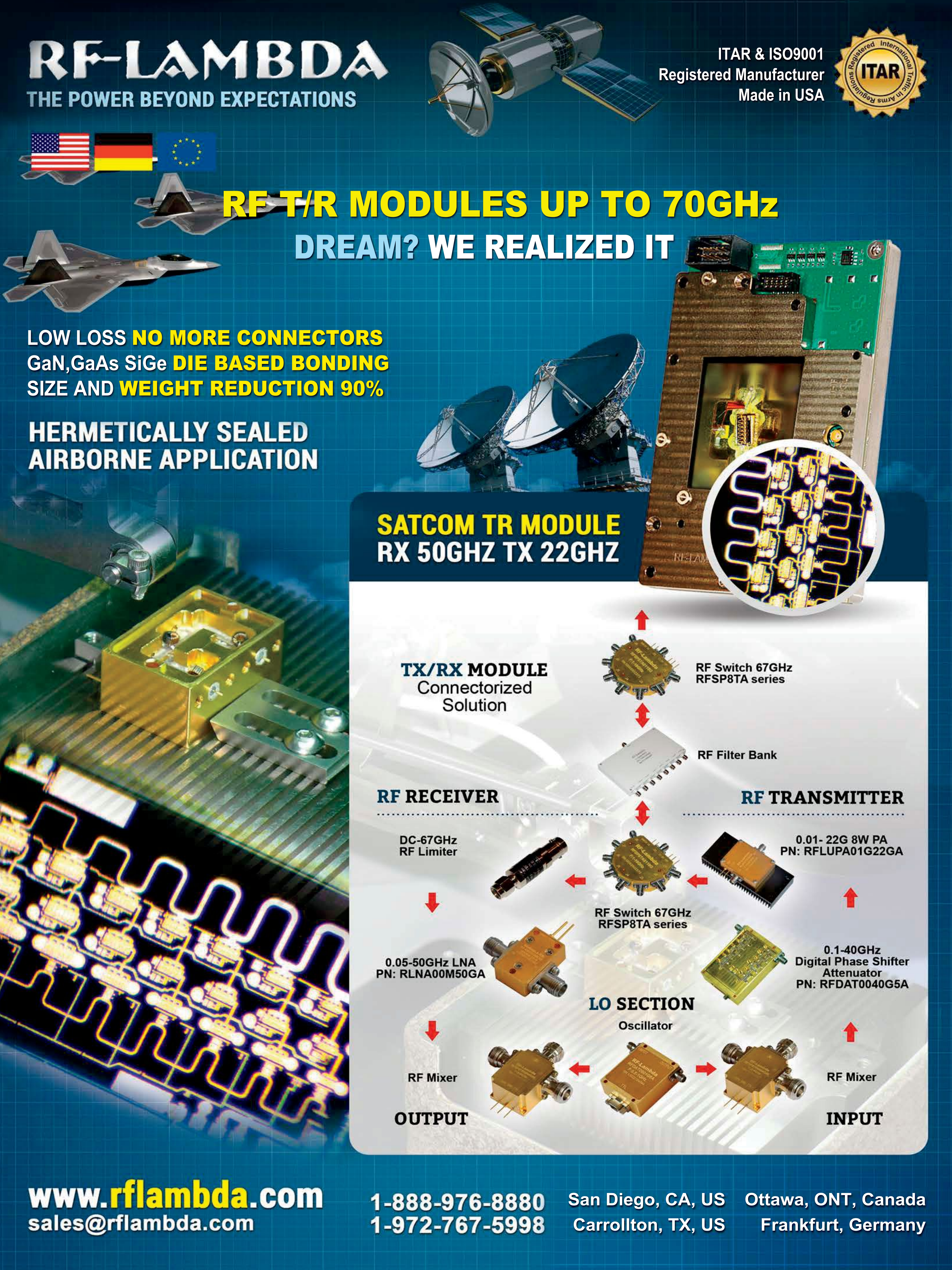
RF-LAMBDA
THE POWER BEYOND EXPECTATIONS
ITAR & ISO9001
Registered Manufacturer
Made in USA
ITAR
Registered International Traffic in Arms Regulations
RF T/R MODULES UP TO 70GHz
DREAM? WE REALIZED IT
LOW LOSS NO MORE CONNECTORS
GaN,GaAs SiGe DIE BASED BONDING
SIZE AND WEIGHT REDUCTION 90%
HERMETICALLY SEALED
AIRBORNE APPLICATION
SATCOM TR MODULE
RX 50GHZ TX 22GHZ
TX/RX MODULE
Connectorized
Solution
RF Switch 67GHz
RFSP8TA series
RF Filter Bank
RF RECEIVER
RF TRANSMITTER
DC-67GHz
RF Limiter
0.01- 22G 8W PA
PN: RFLUPA01G22GA
RF Switch 67GHz
RFSP8TA series
0.05-50GHz LNA
PN: RLNA00M50GA
0.1-40GHz
Digital Phase Shifter
Attenuator
PN: RFDAT0040G5A
LO SECTION
Oscillator
RF Mixer
RF Mixer
OUTPUT
INPUT
www.rflambda.com
sales@rflambda.com
1-888-976-8880
1-972-767-5998
San Diego, CA, US
Carrollton, TX, US
Ottawa, ONT, Canada
Frankfurt, Germany

TechBrief

17 Watt Ka-Band GaN Power Amplifier in QFN Package

Nxbeam expands its MMIC product portfolio with the release of a new GaN Ka-Band QFN packaged power amplifier. The NPQ2107-SM operates from 27.5 to 31 GHz and provides an average saturated output power of 17 W, average power-added efficiency of 29 percent and average linear gain of 22 dB. For linear power, the part provides > 9 W output power at a spectral regrowth of -30 dBc for a QPSK modulated signal (10 MSPS, Alpha = 0.2). The part comes in a QFN package, making it easy to integrate into any system.

The output power level of this MMIC makes it suitable for satellite communications ground terminals as well as point-to-point communication links. The part can be used as a driver amplifier or can be easily power combined to achieve higher output power levels given its superb output return loss of greater than 10 dB.

The design incorporates three independently controlled amplifier stages and is designed to offer customers flexibility to tailor linear power performance over a variety of modulations and use cases.

The RF input and RF output are matched to 50 Ω with DC blocking capacitors for easy system integration.

Since 2018, Nxbeam has been developing high performance GaN power amplifier MMICs and higher-level products for the satellite and terrestrial communications markets. Nxbeam's mission is to deliver the next generation of wireless communication infrastructure products to power the future of information communication technology.

VENDORVIEW

Nxbeam Inc.
Huntington Beach, Calif.
www.nxbeam.com

WirelessPro Introduction

Learn about Keysight's WirelessPro 3GPP AI Simulation Platform, a next-generation software platform designed to meet the evolving needs of wireless communication system engineers.

Keysight Technologies, Inc.

www.keysight.com/us/en/assets/6125-1233/videos/WirelessPro-Introduction.mp4

FR2 Signal Generation Signal Chain using Apollo MxFE

This demonstration highlights a complete wide-band spectrum analyzer signal chain that supports the emerging 6G FR3 band with instrument grade error vector magnitude (EVM) performance of < -50 dB.

Analog Devices

www.analog.com/en/resources/media-center/videos/6355243008112.html

Engineering the Future of Wireless: Inside the Promise and Power of Wi-Fi 8

To help navigate the intricacies of Wi-Fi 8 and its implications for design engineers, Qorvo Connectivity Product Line Directors Kevin Gallagher and Wayne Polonio share their expert insights on what engineers can expect from Wi-Fi 8 and how it will shape the future of wireless networking.

Qorvo

www.qorvo.com/design-hub/blog/engineering-the-future-of-wireless-inside-the-promise-and-power-of-wifi-8

How AI Takes LEO Satellite Communication to the Edge

RFMW Technical Marketing Manager Dan Loomis covers how and why AI and satellite integration matter.

RFMW

https://rfmwblog.com/2025/09/15/how-ai-takes-leo-satellite-communication-to-the-edge/

Precision in Under 5 Minutes: How to Detect RF Interference

RF interference poses a real challenge for operators by disrupting networks and reducing spectrum reliability. In this episode, Masha demonstrates how to detect, locate and analyze interference using the R&S®FPH Handheld Spectrum Analyzer.

Rohde & Schwarz

www.youtube.com/watch?v=Zjd65GGI_Lc

VNA400: Precision Perfected with Rigorous Calibration!

This in-depth exploration showcases how the VNA400 sets new standards in RF engineering and comprehensive signal analysis.

Signal Hound

www.youtube.com/watch?v=qm9Q6xMHBM0

NEW PRODUCTS

FOR MORE NEW PRODUCTS, VISIT WWW.MWJOURNAL.COM/BUYERSGUIDE
FEATURING VENDORVIEW STOREFRONTS

DEVICES/ COMPONENTS/MODULES

Small Steps, Massive Performance

VENDORVIEW

The ADRF5702 is a high-performance 8-bit digital attenuator, delivering a wide 31.875dB attenuation range with ultra-fine 0.125dB step resolution. Built on advanced silicon-on-insulator (SOI) technology, it covers an impressive 50MHz to 20GHz bandwidth, while maintaining a low insertion loss under 2.6dB and outstanding attenuation accuracy over temperature.

Analog Devices
www.analog.com

4×4 Butler Matrix

VENDORVIEW

KRYTAR, Inc. announces a new 4×4 Butler matrix with broadband frequency coverage from 2.4 to 7.25 GHz. A Butler matrix is a beamforming network used to feed a phased array of antenna elements. Its purpose is to control the direction of a beam, or beams, of radio transmission. KRYTAR's long history of excellence in the design of broadband microwave components affords the ability to produce unique broadband passive beamforming network solutions to the wireless communications market.

KRYTAR, Inc.
www.krytar.com

Waveguide Circulator

Power your Ka-Band phased array radar systems with the HMC28-599-35.0-1.0 waveguide circulator from Renaissance Electronics, an AEM company. This device operates from 34.5 to 35.5 GHz with a WR28 interface, offering excellent signal clarity with 0.2 dB insertion loss and 5 W CW power handling. Get the edge in your RF designs and explore more details on the Renaissance website.

Renaissance Electronics
www.aeminc.com

Power Divider/Power Splitter

VENDORVIEW

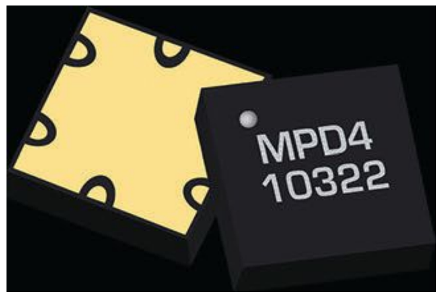

Now available at RFMW, the Marki Microwave MPD4-0218CSP3 is a 2 to 18 GHz MMIC 4-way Wilkinson power divider/power splitter delivering 29 dB isolation and just 0.8 dB excess insertion loss. Housed in a compact 3.5 mm CSP3 chip scale package, it offers superior size reduction compared to PCB-based designs. Ideal for SWaP-critical applications, it supports equal amplitude and phase splitting or combining with excellent isolation and features tight unit-to-unit consistency for reliable system simulations.

RFMW
www.rfmw.com

MATERIALS

PhaseBlue®1500

Blueshift introduces PhaseBlue® 1500, the first product in its Series Circuit Materials (SCM) line. These latest laminates are engineered with a proprietary nanoporous polyimide aerogel core composed of 85 percent air and 15 percent polyimide, enabling an unmatched combination of light weight, flexibility and high frequency performance. As a U.S. made and sustainably compliant material that meets modern environmental standards (formulated without intentionally added per- and polyfluoroalkyl substances), PhaseBlue®addresses growing regulatory and environmental concerns while delivering a next-generation alternative to PTFE-based substrates.

Blueshift
www.blueshiftmaterials.com

Sintered Ferrite Powder

Fair-Rite's brand new product, Sintered Ferrite Powder, expands design flexibility for experimental and production applications. Made from the same base material as our solid components, this powder form is ideal for areas where air gaps naturally exist. While it won't match the full performance of pressed ferrites, sintered powder provides unique advantages for innovation, prototyping and specialized designs. It's a versatile solution for engineers looking to explore new possibilities with trusted Fair-Rite materials.

Fair-Rite
www.fair-rite.com

CABLES & CONNECTORS

BNC Bulkhead Jack

Amphenol RF introductes a tamper-resistant BNC bulkhead jack designed for flexible 1.13 mm micro-coax cable. This panel-mount connector is engineered to offer robust reliability up to 9 GHz to support Wi-Fi 7 technology. This BNC connector is well suited for test and measurement, telecommunications and industrial applications. This new BNC bulkhead jack features nickel-plated brass bodies and gold-plated beryllium copper contacts. These materials are designed to endure harsh environments and ensure constant signal integrity and high frequency capability.

Amphenol RF
www.amphenolrf.com

eLEARNING CENTER

Presented by: Microwave Journal

Now On Demand

Designing with Juliano and Katerina
eLearning Series: Frequency Selective Surfaces

Sponsored by:

Ansys

microwavejournal.com/events/2342

Online Panel: 5G/6G Advances
Sponsored by: Qorvo, MathWorks and CADFEM

Sponsored by:

qorvo all around you

MathWorks

CADFEM

microwavejournal.com/events/2343

Register to attend at mwjournal.com/webinars

ONLINE PANEL SERIES

11/20

Antenna Simulation with COMSOL Multiphysics®

Sponsored by: COMSOL

FEATURED e-Books

mwjournal.com/ebooks

United States Postal Service

Statement of Ownership, Management and Circulation
(All Periodicals Publications Except Requester Publications)

1. Company Name/Publication Title: MICROWAVE JOURNAL/MICROWAVE JOURNAL
2. Publication Number: 396250
3. Filing Date (mm/dd/yyyy): 09/16/2025
4. Issue Frequency: MONTHLY
5. No. Issues Published Annually (required): 12
6. Annual Subscription Price: 120.00

7. Complete Mailing Address of Known Office of Publication (Not printer) — AMS
Address Line 1: 685 CANTON ST
Address Line 2:
City: NORWOOD County: NORFOLK State: MA ZIP+4: 02062 - 2608
Foreign Address:
Contact Person: CARL SHEFFRES
Telephone (include area code): (781) 761 - 1949 Ext.

8. Complete Mailing Address of Headquarters or General Business Office of Publisher — AMS
Address Line 1: Horizon House Publications, Inc.
Address Line 2: 685 Canton St.
City: Norwood State: MA ZIP+4: 02062 -
Foreign Address:

9. Full Names and Complete Mailing Addresses of Publisher, Editor, and Managing Editor (Do not leave blank)

Publisher — AMS
Full Name: Carl S. Sheffres
Address Line 1: Horizon House Publications, Inc.
Address Line 2: 685 Canton St.
City: Norwood State: MA ZIP+4: 02062 - 2610
Foreign Address:

Editor — Same as Publisher — N/A — AMS
Full Name: Patrick Hindle
Address Line 1: Horizon House Publications, Inc.
Address Line 2: 685 Canton St.
City: Norwood State: MA ZIP+4: 02062 - 2610
Foreign Address:

Managing Editor — Same as Publisher — N/A — AMS
Full Name: Jennifer DiMarco
Address Line 1: Horizon House Publications, Inc.
Address Line 2: 685 Canton St.
City: Norwood State: MA ZIP+4: 02062 - 2610
Foreign Address:

10. Owner (Do not leave blank. If the publication is owned by a corporation, give the name and address of the corporation immediately followed by the names and addresses of all stockholders owning or holding 1 percent or more of the total amount of stock. If not owned by a corporation, give names and addresses of the individual owners. If owned by a partnership or other unincorporated firm, give its name and address as well as those of each individual owner. If the publication is published by a nonprofit organization, give its name and address.) — AMS

Full Name	Complete Mailing Address
Horizon House Publications, In	685 Canton St., Norwood, MA 02062-2610
William M. Bazzy, CEO	685 Canton St., Norwood, MA 02062-2610
Ivar A. Bazzy	685 Canton St., Norwood, MA 02062-2610
Jared M. Bazzy	685 Canton St., Norwood, MA 02062-2610
Joan B. Egan	685 Canton St., Norwood, MA 02062-2610

Add / Edit / Delete

Upload Owner Address File — Choose File No file chosen

List of owners is in the publication file at the original entry office.

11. Known Bondholders, Mortgagees, and Other Security Holders Owning or Holding 1 Percent or More of Total Amount of Bonds, Mortgages, or Other Securities. If none, check box: ☑ None

Full Name	Complete Mailing Address

Add / Edit / Delete — AMS

13. Company Name/Publication Title: MICROWAVE JOURNAL/MICROWAVE JOURNAL
14. Issue Date for Circulation Data Below (mm/dd/yyyy): 09/15/2025

15. Extent and Nature of Circulation	Average No. Copies Each Issue During Preceding 12 Months	No. Copies of Single Issue Published Nearest to Filing Date
a. Total Number of Copies(net press run)	23541	24530
b. Paid Circulation (By Mail and Outside the Mail) (1) Mailed Outside County Paid Subscriptions Stated on PS Form 3541 (include paid distribution above nominal rate, advertiser's proof copies, and exchange copies)	15347	15812
(2) Mailed In-County Paid Subscriptions Stated on PS Form 3541 (include paid distribution above nominal rate, advertiser's proof copies, and exchange copies)	0	0
(3) Paid Distribution Outside the Mails Including Sales Through Dealers and Carriers, Street Vendors, Counter Sales, and Other Paid Distribution Outside USPS	6509	6960
(4) Paid Distribution by Other Classes of Mail Through the USPS (e.g. First-Class Mail)	0	0
c. Total Paid Distribution (Sum of 15b (1), (2), (3), and (4))	21856	22772
d. Free or Nominal Rate Distribution (By Mail and Outside the Mail) (1) Free or Nominal Rate Outside County Copies included on PS Form 3541	741	606
(2) Free or Nominal Rate In-County Copies included on PS Form 3541	0	0
(3) Free or Nominal Rate Copies Mailed at Other Classes Through the USPS (e.g. First-Class Mail)	0	0
(4) Free or Nominal Rate Distribution Outside the Mail (Carriers or other means)	966	1039
e. Total Free or Nominal Rate Distribution (Sum of 15d (1), (2), (3), and (4))	1707	1645
f. Total Distribution (Sum of 15c and 15e)	23563	24417
g. Copies not Distributed	58	113
h. Total (Sum of 15f and 15g)	23621	24530
i. Percent Paid (15c divided by 15f times 100)	92.76 %	93.26 %

16. If total circulation includes electronic copies, report that circulation on lines below		
a. Paid Electronic Copies	0	0
b. Total Paid Print Copies (Line 15c) + Paid Electronic Copies	0	0
c. Total Print Distribution (Line 15F) + Paid Electronic Copies	0	0
d. Percent Paid (Both Print & Electronic Copies)	0.00 %	0.00 %

I Certify that 50% of all my distributed copies (Electronic & Print) are paid above a nominal price.

17. Publication of Statement of Ownership
◉ If the publication is a general publication, publication of this statement is required. Will be printed in the 11/01/2025 issue of this publication.
○ Publication not required.

18. Signature and Title of Editor, Publisher, Business Manager, or Owner: Carl S. Sheffres — Title: Publisher — Date: 09/15/2025

Reason for Amendment:

I certify that all information furnished on this form is true and complete. I understand that anyone who furnishes false or misleading information on this form or who omits material or information requested on the form may be subject to criminal sanctions (including fines and imprisonment) and/or civil sanctions (including civil penalties).

RF Connectors

Connectronics Inc. has expanded its product line with the launch of the SMP bullet — a subminiature push-on adapter system designed to ensure reliable RF performance, especially in board-to-board or other gang-mating applications. The SMP bullet provides high-density solutions, supporting both board-to-board and cable-to-board connections. Available for fixed and spring-loaded applications, it accommodates tolerance and misalignment issues during mating, prevents signal degradation and ensures consistent RF performance

Connectronics Inc.
www.connectronics.com

AMPLIFIERS

80 W Solid-State Power Amplifier

VENDORVIEW

With unprecedented power, uncompromising precision and broadband brilliance, AMP20167 covers 18.0 to 40.0 GHz for EMC/lab testing, MIL-STD 461 RS103 and other mission-critical applications. It has 6U form and exceptional power/gain flatness. The smart sensing suite offers real-time monitoring of forward/reflected power in both dBm and watts, plus VSWR, voltage, current and temperature sensing for total control. The solid-state reliability offers no tubes, no compromise. Whether you are stress-testing systems or pushing RF boundaries, AMP20167 delivers precision and power. Exodus doesn't follow standards. We set them.

Exodus Advanced Communications
www.exoduscomm.com

Broadband Ultra-Low Noise Amplifier

Model ABL1800-11-3315 is a two-stage MMIC-based broadband ultra-low noise amplifier module operating in the frequency range from 2.0 to 18 GHz. It offers 33 dB of linear gain and 1.5 dB of typical noise figure with excellent gain flatness and input/output return loss. The unit has a built-in voltage regulator and operates with a single DC power supply voltage. The package size of the amplifier is 1.5 × 1.0 × 0.4 in.

Wenteq Microwave
www.wenteq.com

TEST & MEASUREMENT

PXR Series Spectrum Analyzer

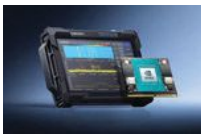

A new industry trend is emerging, as spectrum analyzers with local processing and computing power enable real-time, on-site analysis. Some models even feature high performance GPUs to accelerate the analysis process. The HAROGIC PXR Series is engineered to meet this challenge. It's not only a rugged spectrum analyzer with IP68 standard design and benchtop-grade RF performance, but also the all-in-one AI platform open platform that deeply integrates the open API and cutting-edge AI computing power of NVIDIA.

HAROGIC
www.harogic.com

MICRO-ADS

Reviewed by John F. Sevic

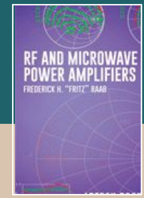

Bookend

RF and Microwave Power Amplifiers

Frederick H. Raab

It is rare to find a single volume that completely captures the knowledge of an entire field. If your goal is first-pass design success backed by rigorous understanding, *RF and Microwave Power Amplifiers* belongs on your shelf.

The book opens with an introduction to applications, emphasizing key specifications such as efficiency definitions, signal fidelity and power gain. The following chapter presents a treatment of signal representation and behavior, along with the implications for power amplifier (PA) design and architecture. The concept of average efficiency is introduced early, as it governs power consumption and thermal loading. The next two chapters provide a PA–specific review of modern RF and microwave power transistors.

The next three chapters cover current-mode amplifiers. A strength of the book is its practical focus, informed by the author's half-century of experience in the field. Topics such as load-line analysis, variable quiescent current methods for efficiency improvement, push-pull configurations, biasing strategies and matching networks are treated in depth. Readers will find these chapters immediately applicable to real-world design.

Subsequent chapters introduce switch-mode RF and microwave PAs. The level of rigor and insight is exceptional, as much of this theory originated with Raab himself. A variety of Class D and E architectures are explored, including complementary, full-bridge and transformer-coupled variants, covering both single-ended and push-pull architectures. Based on the reviewer's own experience, the design equations provided can lead to first-pass success. The following chapter gives advanced treatment of Class E, including non-ideal effects due to finite feed inductance, wideband design and excess output capacitance. Similarly, the final chapters present the Class F mode, beginning with harmonic peaking.

A major feature of the book is the inclusion of end-of-chapter problems and solutions. RF engineering is a full-contact sport, and these problems are essential for developing intuition and understanding time-domain voltage and current behavior at the transistor terminals.

ISBN: 9781685690830
Pages: 550
To order this book, contact:
Artech House
us.artechouse.com

Advertising**Index**

5G 6G SPECIAL FOCUS

ADVERTISERS ARE HIGHLIGHTED IN PURPLE

Sales Representatives

Microwave Journal

Eastern and Central Time Zones
Carl Sheffres
Group Director
(New England, New York, Eastern Canada)
Tel: (781) 619-1949
csheffres@mwjournal.com

Michael Hallman
Associate Publisher
(NJ, Mid-Atlantic, Southeast, Midwest, TX)
Tel: (301) 371-8830
Cell: (781) 363-0338
mhallman@mwjournal.com

Pacific and Mountain Time Zones
Brian Landy
Western Reg. Sales Mgr.
(CA, AZ, OR, WA, ID, NV, UT, NM, CO, WY, MT, ND, SD, NE & Western Canada)
Tel: (831) 426-4143
Cell: (831) 713-9085
blandy@mwjournal.com

Submitting ad material?
Visit: www.adshuttle.com/mwj
(866) 774-5784
outside the U.S. call
+1-414-566-6940

Ed Kiessling
(781) 619-1963
ekiessling@mwjournal.com

International Sales
Michael O'Kane
Tel: +44 (0) 1875 825 700
Cell: +44 (0) 7961 038 245
mokane@horizonhouse.com

Germany, Austria, and Switzerland (German-speaking)
Victoria and Norbert Hufmann
Tel: +49 911 9397 6442
victoria@hufmann.info
norbert@hufmann.info

France
Gaston Traboulsi
Tel: +44 207 596 8742
gtraboulsi@horizonhouse.com

Korea
Jaeho Chinn
JES MEDIA, INC.
Tel: +82 2 481-3411
corres1@jesmedia.com

China
Shanghai
Linda Li
ACT International
Tel: +86 136 7154 0807
lindal@actintl.com.hk

Wuhan
Phoebe Yin
ACT International
Tel: +86 134 7707 0600
phoebey@actintl.com.hk

Shenzhen
Samuel Zhoul
ACT International
Tel: +86 186 8201 0368
samuelz@actintl.com.hk

Beijing
Cecily Bian
ACT International
Tel: +86 135 5262 1310
cecilyb@actintl.com.hk

Hong Kong
Floyd Chun
ACT International
Tel: +86 137 2429 8335
floydc@actintl.com.hk

Taiwan, Singapore
Simon Lee
ACT International
Tel: +852 2838 6298
simonlee@actintl.com.hk

Japan
Katsuhiro Ishii
Ace Media Service Inc.
Tel: +81 3 5691 3335
amskatsu@dream.com

Corporate Headquarters: 685 Canton Street, Norwood, MA 02062 • Tel: (781) 769-9750

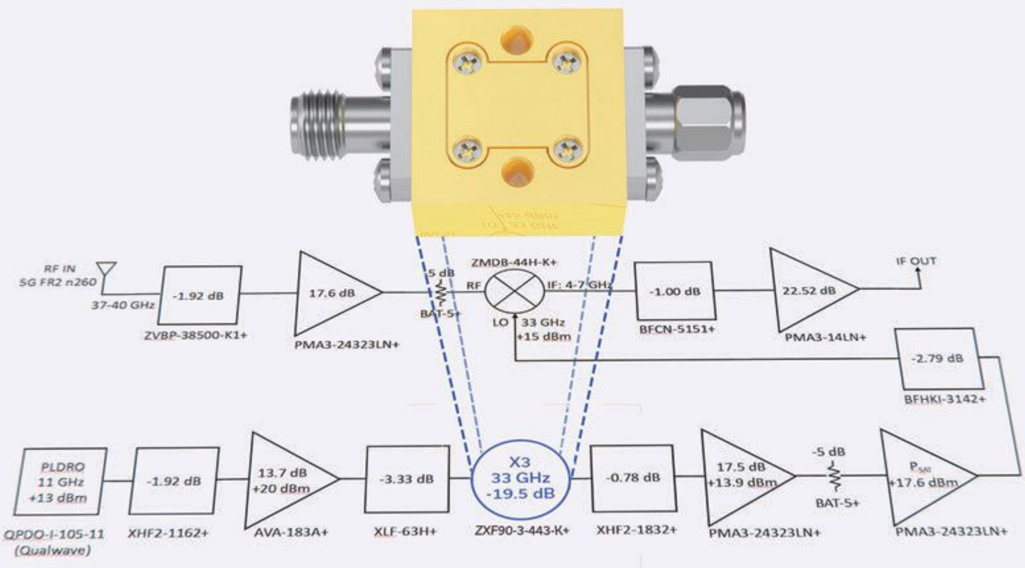

9 TO 72 GHz

Coaxial Frequency Multipliers

For High-Frequency LO Chains,
Upconverters & More

xN

LEARN MORE

High-frequency multipliers cover 9 to 72 GHz with +12 to +20 dBm input in compact, coaxial housings.

Model Name	Description	F Low	F High
ZXF90-3-223-K+	X3 Frequency Multiplier, SMA-F to 2.92 mm-M, 50Ω	10 GHz	22 GHz
ZXF90-3-443-K+	X3 Frequency Multiplier, SMA-F to 2.92 mm-M, 50Ω	20 GHz	43.5 GHz
ZXF90-3-453-V+	X3 Frequency Multiplier, SMA-F to 1.85 mm-M, 50Ω	20 GHz	45 GHz
ZXF90-3-64-E+	X3 Frequency Multiplier, 2.92 mm-F to 1.85 mm-M, 50Ω	30 GHz	60 GHz
ZXF90-3-723-E+	X3 Frequency Multiplier, 2.92 mm-F to 1.85 mm-M, 50Ω	40 GHz	72 GHz
ZXF90-2-44-K+	X2 Frequency Multiplier, 2.92 mm-F to 2.92 mm-F, 50Ω	12.4 GHz	40 GHz
ZXF90-2-153-K+	X2 Frequency Multiplier, 2.92 mm-F to 2.92 mm-F, 50Ω	9 GHz	15 GHz

FABS and LABS

Menlo Micro: Setting a New Standard in Switch Technology

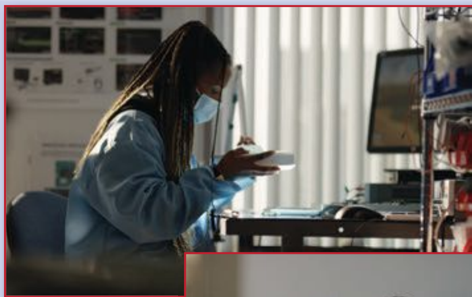


Menlo Micro, founded in 2016, is on a mission to set a new standard in switch technology. Menlo Micro's foundational technology is its Ideal Switch, which incorporates the benefits of electromechanical and solid-state switches. Menlo leverages this technology to create solutions for industries, including test and measurement, aerospace and defense, industrial, medical, telecommunications, consumer and automotive.

The Ideal Switch combines the nuances of semiconductor manufacturing with a micro-mechanical actuator, creating a high isolation airgap when OFF and a near-zero resistance when ON. The foundation of the switch platform is a 100 μm x 100 μm unit cell, approximately 90 percent smaller than traditional switches, and is configurable in series or parallel designs to allow for a multitude of product configurations. In addition to these sizing advantages, the Ideal Switch uses proprietary alloys that are resilient to high temperatures and mechanical stress. The Ideal Switch draws low power compared to EMRs, improving system energy efficiency and eliminating the need for heat sinks. It also has a < 10 μs switching time and operates for over 3 billion switching cycles. The Ideal Switches are hermetically sealed using wafer bonding with through-glass copper vias creating miniaturized, chip-scale packages. They are then implemented in a variety of products designed in collaboration with industry-leading customers.

Menlo believes the path from concept to commercialization for advanced electronic technologies demands a tightly integrated product development cycle that spans design, fabrication and testing while engaging both internal and external ecosystems. At Menlo Micro, this cycle is anchored by engineering labs in Irvine, Calif., complemented by its Product Development Center at the NY CREATES NanoTech Complex in Albany, N.Y. Together, these facilities enable rapid iteration between design, fabrication and test for both new technologies and new product introductions.

Menlo extends this innovation framework through collaborations with university research programs, government initiatives, technology networks and direct customer engagement. By co-creating innovation with Tier-1 customers, Menlo ensures the development process is market-driven, tightly aligned with real-world requirements and responsive to evolving system needs. This approach not only accelerates innovation but also helps customers transition smoothly to leverage the benefits of new technologies, particularly in achieving improvements in size, weight, power and cost (SWaP-C).

The Ideal Switch has been successfully implemented and has significant customer adoption across a variety of high-value markets. Menlo highlights its RF switch in communications and 5G/6G, aerospace and defense, test and measurement and medical applications. Menlo's products are critical for testing AI GPUs and envision the extension of the Ideal Switch's usage in autonomous driving. The Ideal Switch is integrated into switched filter banks, antenna tuning and beamforming systems, high-power RF front-ends, low loss switching matrices and EM relays in RF paths.

Menlo Micro's lab ecosystem and collaborative development model drive technology innovation that is co-created with tier-1 customers to shorten time-to-market and deliver meaningful performance advantages to customers across industries. As Menlo Micro's Ideal Switch gains traction throughout the RF and high speed digital industries, it will continue to carry out its mission of "setting a new standard in switch technology."

https://menlomicro.com/


SPECTRAN® V6
BEYOND REALTIME
Setting the Mobile Benchmark
The ULTIMATE Real-Time Spectrum Analyzer Tablet
8 | 18 | 55 | 140 GHz 2x 490 MHz RTBW
HIGH-END SPECTRUM ANALYZER:
9 kHz up to 140 GHz
Optional Tx (Generator)
2x 490 MHz Bandwidth
3 THz/s Sweep Speed
16-Bit ADC
-170dBm/Hz | 4dB NF
IQ Recording & Playpack
8h Continuous Runtime
Temp. Range -40° to +60°
GPS & Time Server
Opt. Handle & Stand
Incl. RTSA-Software
RUGGED PREMIUM PC POWER:
15.6" 1500nit FullHD Touchscreen
AMD 8-Core 8845HS CPU
64 GB LPDDR5 RAM
Up to 64 TB Highspeed SSD
2x M.2 2280 & 3x M.2 2242
Many I/Os incl. USB4, SD & HDMI
SIM slot, opt. WiFi, Bluetooth, 5G
SFP+ 10G Ethernet, SATA, RS232
Rugged Aluminum Casing
Hot-Swap Batteries
Front & Rear Cameras, Smart Pen
Windows or Linux
MADE IN GERMANY
www.aaroniausa.com
ubuy@aaroniausa.com
+1 (214) 935-9800
www.aaronia.com
mail@aaronia.de
+49 6556 900 310
AARONIA AG®
WWW.AARONIA.COM

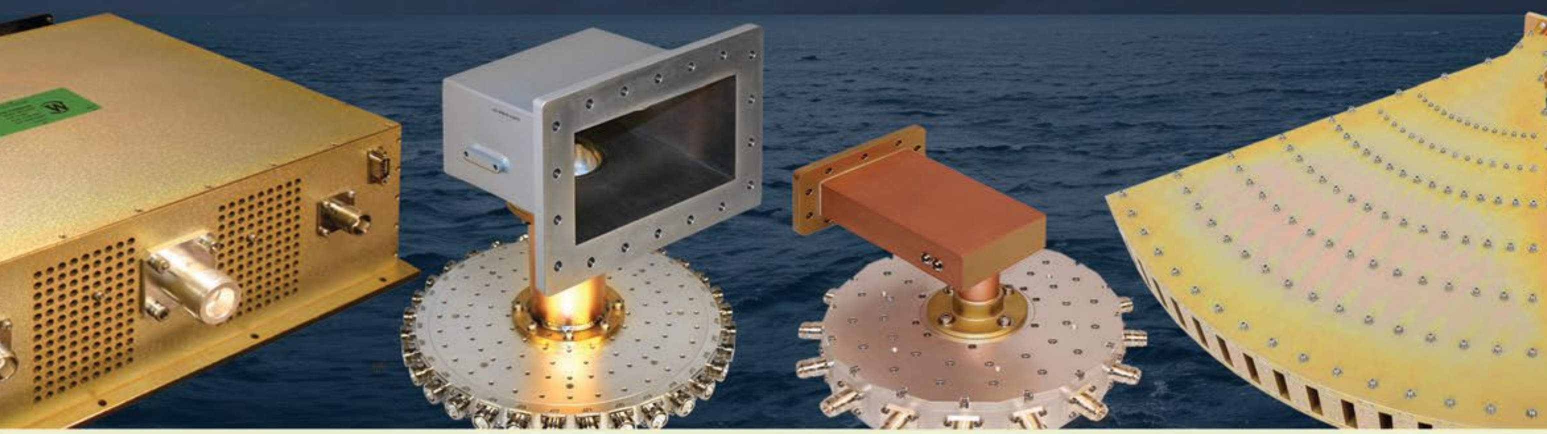

Dual-Band Miniaturized 8 × 8 MIMO Array for 5G Mobile Terminals

Xin Wang, Lu Cheng and Junlin Wang
Inner Mongolia University, Inner Mongolia Autonomous Region, People's Republic of China

A dual-band miniaturized eight-element MIMO antenna array operates in the 5G N77, N78 and N79 frequency bands. The antenna requires no additional decoupling structure, which is achieved with the use of tuning branches.

The -6 dB bandwidth is 3.4 to 3.6 GHz and 4.3 to 5.17 GHz. Isolation in each band is greater than 25.5 and 16.6 dB, while efficiency is over 40 and 42 percent, respectively. The envelope correlation coefficient (ECC) is less than 0.025. The 8×8 MIMO array antenna meets the communication requirements of 5G mobile terminals.

In recent years, MIMO technology has been commercialized in 5G mobile terminals due to its superior data transmission rate, shorter latency and higher reliability. Achieving elevated data throughput rates is possible through the deployment of multiple antennas.[1] In 2015, the 3.5 GHz band was included as a new frequency band in the 5G communications framework.[2] In recent years, a significant number of studies have concentrated on MIMO arrays in the 3.5 GHz (3.4 to 3.6 GHz) band.[3-7] However, as they have demonstrated limited bandwidth, many bandwidth extension studies have followed. These have been conducted in the 3.5 GHz band[8-14] as well as other bands.[15-17] These studies added new resonant points using parasitic branches, slotted structures and inverted-F antennas.

Recent studies have examined dual-band and multi-band antennas.[18-29] Deng et al.[18] demonstrated dual-frequency operation from 3.4 to 3.6 GHz and 4.8 to 5.0 GHz using mode elimination; however, the antenna was large. Ghiat et al.[22] increased bandwidth by coupling the feed; however, there were only four antennas in the MIMO array. Ahn et al.[28] combined two antennas using open and closed stubs to increase the bandwidth, but the isolation was relatively low.

In this work, a miniaturized dual-band MIMO array's design bifurcates the antenna's current path into three distinct dipole modes by a separating branch, thereby facilitating dual-frequency operation. By adding a coupled feed port with a T-shaped tuning branch, a new resonant frequency point is introduced. This further widens the bandwidth. The T-shaped tuning branch is used for optimizing impedance matching and enhancing isolation between ports.

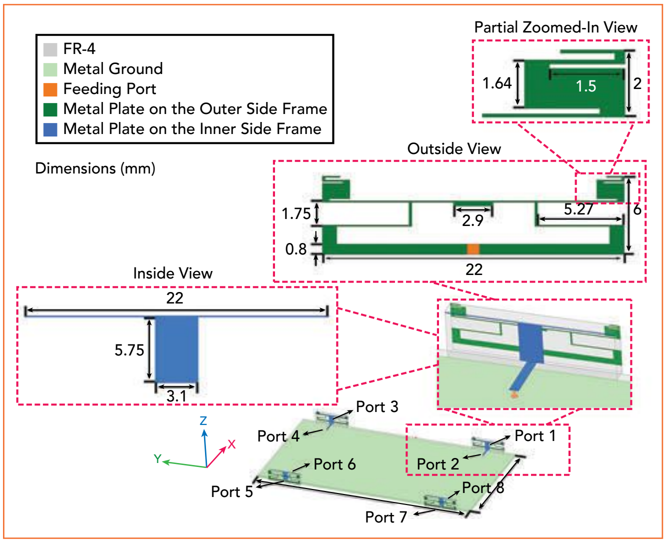

Fig. 1 8 × 8 MIMO system and individual antenna element design.

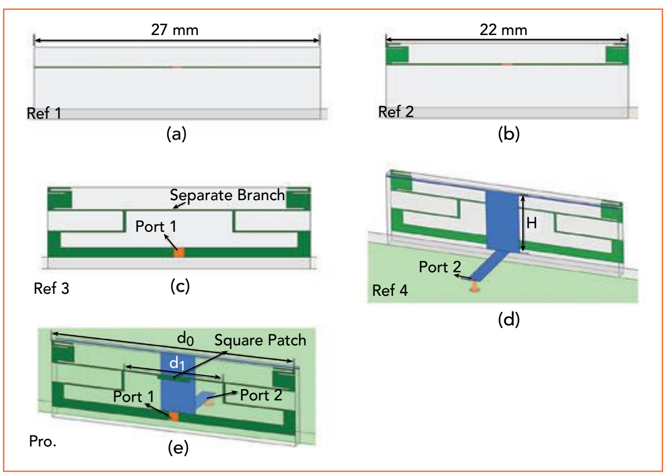

Fig. 2 Antenna design evolution: (a) Ref 1, (b) Ref 2, (c) Ref 3, (d) Ref 4 and (e) final prototype.

ANTENNA DESIGN EVOLUTION

Antenna Configuration

Figure 1 shows the configuration of an eight-element MIMO array designed for the study of 5G smartphone applications. The main antenna body with a split branch is located on the outside of the phone's side frame. It covers the 3.4 to 3.6 GHz and 4.3 to 5.17 GHz frequency bands. The T-shaped coupled feed element consists of a T-shaped tuning branch and a microstrip feed located on the inside of the side frame of the smartphone and on the top of the base plate of the smartphone, respectively.

The antenna is copper. The gray component in the Figure 1 is an FR4 dielectric substrate (ε_r = 4.4, tanδ = 0.02). The dimensions of the bottom substrate are 150 × 75 × 1 mm, and the dimensions of the side substrate are 22 × 7 × 2 mm. A metal floor is located under the bottom substrate and has a size of 150 × 75 mm. On the upper surface of the bottom substrate, the end of the 50 Ω microstrip feed has a 0.4 mm via hole that facilitates the transmission of energy to the microstrip with a coaxial line.

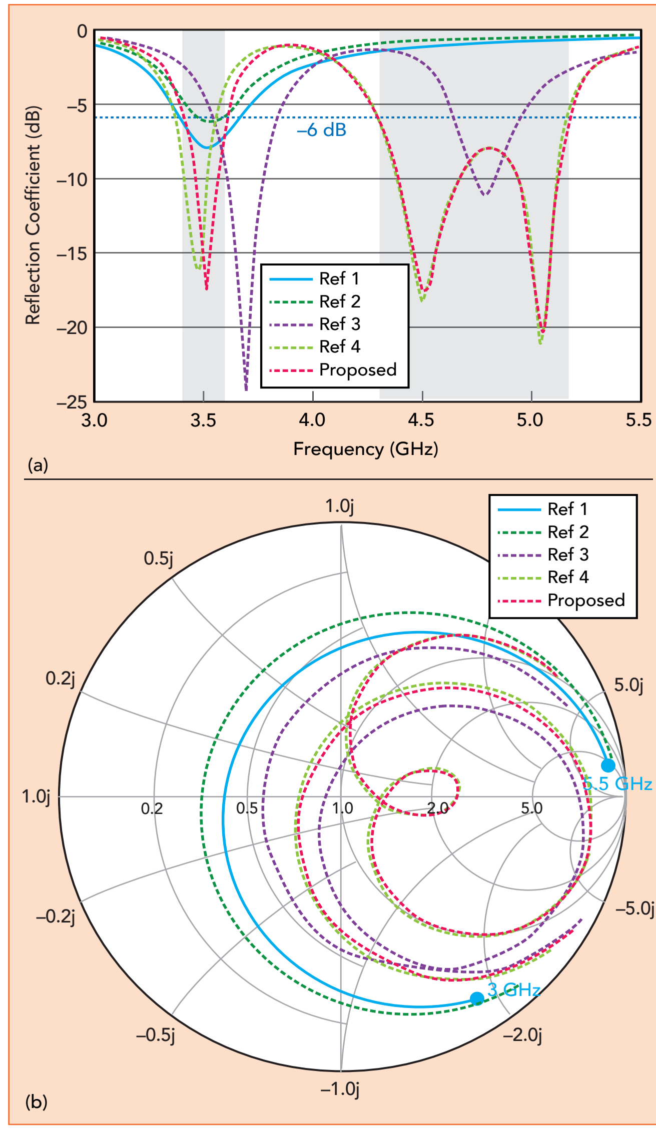

Fig. 3 (a) Reflection coefficient magnitudes and (b) Smith chart representation for the antenna configurations shown in Figure 2.

Antenna Evolution and Analysis

Dipole antennas are distinguished by their simplicity of structure and efficiency in signal reception. The initial configuration uses a dipole antenna (see ***Figure 2a***) that has a resonant frequency at 3.5 GHz. This antenna measures 27 mm in length. To reduce its size, it is folded, thereby reducing its length to 22 mm (see ***Figure 2b***). $|S_{11}|$ and Smith chart displays for these and subsequent configurations are shown in ***Figures 3a*** and ***3b***.

It is evident from Figure 3 that the impedance matching for these two configurations is not satisfactory. To broaden the bandwidth and optimize the impedance match, a second dipole antenna structure is stacked below the configuration in Figure 2b, and the port position is replaced by a separate branch. The entire antenna is directly fed from Port 1 (see ***Figure 2c***). As shown in Figure 3a, a new resonance emerges in the high frequency range, while the impedance matching level in the low frequency band is significantly enhanced. The integration of a T-shaped capacitive coupling feed,

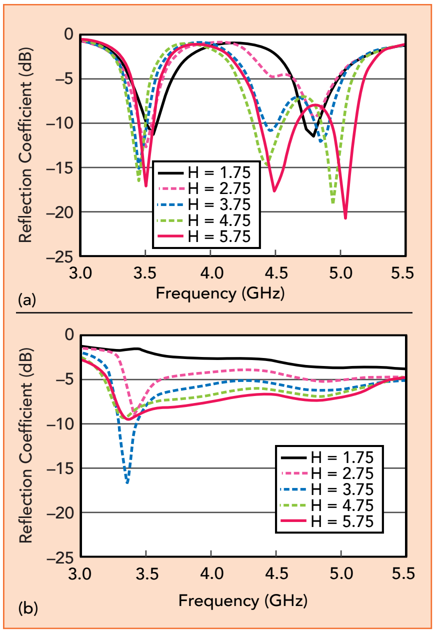

Fig. 4 Effect of the length of H on reflection coefficient magnitudes of (a) Port 1 and (b) Port 2.

Port 2, on the opposite side of Port 1 (see ***Figure 2d***) further optimizes the impedance match, as seen by the bandwidth broadening at higher frequencies.

As shown in Figure 3b, the impedance curve is closer to the 3:1 voltage standing wave ratio circle. Furthermore, feeding a dipole antenna directly through a coaxial line is equivalent to short-circuiting the antenna, increasing its inductive reactance. By introducing a capacitive reactance, the inductive reactance is cancelled and isolation between the ports is improved.

A square patch is added in the middle of the separate branch (see ***Figure 2e***) to yield the final dipole antenna prototype design. The square patch further adjusts the impedance match at lower frequencies, moving the low-band resonant frequency to 3.5 GHz. The final antenna operates in the 3.4 to 3.6 GHz and 4.3 to 5.17 GHz frequency bands.

By modifying the height of the T-shaped tuning branch, impedance matching is optimized at Ports 1 and 2 (see ***Figures 4a*** and ***4b***), further increasing the bandwidth. For Port 1, increasing H from 1.75 to 5.75 mm introduces a new resonance in the high frequency region. The bandwidth at Port 2 gradually increases to span from 3.22 to 5.16 GHz. The dual-port antenna covers the 3.4 to 3.6 GHz and 4.3 to 5.17 GHz frequency bands.

Figure 5 shows the distribution of the three vector currents. At 3.5 GHz, the antenna is split into upper and lower parts, with each part constituting a dipole current that operates in the fundamental mode. At 4.5 and 5.05 GHz, the entire antenna participates in the resonance in the high frequency region as a dipole antenna operating in the third mode. The T-branch always operates in the fundamental mode.

Parameter Analysis

The antenna width d_0 and the length of the branch d_1 are significant parameters that affect the antenna's resonances; therefore, a parametric sweep is conducted on these two parameters (see ***Figure 6***). For Port 1, as d_0 increases from 20 to 22 mm, both the lower and higher resonances shift lower in frequency (see Figure 6a). For Port 2, the increase in d_0 optimizes the impedance match in the lower frequency band, causing the resonant frequency point in that band to shift lower, thereby expanding the bandwidth (see Figure 6b).

For Port 1, increasing d_1 shifts the upper band resonance higher in frequency, while the resonances at 4.5 and 3.5 GHz remain relatively unchanged (see ***Figure 6c***). For Port 2, increasing the length of d_1 expands the bandwidth in the lower frequency band (see ***Figure 6d***).

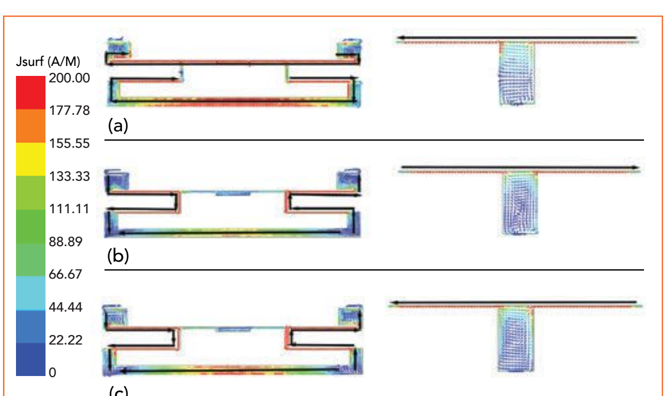

Fig. 5 Surface current distribution at frequencies (a) 3.5, (b) 4.5 and (c) 5.05 GHz.

Array Configuration

MIMO arrays are employed in 5G mobile terminals for elevated data throughput and enhanced spectral

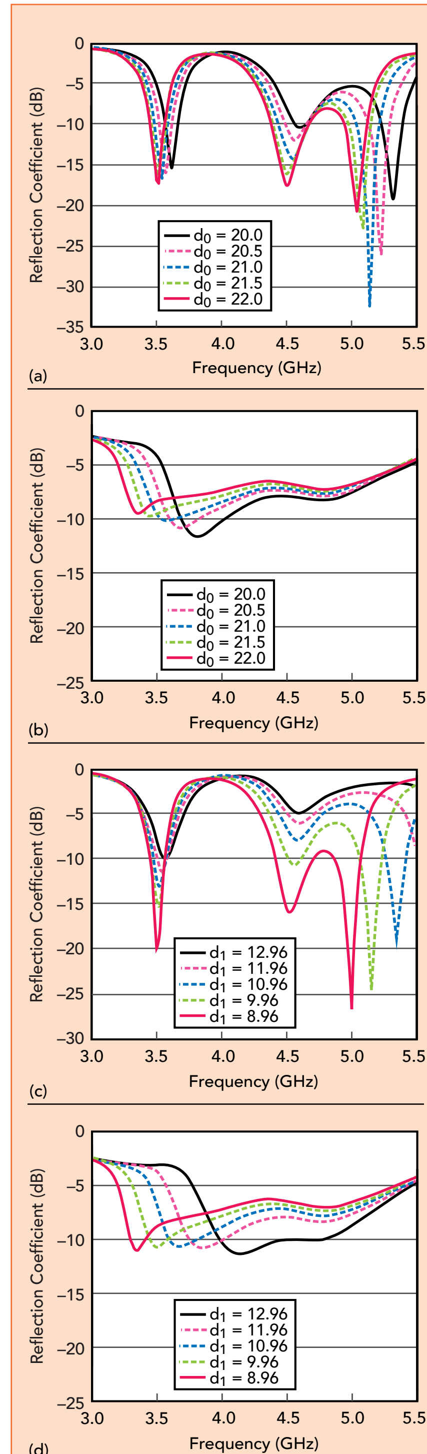

Fig. 6 Effect of antenna width d_0 on resonant frequencies at (a) Port 1 and (b) Port 2. Effect of branch length d_1 on resonant frequencies at (c) Port 1 and (d) Port 2.

efficiency. This is accomplished by configuring the dual-port antenna described above into an 8×8 MIMO array (see ***Figure 7***). The use of spatial diversity between dual-port antennas serves to enhance isolation. The dual-port antenna elements are placed along the long edges of the phone. The distance w between the antennas mainly affects isolation between Ports 1, 3 and Ports 2, 4 (see Figures 7b and 7c) and by similarity Ports 5, 7 and Ports 6, 8. As w increases from 28.2 to 88.2 mm, $|S_{13}|$ decreases from a maximum -22 dB to a maximum -26 dB and $|S_{24}|$ decreases from a maximum -12 dB to a maximum -16.6 dB.

MEASUREMENT RESULTS AND DISCUSSION

MIMO Performance

A prototype of the 8×8 MIMO array (see ***Figure 8***) is tested and results are compared with simulation (see ***Figures 9*** and ***10***). Because the antennas are arranged symmetrically, only data from Ports 1 and 2 are displayed. The -6

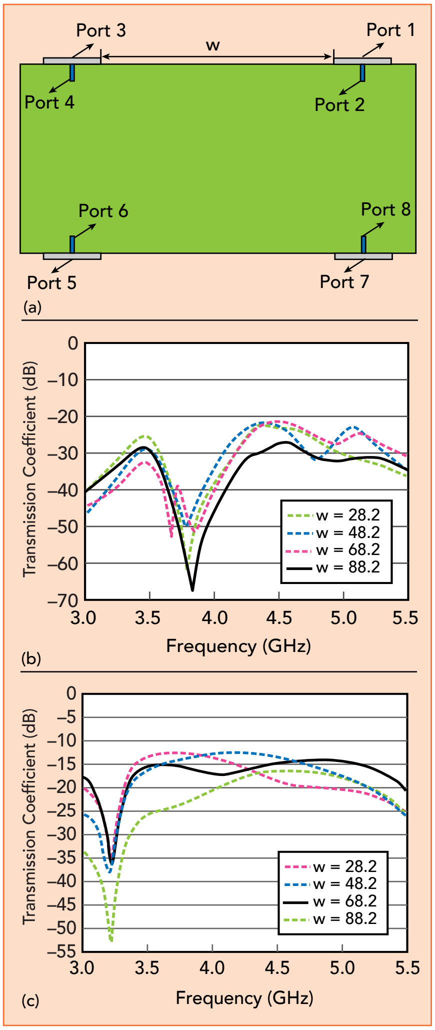

Fig. 7 (a) Top view of the 8 × 8 MIMO system. Effect of the length of w on (b) $|S_{13}|$ and (c) $|S_{24}|$.

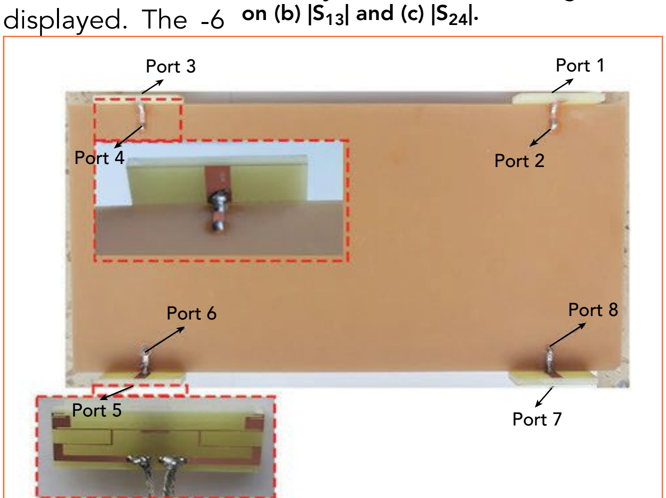

Fig. 8 8 × 8 MIMO antenna system prototype.

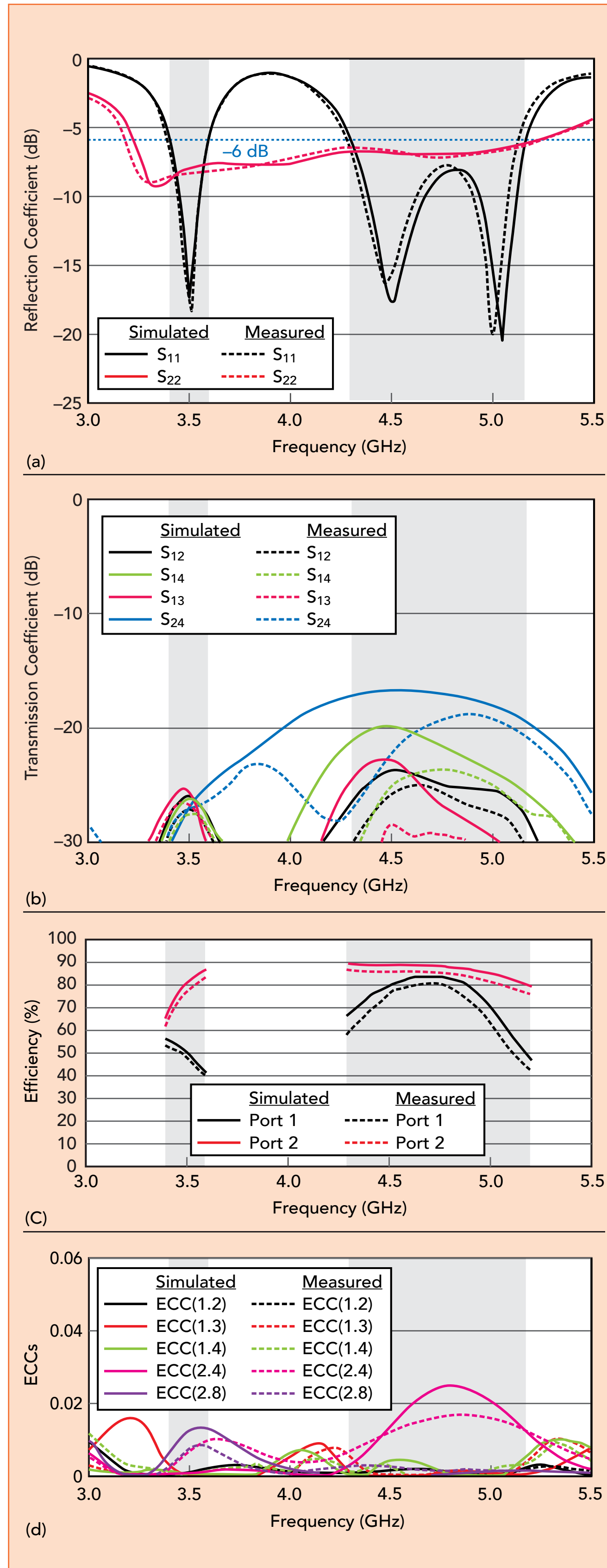

Fig. 9 Prototype MIMO antenna system (a) reflection coefficient magnitudes, (b) transmission coefficients magnitudes, (c) efficiency and (d) ECCs.

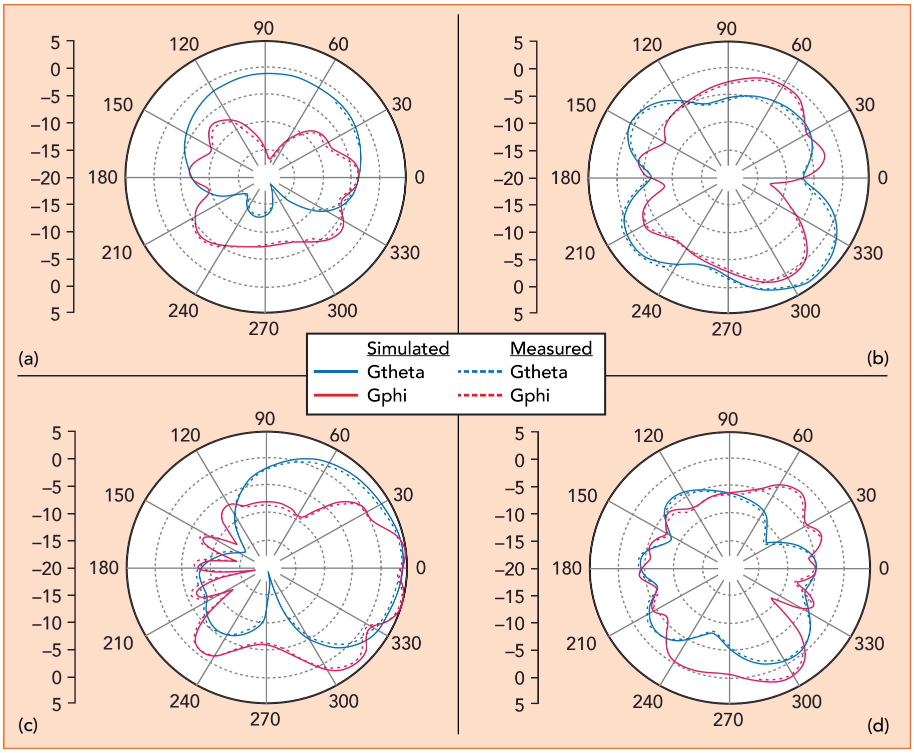

Fig. 10 **Antenna radiation patterns: (a) Port 1 at 3.5, (b) Port 2 at 3.5, (c) Port 1 at 5.05 and (d) Port 2 at 5.05 GHz.**

TABLE 1

COMPARISON WITH OTHER WORK

Reference	Frequency (GHz)	Isolation (dB)	Efficiency (%)	Size (mm^2)	ECC
3	3.4 to 3.6	> 15	> 73	13.45 × 5.5	< 0.02
5	3.4 to 3.6	> 16	> 48	23.2 × 5.6	< 0.08
8	3.2 to 4.4	> 12	> 46	20 × 7	< 0.11
10	3.3 to 3.8	> 19.5	> 43	24 × 4	< 0.06
17	4.4 to 6.0	> 10.5	> 46	35 × 7	< 0.32
22	3.4 to 3.6 3.6 to 3.8 4.8 to 5	> 14	> 82	10.5 × 5	< 0.02
24	3.37 to 3.61 3.11 to 4.15	> 14 > 21	> 48 > 60	20 × 11.8	< 0.05
29	3.43 to 3.8 5.15 to 5.85	> 12 > 16	> 61 > 53	28.92 × 9	< 0.05
This Work	3.4 to 3.6 4.3 to 5.17	> 25.5 > 16.6	> 40 > 42	22 × 6	< 0.025

dB impedance bandwidth encompasses a frequency range of 3.4 to 3.6 GHz and 4.3 to 5.17 GHz (see Figure 9a). Isolation is greater than 25.5 and 16.6 dB (see Figure 9b), and efficiency is higher than 40 and 42 percent (see Figure 9c) in the lower and upper bands, respectively. ECCs are less than 0.025 (see Figure 9d). The antenna has good diversity performance.

The radiation patterns are shown in Figure 10. The maximum radiation directions of the patterns of Ports 1 and 2 are different, which helps to improve the isolation between the ports.

Comparison

The advantages of this antenna in 5G applications are illustrated by a comparison with other reported work (see ***Table 1***). Antennas designed by Abbasi et al.[3] and Zhang et al.[5] achieve the required efficiency and diversity performance but have narrow bandwidths. Zhao et al.[8] improves the bandwidth through the introduction of new branches, but the isolation level is low, and the ECC is significantly higher compared to this antenna. Zeng et al.[10] and Ren et al.[17] use a phase shifter and current cancellation to achieve high isolation. However, the antenna size is large. All the above cover only a single frequency band.

Ghiat et al.[22] achieve multiple frequency operation using a coupled feed, but the bandwidth is still relatively narrow. Abubakar et al.[24] further extend the bandwidth by loading the slot structure. Bandwidth extension is achieved by Boufouss and Najid[29] using a PIFA pattern and parasitic elements. However, the antenna dimensions are still larger than those of this antenna. Compared to the other designs, this antenna offers broad bandwidth, miniaturization, high isolation and good diversity performance.

CONCLUSION

An 8×8 MIMO antenna array for 5G mobile terminals combines three dipole current modes in one antenna with a separate branch for dual-band operation, which also enables miniaturization. Bandwidth is increased and isolation between ports is improved by adding a coupled feed port with a T-shaped tuning branch.

The antenna operates in the 3.4 to 3.6 GHz and 4.3 to 5.17 GHz frequency bands. The dual operating bands demonstrate an isolation greater than 25.5 dB and 16.6 dB, respectively. The antenna is small, with dimensions of 22 × 6 mm. With an ECC of less than 0.025, the antenna has good diversity performance as well. ■

References

1. M. A. Jensen and J. W. Wallace, "A Review of Antennas and Propagation for MIMO Wireless Communications," *IEEE Transactions on Antennas and Propagation*, Vol. 52, No. 11, November 2004, pp. 2810–2824.
2. "World Radiocommunication Confer-

ence Allocates Spectrum for Future Innovation," *ITU*, Nov. 27, 2015, Web: http://www.itu.int/net/pressoffice/press_releases/2015/56.aspx.
3. D. Abbasi, A. Aziz, K. Aljaloud, A. H. Alqahtani, A. Zerguine, A. Al-Garni, A. R. Chishti and R. Hussain, "Higher Order MIMO Antenna Design Using Capacitively Coupled Meandered Loop Element for 5G Smartphone Applications," *IEEE Transactions on Circuits and Systems II: Express Briefs*, Vol. 70, No. 8, August 2023, pp. 2889–2893.
4. S. K. Gupta, A. Bage and P. Ranjan, "A Compact, High Isolation Building Block for 8×8 Multi-Input Multi-Output Antenna Array Suitable for 5G Smartphone Applications," *International Journal of RF and Microwave Computer-Aided Engineering*, Vol. 32, No. 12, October 2022.
5. H. H. Zhang, G. G. Yu, X. Z. Liu, G. S. Cheng, Y. X. Xu, Y. Liu and G. M. Shi, "Low-SAR MIMO Antenna Array Design Using Characteristic Modes for 5G Mobile Phones," *IEEE Transactions on Antennas and Propagation*, Vol. 70, No. 4, April 2022, pp. 3052–3057.
6. H. Chen, D. He, M. Zhang and Y. Dou, "Self-Decoupled Coupled Line Antenna Pair (CLAP)," *IEEE Antennas and Wireless Propagation Letters*, Vol. 23, No. 10, October 2024, pp. 2944–2948.
7. Y. Fang, Y. Jia, J. -Q. Zhu, Y. Liu and J. An, "Self-Decoupling, Shared-Aperture, Eight-Antenna MIMO Array With MIMO-SAR Reduction," *IEEE Transactions on Antennas and Propagation*, Vol. 72, No. 2, February 2024, pp. 1905–1910.
8. C. Zhao, S. Lei, M. Chen, K. Sun, W. Yang and J. Tian, "A Compact Broadband Self-Decoupled MIMO Array Based on Dual Transmission Path Cancellation," *IEEE Antennas and Wireless Propagation Letters*, Vol. 23, No. 12, December 2024, pp. 4403–4407.
9. L. Qu and H. Piao, "A Dual-Port Single-Dipole MIMO Antenna Pair Based on Selective Modal Excitation for 5G Metal-Rimmed Terminals," *IEEE Access*, Vol. 10, September 2022, pp. 100208–100214.
10. W. -F. Zeng, F. -C. Chen and Q. -X. Chu, "Bandwidth-Enhanced 5G Mobile Phone Antenna Pair with Tunable Electric Field Null," *IEEE Transactions on Antennas and Propagation*, Vol. 71, No. 2, February 2023, pp. 1960–1964.
11. H. Zhou, D. Wu, M. Zhu, Y. Qiu, G. Yu and H -M. Zhou, "Wideband Low-Profile 8×8 MIMO Antenna Based IFA Pair for Ultrathin 5G Smartphones," *International Journal of Antennas and Propagation*, Vol. 1, No. 10, May 2022.
12. J. Sui, C. Huang and Y. -F. Cheng, "Multi-Element Fully Decoupled Inverted-F Antennas for Mobile Terminals," *IEEE Transactions on Antennas and Propagation*, Vol. 70, No. 11, November 2022, pp. 10076–10085.
13. J. You and Y. Dong, "Pattern-Reconfigurable Dipole Antenna Based on Odd- and Even-Mode Principle for 5G-NR Communications," *IEEE Transactions on Antennas and Propagation*, Vol. 72, No. 10, October 2024, pp. 8028–8033.
14. M. Han, L. Chang and A. Zhang, "Shared-Aperture Three-Antenna Module Using a Single Floating Metal with Small Clearance for 5G Mobile Terminals," *IEEE Antennas and Wireless Propagation Letters*, Vol. 23, No. 10, October 2024, pp. 3053–3057.
15. A. T. Z. Moses and N. Moses, "Highly Efficient 4-Port Self-Decoupled Multiple-Input Multiple-Output Antenna Pairs Operating in N46 Band for 5G Smartphone Applications," *International Journal of RF and Microwave Computer-Aided Engineering*, Vol. 32, No. 12, December 2022.
16. J. Sui, C. Huang, J. Li, X. Zhu and D. Li, "Wideband Aperture-Overlapped MIMO Antennas Naturally Integrating Mode Orthogonal and Parasitic Decoupling Schemes," *IEEE Antennas and Wireless Propagation Letters*, Vol. 23, No. 8, August 2024, pp. 2441–2445.
17. A. Ren, H. Yu, L. Yang, Z. Huang, Y. Liu and J. Hou, "Massive 16-Element Wideband Decoupled Pairs with High Integration for 5G Smartphones," *IEEE Antennas and Wireless Propagation Letters*, Vol. 23, No. 12, December 2024, pp. 4114–4118.
18. C. Deng, X. Cao, D. Li and W. Yu, "Compact Dual-Band MIMO Antenna with Shared Decoupling Structure for 5G Mobile Terminals," *IEEE Antennas and Wireless Propagation Letters*, Vol. 22, No. 6, June 2023, pp. 1281–1285.
19. W. Tang, J. Sui, Y. Wang, D. Li, J. Li and X. Zhu, "Dual-Band and Wideband Self-Decoupled MIMO Antennas With Four Hybrid Modes," *IEEE Antennas and Wireless Propagation Letters*, Vol. 23, No. 10, October 2024, pp. 3272–3276.
20. J. Hatte and V. Hendre, "Simplified Compact 4 Element MIMO Loop Antenna Structure with Decoupling Set-Up and Dual Band for 5G Wireless Terminal Devices," *Sadhana*, Vol. 48, No. 259, November 2023.
21. Z. Chen, Y. Liu, T. Yuan and H. Wong, "A Miniaturized MIMO Antenna with Dual-Band for 5G Smartphone Application," *IEEE Open Journal of Antennas and Propagation*, Vol. 4, January 2023, pp. 111–117.
22. A. Ghiat, A. Tribak, J. Terhzaz, A. Mimouni and H. Akhdar, "Triple-Band MIMO Antenna for 5G Terminals," *International Journal of Antennas and Propagation*, Vol. 2024, March 2024.
23. R. Xiao, W. Geyi, G. Yang and W. Wu, "Application of Resonant Modal Theory to the Design of Dual-Band Wideband Dipole Antenna," *IEEE Antennas and Wireless Propagation Letters*, Vol. 23, No. 8, August 2024, pp. 2551–2555.
24. H. S. Abubakar, Z. Zhao, M. E. Munir, W. U. K. Tareen, B. Wang, S. H. Kiani and T. Ali, "Enhanced Smartphone Connectivity: Dual-Band MIMO Antenna with High Isolation and Low ECC," *Physica Scripta*, Vol. 99, No. 6, May 2024.
25. M. N. Zahid, Z. Gaofeng, S. H. Kiani, U. Rafique, S. M. Abbas, M. Alibakhshikenari and M. Dalarsson, "H-Shaped Eight-Element Dual-Band MIMO Antenna for Sub-6 GHz 5G Smartphone Applications," *IEEE Access*, Vol. 10, July 2022, pp. 85619–85629.
26. Y. Luo, L. Zhu, Y. Liu, N. -W. Liu and S. Gong, "Multiband Monopole Smartphone Antenna With Bandwidth Enhancement Under Radiation of Multiple Same-Order Modes," *IEEE Transactions on Antennas and Propagation*, Vol. 70, No. 4, April 2022, pp. 2580–2592.
27. V. Thakur and N. Jaglan, "A T-Shaped Compact Dual-Band MIMO Antenna System for 5G Smartphone Applications," *Wireless Networks*, Vol. 30, 2024, pp. 1683–1695.
28. J. Ahn, Y. Youn, B. Kim, J. Lee, N. Choi, Y. Lee, G. Kim and W. Hong, "Wideband 5G N77/N79 4×4 MIMO Antenna Featuring Open and Closed Stubs for Metal-Rimmed Smartphones with Four Slits," *IEEE Antennas and Wireless Propagation Letters*, Vol. 22, No. 12, December 2023, pp. 2798–2802.
29. R. Boufouss and A. Najid, "A Dual-Band MIMO PIFA Antenna with a Printed Rectangular Open-Ended Ring for 5G/WLAN Mobile Terminal," *Engineering Research Express*, Vol. 6, No.1, March 2024.